MASTER'S THESIS 2023

Methods to study device induced aggregation of proteins

Therese von Wowern

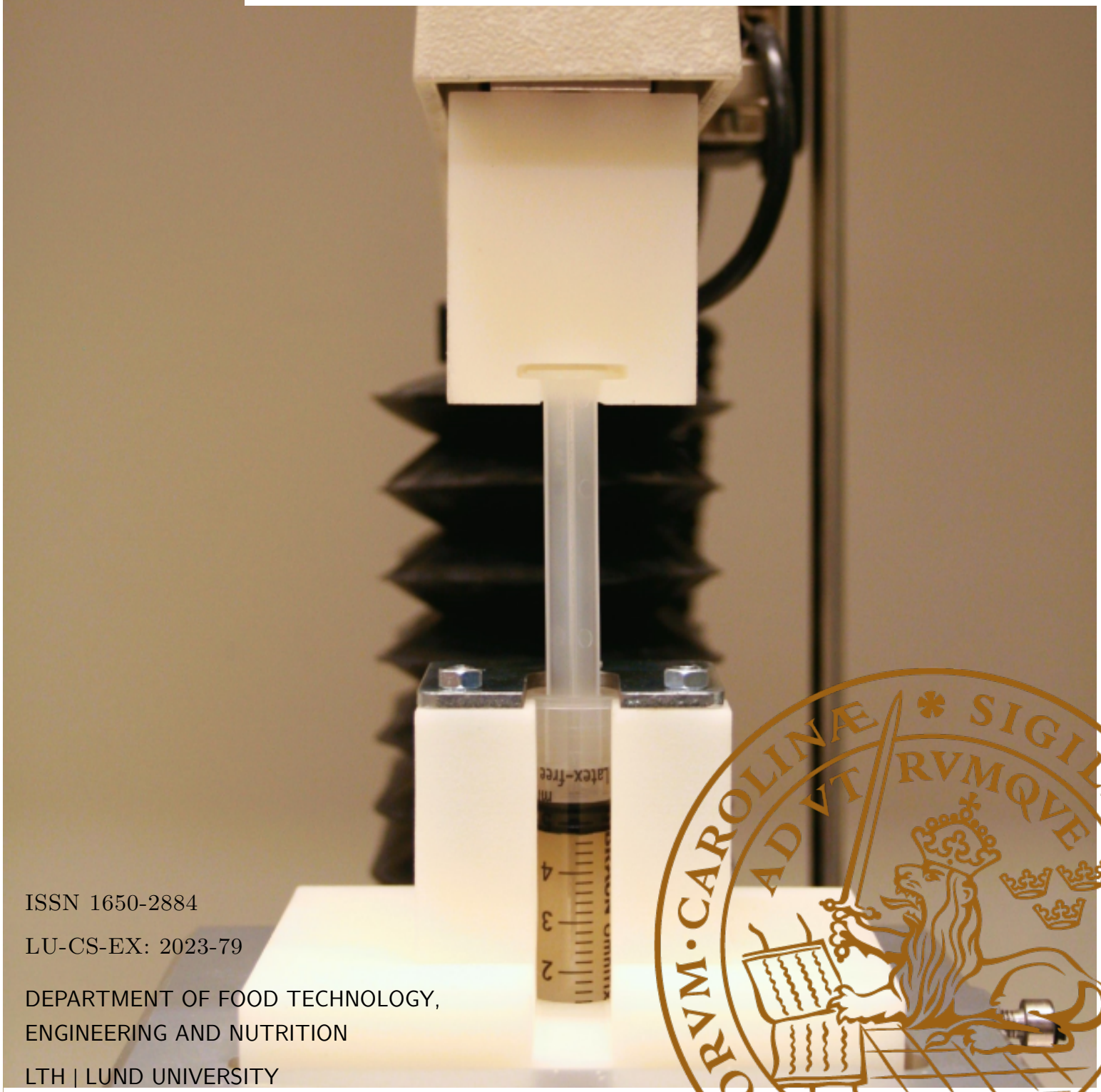

ISSN 1650-2884

LU-CS-EX: 2023-79

DEPARTMENT OF FOOD TECHNOLOGY,
ENGINEERING AND NUTRITION

LTH | LUND UNIVERSITY

EXAMENSARBETE

Läkemedelsteknologi
KLGM15

LU-CS-EX: 2023-79

Methods to study device induced aggregation of proteins

Therese von Wowern

Methods to study device induced aggregation of proteins

Degree Project in Pharmaceutical Technology

KLGM15

Therese von Wowern
ma5837vo-s@student.lu.se

September 6, 2023

Master's thesis work carried out at
the Department of Food Technology, Engineering and Nutrition,
Lund University.

Supervisors:
Marie Wahlgren, marie.wahlgren@food.lth.se
Anna Kjellström, anna.kjellstrom@food.lth.se
Examiner:

Lars Nilsson, lars.nilsson@food.lth.se

Acknowledgements

With this diploma work, I conclude my master studies in Chemical Engineering at Lund University and want to convey my sincere appreciation to everyone who have supported me through this journey.

I would like express my deep gratitude to my subordinate supervisor Anna Kjellström. Without you this work would not have been possible. Thank you for your generous patience with explaining and the countless hours you have spent helping me, always with a smile.

I would also like to express my gratitude to my supervisor Marie Wahlgren. I have truly appreciated your input, support and positive energy.

I would like to thank my father, Bo von Wowern, for his help with designing and welding the first version of the syringe setup.

Further, I would like to thank Jonny Nyman at the 3D printing laboratory of LTH. Your input was crucial for the final syringe setup design and your help made it possible to put it into reality.

I would also like to show my appreciation to Marie Svensson Coelho for the demo and help regarding the operation of FlowCAM.

Thank you Basel Al-Roudainy for the walktrough of the DLS, Ia Rosenlind for letting me borrow laboratory equipment and Jeanette Purhagen for your input regarding the texture analyser. Thank you Olexandr Fedkiv, for your help with ordering and helping me find material at the institution.

I would also like to thank my fiance and my friends for all the encouragement throughout my studies. Last, but not least, I would like to express my thankfulness to my parents for their endless support and for taking care of my daughter Elin during the days while I worked on this project.

Thank you!

Therese von Wowern, September 6, 2023. Lund

Abbreviations

AR	-	Aspect ratio
DLS	-	Dynamic light scattering
EDQM	-	European Directorate for the Quality of Medicines and HealthCare
ESD	-	equivalent spherical diameter
PDI	-	Polydispersity Index
SEC	-	Size exclusion chromatography
SVP	-	Subvisible particulate
USP	-	US Pharmacopoeia

Abstract

This work developed a method for the investigation of how medical devices, such as syringes and needles, affect the formation of subvisible particles in a protein drug without excipients. Protein-based pharmaceuticals are well known to be sensitive to different kinds of stress, and exposure to stress during the use of this device is unavoidable.

To study this phenomenon, an in-house built probe for the operation of syringes with a texture analyser was created. Mechanical stress was modulated by varying the expulsion speed, and related forces were captured by the texture analyser. The formation of particles was evaluated by dynamic light scattering(DLS), size exclusion chromatography(SEC) and flow imaging microscopy by FlowCAM.

The insulin was found to be primarily present in its hexamer form, with a hydrodynamic diameter of 5.6 nm. FlowCAM showed increased concentration of particles in both siliconized and non-siliconized syringes after mechanical stress. The increase was associated with protein aggregates in the non-siliconized syringe, while increase in the the siliconized was mainly associated to silicone oil droplet formation. The particles were categorized by sphericity using circle fit and aspect ratio, with spherical cutoff at 0.85. The siliconized syringe had no increase in protein aggregates after stress and displayed a substantial loss of native protein (2.5 %) according to SEC. This concedes with findings from other studies and might be due to oil interface adsorption. Although, the size distribution from FlowCAM yielded particle counts, which were theoretically too low to account for this loss alone.

Keywords: protein formulation; protein aggregation; insulin; silicone oil; syringe; shear stress; subvisible particle; size exclusion chromatography; flow imaging microscopy

Table of Contents

Chapter 1

Introduction

This work was part of the project RealHope, which is working towards improving patient safety by addressing the concerns regarding protein drug instability (RealHope, n.d.). The formation of subvisible particulates (SVP) in protein-based injectabelia, represents one way by which this type of drug can be destabilized. Their presence is of great interest as the particles have the potential to cause harm in the patient, and are therefore regulated via standards by the USP and the European directorate. Further,the surveillance of particulates serves as a quality parameter in the pharmaceutical industry, where increased numbers might indicate problems during manufacturing, storage or handling of the product (Pharmacopea Europaea, 2008; Gecsey, 2015; Carpenter et al., 2015). Studies have shown that medical devices such as syringes and silicone lubrication can promote the emergence of subvisible particles during handling, especially after having been subjected to different types of mechanical stress. Totally preventing the medical device from inflicting some sort of mechanical stress on the injectabelia is virtually impossible, as force needs to be applied to operate it. But, questions remains regarding what type and how high amount of stress the system can be allowed to experience, before it should give rise to concerns. There have also been indications that the type of mechanical stress will affect the morphology of the formed protein aggregates, and it remains to see whether or not this differences reflect their potential to harm the patient (Li et al., 2012; Kim et al., 2020).

1.1 Aim and objective

The aim of this work was to develop a method to investigate the formation of of subvisible particles in a protein drug, which had been subjected to aspiration and expulsion by a syringe with needle.

The specific objectives were:

- To design and manufacture a probe, which enabled a texture analyzer to operate a syringe.
- To delimitate and design the scope of the work in a sensible and justifiable way.
- To explore the impact of mechanical stress at laminar flow.
- To investigate the effect of silicone oil lubrication.
- To analyze the mechanically stressed protein drug with three commonly deployed techniques in the field; size exclusion chromatography (SEC), dynamic light scattering (DLS) and flow imaging microscopy by FlowCam.
- To evaluate if any of the investigated conditions had the potential to occur in a clinical setting.

1.2 Expected result

During this investigation, the subvisible particulates were expected to mainly be composed of protein aggregates and silicone oil particles. It is known that mechanical stress in the form of flicking or dropping increases the concentration of these particles (Kim et al., 2020). Thus, it is expected that increased expulsion force, which in turn causes increased shear stress, will lead to increased levels of particulate, both proteinaceous and silicone. The question remains though, whether the magnitude of the forces during this investigation are enough to cause an observable increase.

Chapter 2

Theory and Background

2.1 Protein-based Pharmaceuticals

2.1.1 Introduction to Protein-based Pharmaceuticals

Protein-based pharmaceuticals is one of the fastest growing class of drugs. Even though the class itself is small, the monetary value involved is significant as the drug cost is high. In 2018, the global market for the class was worth approximately $147 billion, and the market is predicted to experience a substantial growth during the next couple of years, reaching $240 billion by year 2025 (Pandya and Patravale, 2021; Makurvet, 2021).

The class has gained attention, as proteins can be tailored to treat a wide range of diseases, some of which have been formerly incurable. It is estimated that over 250 proteins are currently being used clinically, both in a hospital setting and at home. For example insulin analogues for treating diabetes mellitus and trastuzumab to treat breast and stomach cancer (Dingman and Balu-Iyer, 2019). Another advantage is the proteins high specificity to their target molecule, which leads to less side-effects compared to classical small drug molecules (Pandya and Patravale, 2021).

2.1.2 Protein aggregates and SVPs

The downside is that protein-based pharmaceuticals mainly consist of water-based solutions intended for parenteral administration. Injectabelia with proteins are more sensitive during

manufactoring, storage and in-house handling than for example tablets. To ensure patient safety when injected, the finished formulation has to fulfill specifications regarding for example particulate matter content (Anselmo et al., 2019; Correia et al., 2012; Gecsey, 2015; Schellekens, 2002).

Protein aggregation represents one way by which the formulation can suffer from degradation and a common source of subvisible particulates. Aggregation can be promoted by a number of factors, such as agitation, shear force, surface/air interfaces, heat, light, medical container materials and presence of other contaminants serving as nuclei for aggregation. This degradation will lead to loss of active pharmaceutical ingredient in the product.. There are concerns that aggregates might clog vessels, promote immune responses which reduce the bioavailability or induce harmful immunogenic complexes in the patient. Thus, the stability of protein-based pharmaceuticals is of great importance and preventing aggregation presents a hurdle for the future development and usage of of protein-based pharmaceuticals (Anselmo et al., 2019; Correia et al., 2012; Gecsey, 2015; Schellekens, 2002).

2.1.3 SVP in protein injectabelia

Minimizing the content of particulate matter represents one of the major challenges with parenteral formulations and is regarded a critical quality parameter. Particulate matter is divided into visible and subvisible particles, where visible are larger than 100 µm and subvisible are 0.1 - 100 µm (Gecsey, 2015; Carpenter et al., 2015).

They can be further classified according to their origin as extrinsic, intrinsic or inherent. Extrinsic are introduced from the surrounding environment and are truly foreign. They do not originate from the manufacturing process or equipment. Intrinsic originate from the process, for example silicone oil or plastic scraping from containers. Inherent relates to the product reforming itself. For example loss of the proteins desired native form by different types of degradation, leading to the formation of aggregates, unwanted quaternary structures or disassociation (Gecsey, 2015; Carpenter et al., 2015).

SEC and DLS are commonly used techniques in the industry for the surveillance of protein aggregate formation (Jiao et al., 2020). While SVP in general, are monitored via light obscuration, where the size of the particle is determined by the amount of light that the product blocks when passing between the light source and the detector (Gecsey, 2015).

Many medical devices, such as syringes and needles, are lubricated with silicone oil which sheds subvisible droplets into the product. The presence of these particles are of concern due to their foreign nature. There have been indications that they also might be able to act as adjuvants and provoke antibody production after repeated injections. Further, silicone oil droplets can promote protein aggregation or cause other perturbations of the proteins

native form. Thus, the monotoring of silicone oil droplets in the SVP range is important for the industry and the count can be used to detect detrimental changes in the production (Jiao et al., 2020; Chisholm et al., 2016).

2.1.4 Regulation regarding SVP

The US Pharmacopoeia (USP) and European Directorate for the Quality of Medicines and HealthCare (EDQM) has created standards regarding subvisible particulate content. The general standards, USP<788> and Ph. Eur. 2.9.19, define limits for subvisible particulate count in injectabelia and test methods to verify the content. The goal was to secure that the parenteral solutions were virtually free of subvisible particles which could be harmful when introduced to the patient (Pharmacopea Europaea, 2008; Gecsey, 2015; Carpenter et al., 2015).

The limits only involve particles of size $\geq$ 10 µm, the main motivation being concerns regarding blood vessel blockage, as the lumen of capillaries is around 5 - 10 µm and lumen for small veins are 10 - 50 µm. The standards describes two analyzing methods for obtaining the count, light obscuration and membrane microscopy. For clear injectabelias, the first method is recommended as it is faster, less subjective and less labor intensive. The standards state that for containers with a volume of less than 100 mL, the limit for subvisible particulate count per container is 6000 particles of size $\geq$ 10 µm and 600 particles of size $\geq$ 25 µm during light obscuration (Pharmacopea Europaea, 2008; Gecsey, 2015; Carpenter et al., 2015).

In 2014 an alternative to USP<788> was introduced, USP<787>, which specifically addresses protein-based formulations. Light obscuration is still the primary investigation method and it has similar thresholds regarding particles as USP<788>. It allows test methods which involves smaller sample volumes and is more adapted to the nature of protein-based injectabelia. Another addition came in 2015, USP<1787> which recommends monitoring of particles in the 2 - 10 µm range and to characterize their origin, as it is an important quality parameter. One of the challenges with light obscuration as the main method, is that it is not able characterize the morphology of the particles and has problems with estimating transparent particles such as protein aggregates. Thus, several suggestions regarding future combination with other techniques, to facilitate the characterization of subvisible particulates has been made. For example by dynamic flow imaging microscopy based techniques like micro-flow imaging and FlowCAM (Gecsey, 2015; Vargas et al., 2020; Roy T Cherris, 2018).

2.1.5 Insulin analog

Insulin is a hormone and regulates the blood sugar by facilitating the cells uptake of glucose. Injectabelia with insulin is widely used to manage diabetes both in hospital settings and at

home today (Nagel et al., 2019).

The insulin analog in this investigation was designed to have a faster onset of biological action after injection. The effect arises because two amino acids have been replaced, which makes the oligomer dissociate more easily into the biologically active monomer than human insulin. The analog is formulated as 3.5 mg/mL at pH 7.4 by the manufacturer. During these conditions, the protein is primarily present as a hexameric structure. But, studies have indicated that a significant amount of the native protein might be present as monomeres or dimeres and dodecameres (Zhou et al., 2016; Nagel et al., 2019; Adams et al., 2018).

The study by Nagel et al. (2019) suggested that the primary form shifted to monomeric when the commercially formulated insulin analog was diluted to approximately 0.9 mg/mL. Thus, the protein concentration seems to affect the preference of form. In studies, the extinction coefficient of this analog is most commonly assumed to be the same as for human insulin ($0.9521\ cm^{-1}/mL/mg^{-1}$) (Harrison and Garratt, 1969; Zhou et al., 2016; Woods et al., 2012). The molecular weight of the analog is 5823 g/mol, and its pure monomer has an isolectric point of 5.1. However, studies have found that the distribution of the native form will affect the surface charge and the isoelectric point will therfore depend on which type of oligomere that is inhabited (Poulsen et al., 2007; PubChem, 2023).

2.1.6 Insulin aggregation

Insulin was regarded as a good model protein for this investigation. It is well-known and studied, that this protein have an inclination to readily form aggregates when exposed to different types of mechanical stress. Especially in conjunction with hydrophobic interfaces, which arises for example during introduction of air, silicone oil or medical devices, (Chouchane et al., 2022). The mechanism behind the aggregation has been proposed (Fig. 2.1) to be because the interface will cause the protein monomers to be destabilized and transiently unfold, while at the same time facilitating protein-protein interaction as they are kept in close proximity of each other (Rudiuk et al., 2012).

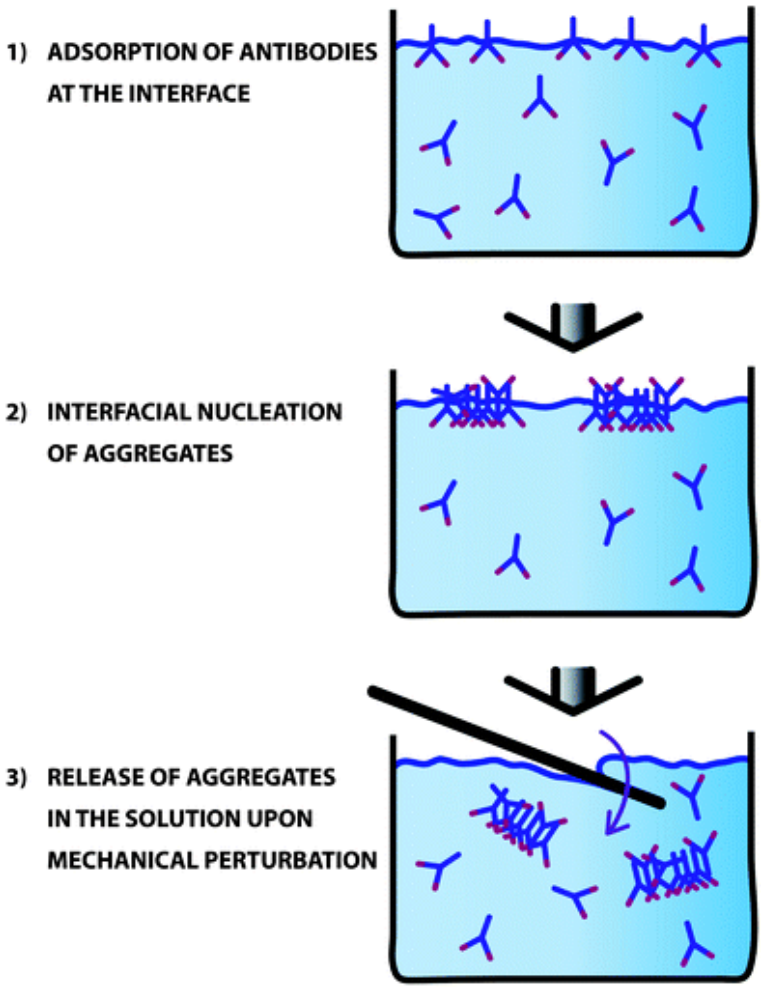

Figure 2.1: Schematic drawing of proposed mechanism behind protein aggregation during mechanical disturbance of interfaces (Rudiuk et al., 2012)

This will create a film of aggregates at the interface, which will be released to the bulk of the solution when disturbed mechanically. Thus, the mechanical stress facilitates continued growth of aggregates, as it will clear the interface. This allows the interface to continue to adsorb monomeric native insulin from the bulk (Rudiuk et al., 2012). As a consequence, formulations with the native insulin in hexameric form are preferred over monomeric, as it will increase the stability of the product (Adams et al., 2018).

Insulin have been shown to be able to form aggregates with widely different morphology, both in the subvisible and visible particle region. Studies have identified the formation of elongated unbranched fibrilar structures and amyloyid-like fibrils ranging in nm to microns in length. Other studies have found spherical aggregates, such as spherulites and particulates. The spherulites ranged from a couple microns to mm in diameter and consisted of multiple fibrils gathered in a common center. Particulates were compact and their diameter was 0.01 - 2 µm (Thorlaksen et al., 2022).

2.1.7 Silicone lubrication

It is acknowledged that syringes will release silicone oil particles during normal use, and this amount increases after having been subjected to mechanical stress such as flicking, dropping or other forms of agitation (Dias Júnior et al., 2020). Studies have found that the presence of silicone oil can decrease the concentration of soluble native protein. It is suggested that this phenomenon primarily arises due to protein adsorption to the hydrophobic surface of the oil particles and the medical device (Fig. 2.2) (Li et al., 2012; Kim et al., 2020).

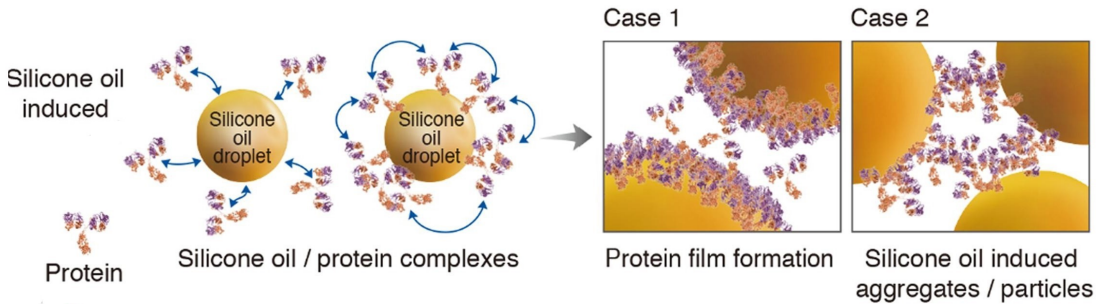

Figure 2.2: Schematic drawing of proposed mechanisms behind silicone oil induced protein aggregation. When the native protein is adsorbed, they will form a film on the oil particle surface (Case 1) or form mixed protein-silicone oil aggregates (Case 2) (Kim et al., 2020)

The associated reduction in native form was further confirmed in the study by Ludwig et al. (2010), which identified that protein will readily adsorb to surfaces of silicone oil droplets. The protein will act as an stabilizing emulsifier, covering roughly 50 % of the available interface area. The surface load of protein was approximated to 1 – 2 mg per m^2 of oil particles. Further, the author found that the emulsion suffered from destabilisation due to creaming as the density of silicone oil (0.972g/mL) was lower than both water and protein (1.3 g/mL).

2.2 Medical devices

2.2.1 Syringes and needles

Polypropylene is the most commonly used plastic for producing disposable plastic syringes. The material is viewed as inexpensive, inert and its safety in regards to medical devices well

explored. The syringes are in general referred to as being 3-piece or 2-piece and are manufactured with or without lubrication in the form of silicone oil. The 3-piece syringes differs by having a stopper and are siliconized to ease the action of the stopper (Fig. 2.3). The 2-piece syringe design generally lack lubrication (Melo et al., 2021).

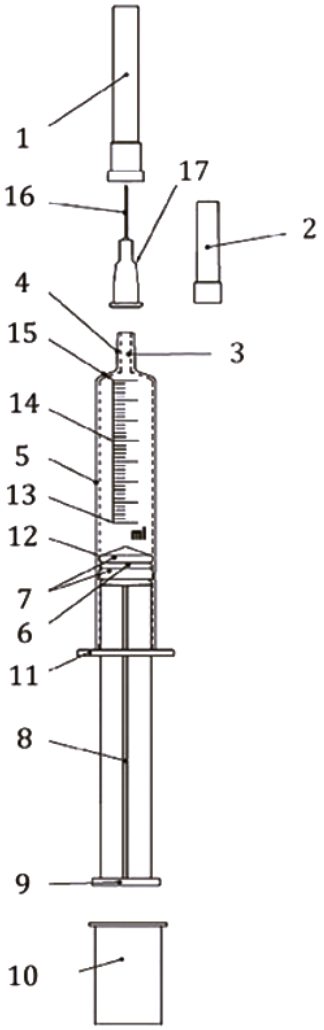

Figure 2.3: Schematic drawing of a syringe with needle.

1. Needle cap or shield
2. Nozzle cap
3. Nozzle lumen
4. Nozzle
5. Barrel plunger
6. Stopper
7. Seals
8. Plunger
9. Push-button
10. Plunger cap
11. Barrel flanges
12. Fiducial line
13. Nominal capacity
14. Graduation lines
15. Zero line
16. Needle tube
17. Hub

Only 3-piece syringes are equipped with a stopper (Svenska Institutet för Standarder, 2016).

The needle tube (Fig. 2.3) consist of medical grade stainless steel and the unit gauge (G) is

used for the description of its diameter, where larger gauge number indicates a thinner needle. It is common practice for the manufacturer to also coat the needle tube with silicone oil to minimize friction at the site of injection, and it can prove difficult to acquire needles without coating. This practice of coating is worth to note, as the use of needles will be expected to introduce silicone to some degree during the investigation even though a silicone free syringe has been used. Further, silicone particles have been associated with the formation of floaters in the eye after injection, which can impair quality of vision and require surgery for removal. They are therefore highly unwanted during intraocular injections (Melo et al., 2021; Narhi et al., 2022; Svenska Institutet för Standarder, 2016).

2.2.2 Syringeability and rheology

The investigated system in this study consisted of a medical device in the form of a syringe with a needle, where fluid was expelled at laminar flow due to the action of the plunger (Fig. 2.4).

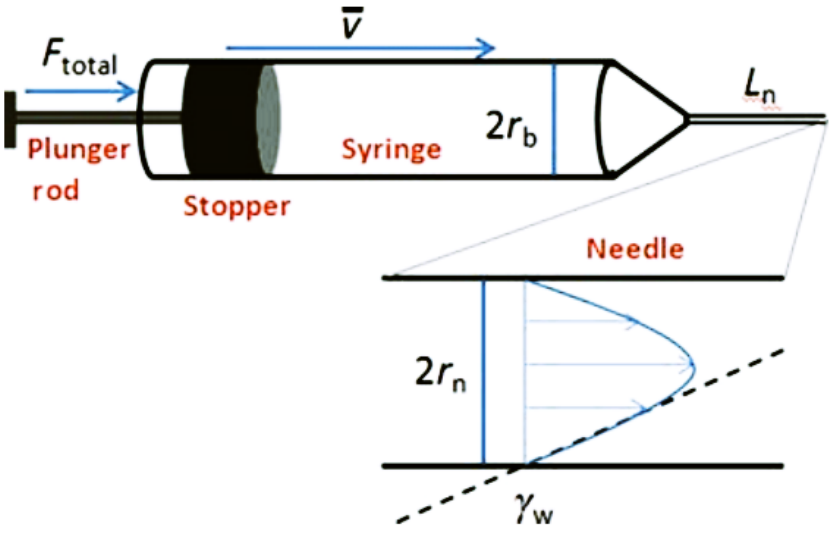

Figure 2.4: Schematic drawing of a syringe with needle during expulsion. The total extrusion force,F_{total}, corresponds to the total force required to move the plunger with an injection speed $\bar{v}$. r_b is the inner radius of the syringe barrel and r_n the inner radius of the needle. The length of the needle is denoted by L_n, while γ_w corresponds to the shear rate at the wall during laminar flow (Rathore et al., 2012)

The study by Rathore et al. (2012) was used as an inspiration for the characterization of the system and its rheology during laminar flow. In this study, gliding force was defined as the force required to sustain a constant speed of the plunger, after static friction had been

overcome. The friction force of the system was defined as the gliding force required to operate the wetted syringe without needle (Rathore et al., 2012).

The setup design for investigation of the protein-device interaction in this Master thesis was inspired by the setup in the study by Burckbuchler et al. (2010). Where the rhelogical study was performed with a texture analyser.

Purely laminar flow is most often defined as flow occurring at Reynolds number (Re) below 2000. The flow will gradually start to gain a turbulent character above this number and be referred to as transitional flow. When Re reaches ≥ 4000, the flow will be regarded as completely turbulent. Reynolds number can be estimated via Equation 2.1 (Connor, 2019).

$$Re = \frac{VD}{v} \tag{2.1}$$

Where V is the flow velocity, D is the hydraulic diameter and v is the kinematic viscosity of the fluid (Connor, 2019).

According to Rathore et al. (2012), the shear stress (τ_w) at the barrel wall of a Newtonian fluid at laminar flow, can be theoretically estimated from the hydrodynamic force (F_{hydro}) by Equation 2.2.

$$\tau_w = \left(\frac{F_{hydro}}{\pi r_b^2}\right)\frac{r_n}{2L_n} \tag{2.2}$$

r_b is the inner radius of the syringe barrel. r_n is the inner radius of the needle and L_n the length of the needle. Equation 2.2 originate from an adaption of the Hagen–Poiseuille equation (Rathore et al., 2012).

The hydrodynamic force was then estimated from the measured total extrusion force (F_{total}) and friction force ($f_{friction}$) by:

$$F_{hydro} = F_{total} - f_{friction} \tag{2.3}$$

When deploying Equation 2.3, it was assumed that the hydrodynamic force only originated from the pressure drop which was required to drive the fluid out of the device. The contribution from other forces, such as the force associated with needle entry was assumed to be negligible (Rathore et al., 2012).

Also, the expected hydrodynamic force be theoretically calculated according to Rathore et al. (2012), by the following equation:

$$F_{hydro} = \left(\frac{8\pi\mu L_n r_b^4}{r_n^4}\right)\bar{v} \tag{2.4}$$

Where μ is the viscosity of the Newtonian liquid and $\bar{v}$ is the linear speed of the plunger. It is assumed that the flow of the fluid is laminar. The equation above (Eq.2.4) can be used to estimate how large the force will be during different combinations of syringe and sizes, along with different injection speeds (Rathore et al., 2012).

2.2.3 Parenteral injections

The most commonly used sites for parenteral administration are the intravenous (in a vein), the subcutaneus (under skin) and the intramuskular (in muscle) route (Fig. 2.5) (Ruiz and Scioli Montoto, 2018).

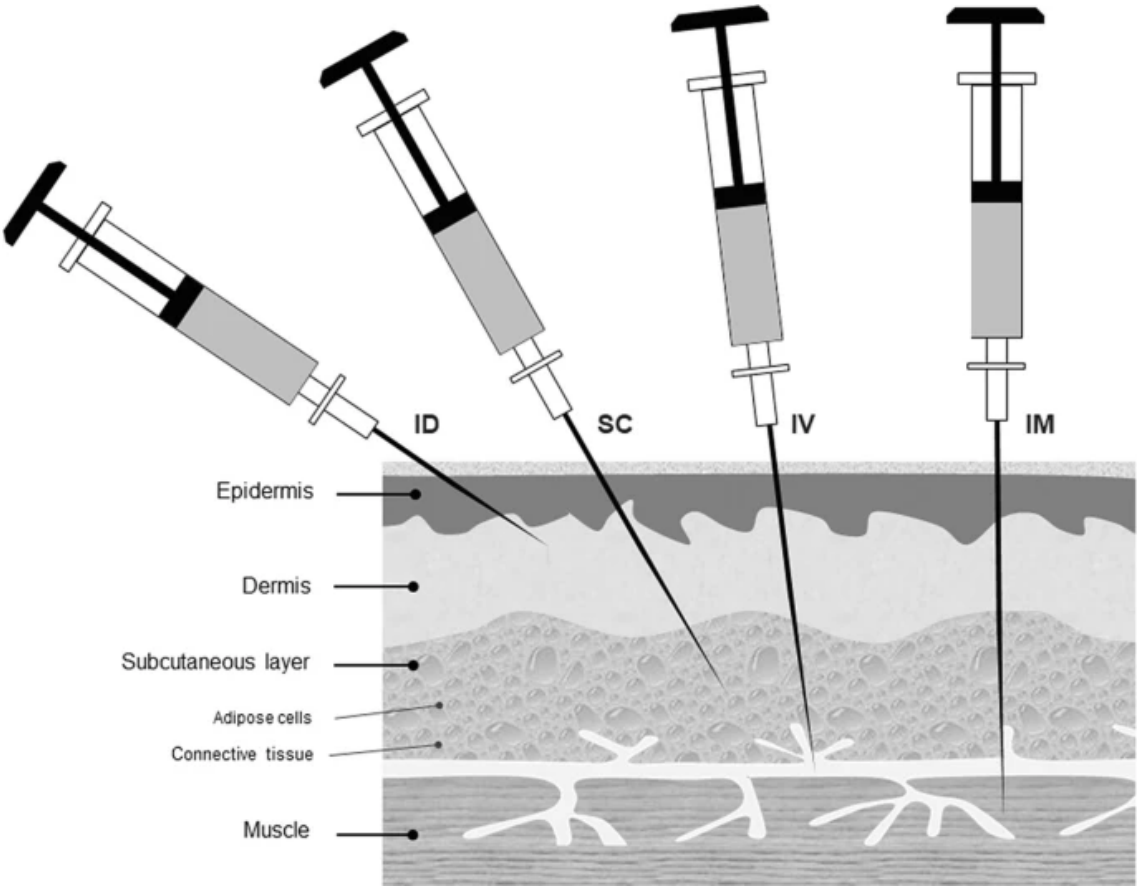

Figure 2.5: Schematic drawing of intramuscular (IM), subctaneous (SC), intravenous (IV) and intradermal (ID) injection (Ruiz and Scioli Montoto, 2018)

Intravenous treatment with protein-based pharmaceuticals is most often given through a peripheral venous catheter. Thus, protein drugs are most often injected (expelled from a syringe with a needle) during subcutaneus or intramuskular administration (Irvine et al., 2013).

A study showed that injection volumes of up to 3 mL and injection rates of 0.3 mL/s were acceptable during subcutaneous injections in the abdominal area. The needles for this type of site are thin (25G - 30G) and short (12.5 - 16 mm). Needles and syringes for subcutaneous injection of insulin are conventionally on the smaller side. Where, the syringe usually holds 0.5 - 1.0 mL and the needle is 31G and approximately 8 - 13 mm long (Berteau et al., 2015; Galan, 2022; Melo et al., 2021; SWEMED, n.d.).

The recommended injection rate during intramuscular injection is slower (0.1 mL/s). This site requires thicker and longer needles, which are 20G - 22G and 25 - 38 mm. The maximal intramuscular injection volume depends on the size of the involved muscle. For the deltoid muscle (arm muscle) it is regarded as 2 mL, while it is 5 mL for the large muscles located at the thigh and buttock (Polania Gutierrez and Munakomi, 2022; Galan, 2022; Hopkins and Arias, 2013).

Other, less common and more locally acting routes are for example intravitreal (inside back chamber of the eye) injections, and these often often involve needles belonging to the thinnest range. For example 30G is commonly used for the injection of the protein-based drug Ranibizumab. The thinner the needle, the less associated trauma or pain, so some physicians have started using even thinner needles such as 31G for intravitreal injections. The use of even thinner needles, such as 32G - 34G, have been considered. It should be noted though, that they will exert approximately the same shear stress as a normal 30G or 31G needle. The reduction in size is typically due to reduction of needle wall thickness, and not the lumen diameter (Melo et al., 2021; JAPAN BIO PRODUCTS, n.d.).

A thinner needle is also associated with better patient compliance because a smaller needle will be perceived as less intimidating. But, this should be weighted against how large the resulting injection force will be, as a small inner lumen will result in a greater hydrodynamic force (view Eq. 2.4). An article by Watt et al. (2019) concluded that the injection force should ideally be no greater than 20N to assure that manual injection can be performed by everyone. The authors found that the maximal acceptable injection force was 40N, and that injections forces near 80N led to difficulties for most of the participants in the study.

2.3 The principle of each method

2.3.1 Texture analyser

Texture analysers (Fig. 2.6a) are used for the scientific studying of materials and rheology. It functions by applying a tensile or compressive force with the arm on the sample, while recording the force, distance and time. The output can then be visualized in graphs for further investigation (Stable Micro Systems, n.d.a).

(a) **(b)**

Figure 2.6: Texture analyser, TA.XTplusC (a) and Universal syringe rig (b) from Stable Micro Systems (Stable Micro Systems, n.d.b; Smewing, 2014)

The equipment enables the investigator to subject samples to repeatable stress under controlled circumstances. Making the user able to reliably characterize the mechanical properties a of wide variety of samples, by equipping the analyser with different types of probes, to which the investigated product can be fitted. For example medical devices such as syringes (Fig. 2.6b). The ready available probe kits from the manufacturer can sometimes prove expensive, which makes in-house design and 3D printed probes a cost-effective alternative. (Stable

Micro Systems, n.d.a).

2.3.2 DLS

DLS (dynamic light scattering) is a noninvasive method, which builds upon Brownian motion to estimate the size of small particles. The Brownian motion arises due to the push of the suspended particles by the molecules in the solution, making them move randomly and diffuse. In DLS, this is measured by illuminating the sample cell with a laser (Fig. 2.7) and recording the change in intensity pattern of the scattered light over time (Malvern Panalytical, 2010).

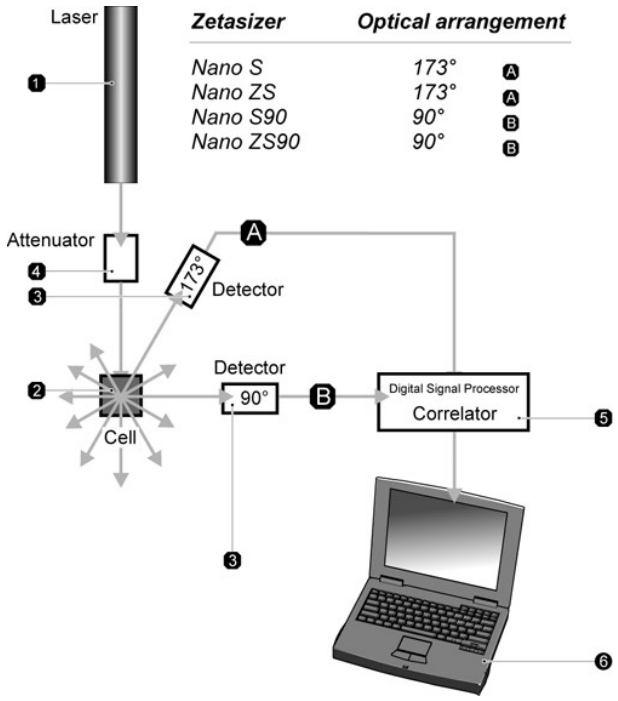

Figure 2.7: Schematic of a Zetasizer Nano series DLS from Malvern Panalytics. A laser illuminates the sample in the cell, where the particles in sample will scatter some of the light, which is then read by the detector at an angle of 173° (back scatter) or 90° (side scatter). The attenuater is used for regulating the amount of light hitting the sample, as the detector is only able to function within a narrow range of light intensity. The correlator will compare snapshots of the intensity at specific time intervals to calculate the decay rate of similarity between the intensity pattern at t = 0 and successive snapshots. This is then passed to a computer, where software estimate the particle size from the decay rate (Malvern Panalytical, 2010). The DLS instrument in this study, Malvern panalytical Zetasizer Nano ZS, is able to describe particles ranging from 0.3 nm up to 10 µm (Malvern Panalytical, n.d.)

The smaller the particles are, the faster will the particles diffuse and the faster will the detected intensity fluctuate (Fig. 2.8), which ultimately leads to a faster loss of the original intensity pattern (Malvern Panalytical, 2010).

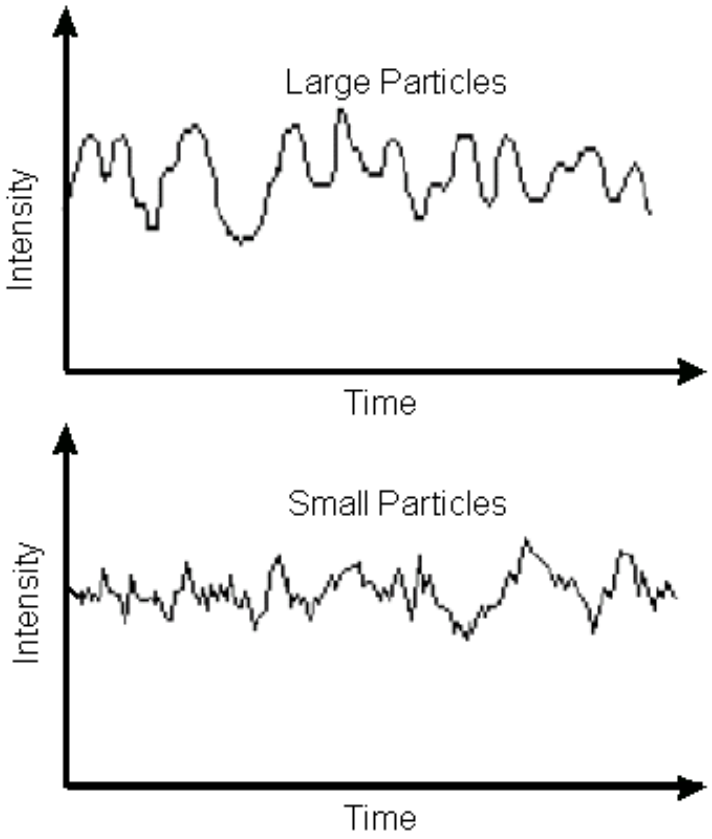

Figure 2.8: Comparison of intensity over time for larger versus smaller particles. The fluctuation rate is faster for smaller particles (Malvern Panalytical, 2010).

The decay and total loss of correlation from the original intensity pattern over time is translated into a correlation factor by the correlator, which is then characterized as a function ($G(\tau)$) of time on a logarithmic scale. The function can then be plotted in the form of a correlogram, view Figure 2.9 (Malvern Panalytical, 2010).

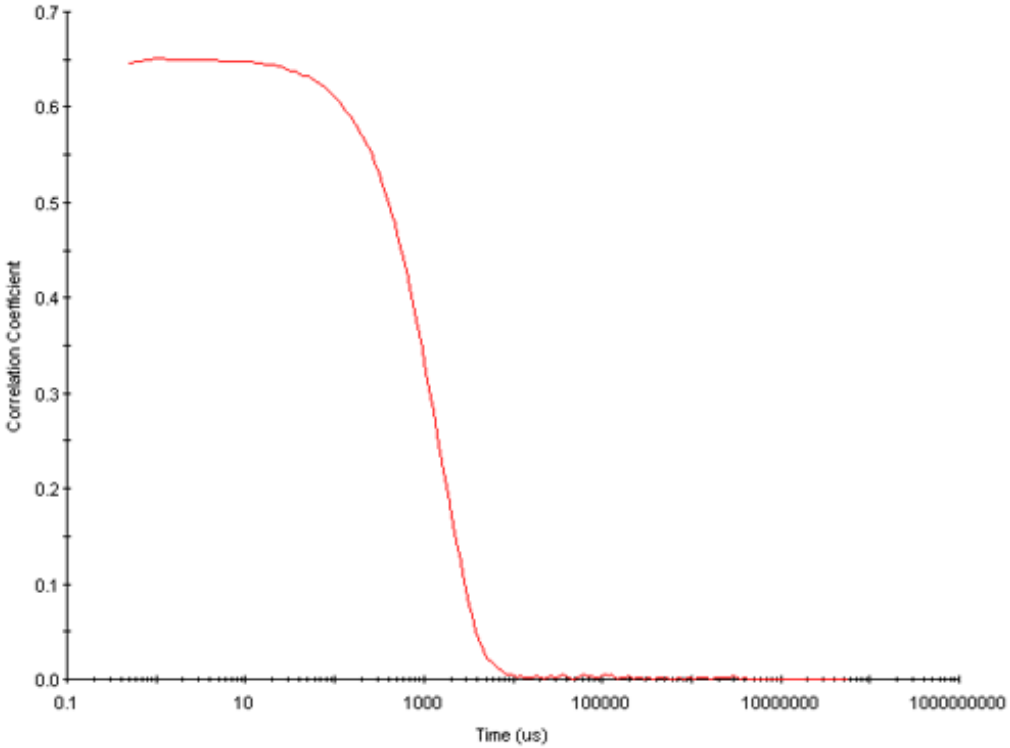

(a) Large particle

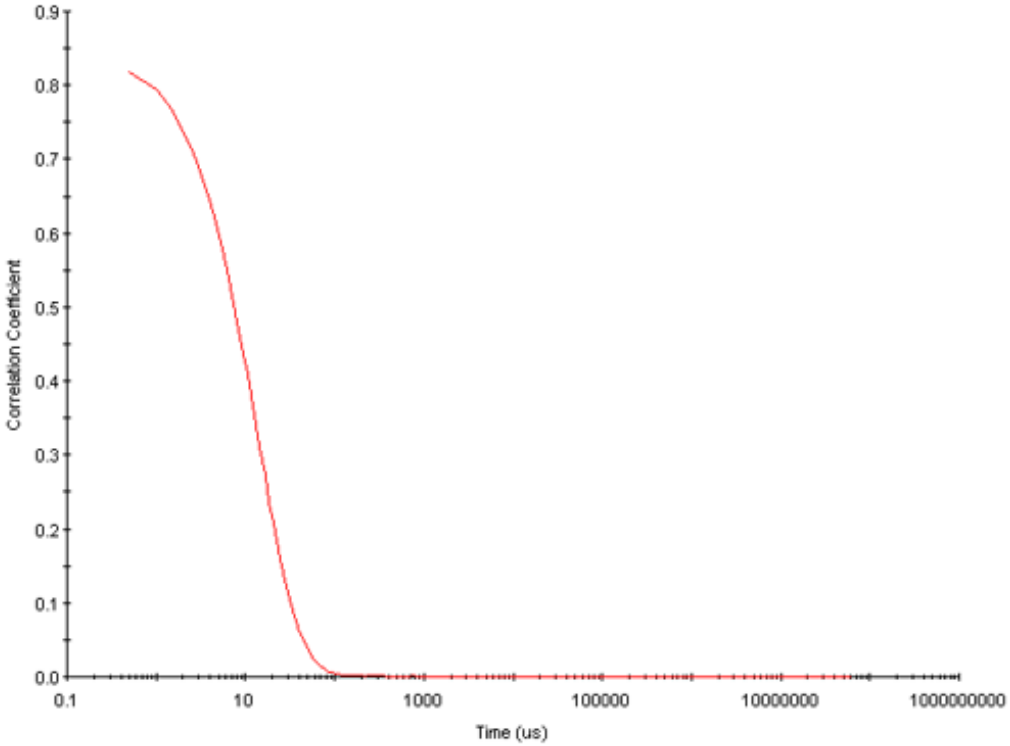

(b) Small particle

Figure 2.9: DLS correlogram. The correlation factor of the intensity pattern is plotted as a function of time (µs). The factor decay is faster for smaller particles (b), approximately 10 µs, compared to several microseconds for the larger particles (a) (Malvern Panalytical, 2010).

Visual inspection of the correlogram can be used to roughly evaluate the nature of the particles. The start of a significant decay in correlation factor in the correlogram is related to the mean size of the particles. The steepness is affected by sample mono- or polydispersity, where monodispersity leads to a steeper loss of factor and polydispersity to a less steep decay (Malvern Panalytical, 2010).

The correlation function of a monodisperse sample (Eq. 2.5) and a polydisperse sample (Eq. 2.6) can be related to the translational diffusion coefficient of particles (D) by:

$$G(\tau) = A[1 + Be^{(-2D((4\pi n/\lambda_0)sin(\theta/2))^2\tau)}] \tag{2.5}$$

$$G(\tau) = A[1 + Bg_1(\tau)^2] \tag{2.6}$$

Where n denotes the refractive index of the solvent, λ_0 the laser wavelength and θ the scattering angle. A and B corresponds to the baseline and the intercept of the correlation function. $g_1(\tau)$ denotes the sum of all the exponential decays within the correlation function (Malvern Panalytical, 2010).

The translational diffusion coefficient can then be translated into particle size, in the form of the hydrodynamic diameter ($d(H)$) (Eq. 2.7), with the Stokes-Einstein equation:

$$d(H) = \frac{k_B T}{3\pi\eta D} \tag{2.7}$$

Where k_B is Boltzmann's constant, T is the absolute temperature and η is the dynamic viscosity of the solution. The three equations above work under the assumption that the particles are completely spherical, which is rarely the case. Further, small changes in particle appearance will affect the measured size of the particle. The hydrodynamic diameter should therefore be regarded as an estimation rather than an absolute value of the actual particle size. It is assumed that $d(H)$ is directly proportional to the diffusivity of the particle. Thus, it is important to keep the temperature constant, as well as other factors such as particle surface charge or ion strength of solution in order to be able to compare results (Malvern Panalytical, 2010).

The concentration is an important factor to consider when performing DLS analysis. Sample concentrations of 1 - 10 mg/mL are generally recommended. A dilution series can be performed to identify the optimal range (Fig. 2.10) (LS Instruments, n.d.) (Brookhaven Instruments, 2019).

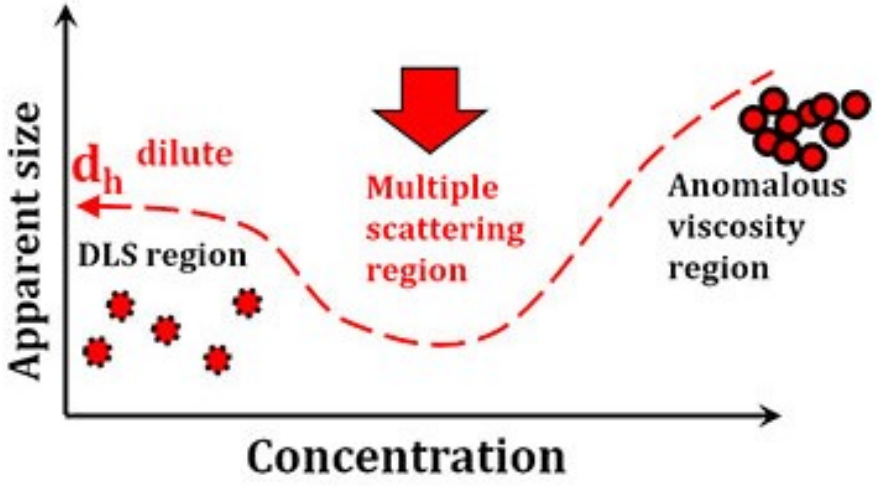

Figure 2.10: Hydrodynamic diameter plotted as a function of sample concentration. If the concentration is too high it will lead to underestimation of particle size (Multiple scatter region), as Equation 2.7 assumes the recorded light only have been scattered once by a particle. High concentrations will also affect the viscosity, which in turn will distort the measurement (Anomalous viscosity region). On the other hand, if the concentration is too low, the signal-to-noise ratio will be too low for appropriate interpretation, resulting in bad cumulative fitting. The optimal range is the plateau referred to as the DLS region (Brookhaven Instruments, 2019)

.

The concentration should be kept as low as possible while still facilitating a good signal-to-noise ratio. This corresponds to the plateau where the hydrodynamic diameter no longer changes when the sample is further diluted (Brookhaven Instruments, 2019).

The quality of measurements at different concentrations can also be evaluated by examining the y-intercept of the correlogram or the count rate (the number of photons detected). The y-intercept is an indicator of the signal-to-noise ratio, where the ideal signal brings intercept value of 1. A value above 0.6 is considered a good signal and the best signals are above 0.9 (Malvern Panalytical, 2017). Measurements involving count rates above 500 - 600 kcps are not recommended. It is recommended that no further dilution of sample is needed, if the diluted sample displays lowering of the count rate by the same factor as the dilution in unison with no change in apparent size (Brookhaven Instruments, 2019).

The risk of multiple scattering can be regulated by the choice of detection angle. Back scatter (detection at 173°) will minimize the amount of sample through which the scattered light will travel, thus extending the plateau and facilitate measurements on samples of higher concentrations (Anton Paar, n.d.).

The parameters of interest when interpreting DLS results primarily consist of the Z-average and the Polydispersity index (PDI). Both are produced by cumulative analysis of the correlation function. Z-average is the mean value for particle size and regarded as the most stable parameteris, hence included in ISO standards. PDI is a dimensionless parameter, which describes how broad the particle size distribution is and serves information about how polydisperse the sample is. In theory, a completely ideal monodisperse sample would have a PDI of 0. Samples with PDI below 0.1 are regarded as monodisperse, PDI 0.1 - 0.4 as moderately polydisperse and above 0.4 as polydisperse. Thus, an increase in PDI shows that the solution has become more heterogenous and will signal that protein aggregates have formed (Malvern Panalytical, 2017) (Nobbmann, 2017).

The intensity distribution will also be of interest, because the intensity is proportional to the sixth power of the hydrodynamic diameter during DLS. Thus, the larger the aggregate, the more amplified will the signal be, enabling the method to track the emergence of small amounts of aggregates. Other studies have found the hydrodynamic diameter of insulin mono- or dimer to be around 2 - 3 nm, while the hexamer form was around 5.6 nm (Zhou et al., 2016).

2.3.3 Flow imaging microscopy

The flow imaging microscopy technique works similar to direct microscopy. It was developed to enable a fast characterization of particles in a fluid sample. The differences are that the sample continuously flows by the objective, and the operator is replaced by a digital camera and a computer software which analyzes the captured images. The captured output can then be used to estimate the concentration of particles and to depict their morphology. Instruments such as FlowCAM utilize this method (Fig. 2.11) (Vargas et al., 2020).

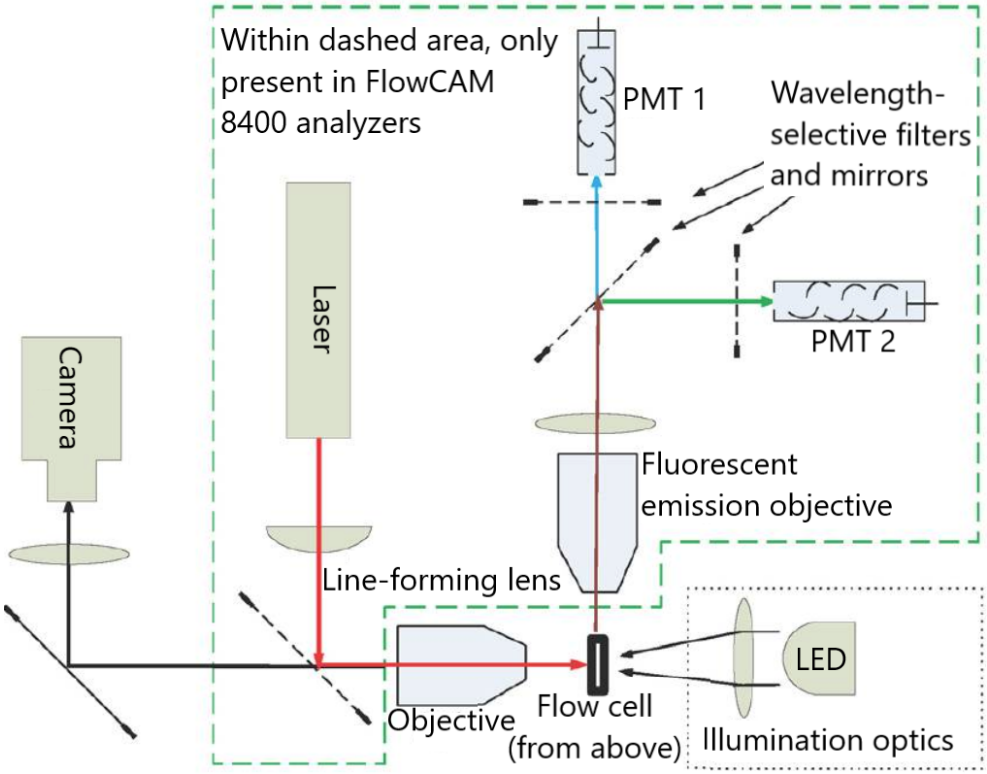

Figure 2.11: Diagram displaying the general components of a FlowCAM instrument. The flow cell is illuminated by the illumination optics and magnified by the objective. Meanwhile, the sample is pumped through the flow cell and thousands of particles per second are captured by the camera. The green dashed area represents components of FlowCAM instruments with the ability to depict fluorescent samples. The photo-multiplier tubes (PMT 1 and PMT 2) detect the light from the fluorescent particles (Fluid Imaging Technologies, Inc., 2017)

.

The currently developed instruments can digitally image a mixumum of 50 000 particles per minute. FlowCAM is able to measure particles in the 300 nm - 5 mm range, depending on the model. The Nano model measures particles of 300nm - 2 µm, and particles larger than 2

µm are measured by the 8000 or LO model. The software is able to construct particle distributions based on up to 40 particle properties. Making it an useful tool for the morphological investigation of subvisible particles (Yokogawa Fluid Imaging Technologies, Inc, 2023, n.d.).

The model in this study (VS-IV-C B3) was equipped with autoimaging and able to to capture fluorescent particles as it had two fluorescence trigger channels and one scatter trigger channel. It could depict particles in the 2 µm - 2 mm range and had 30 different particle properties (Spaulding, 2014).

Three particle properties was of interest to this investigation; equivalent spherical diameter (ESD), circle fit and aspect ratio (AR). The ESD was used for the characterization of diameter, while the sphericity was characterized by the circle fit and the AR. The ESD is determined as the mean of 36 feret measurements, where 5° increments of the feret angle was performed between each measurement. The feret measurement is defined as perpendicular distance between parallel tangents touching opposite sides of the particle (Fig. 2.12) (Spaulding, 2014).

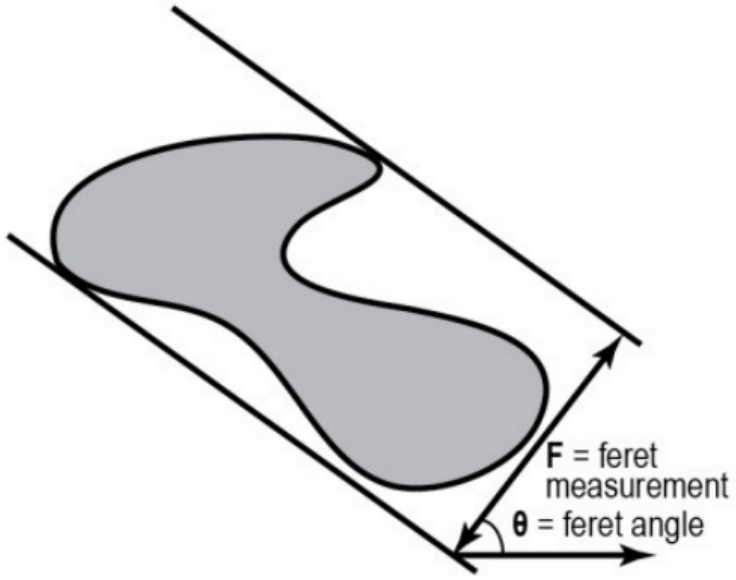

Figure 2.12: FlowCAM software definition of feret measurement (F) and angle (θ) (Spaulding, 2014)

.

Circle Fit is characterized in the following way (Fig. 2.13)

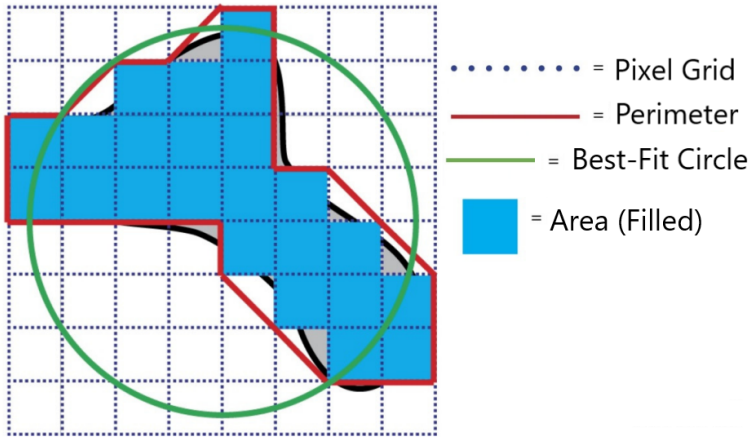

Figure 2.13: FlowCAM software definition of circle fit, which describes how much the perimeter (red) deviates from a best-fit circle (green). A best-fit circle, is the circle where the radial distance between the particle perimeter and the fitted circle is at minimum. The fit is normalized between 0 - 1, where the particle resembles a perfect circle at 1 (Spaulding, 2014)

.

Another particle property which can be used to characterize sphericity is the AR. The estimation of AR during FlowCAM analysis is described in Figure 2.14 (Spaulding, 2014).

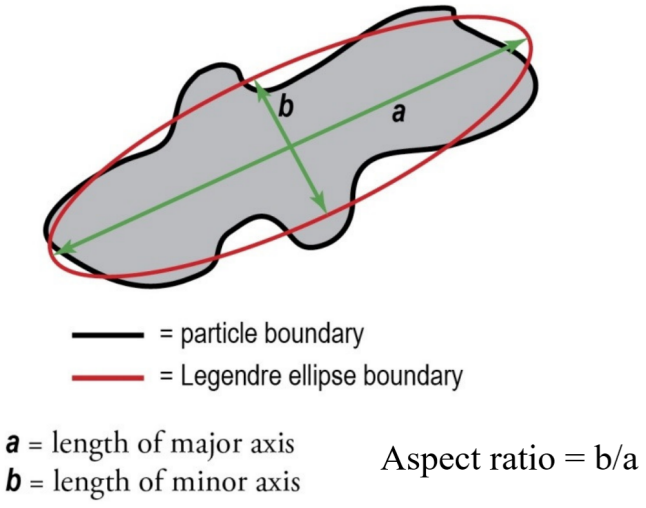

Figure 2.14: FlowCAM software definition of aspect ratio, which is the ratio between the shortest length (b) and the longest length (a) of an ellipse centered at the centroid of the particle. The particle resembles a perfect circle if its 1 while the particle is long and thin if its close to 0 (Spaulding, 2014)

.

A study by Kim et al. (2020) used FlowCAM to investigate the effect of flicking syringes containing a protein solution. Images of air bubbles and silicone oil were artificially generated for comparison against output. Their morphology can be viewed below in Figure 2.15.

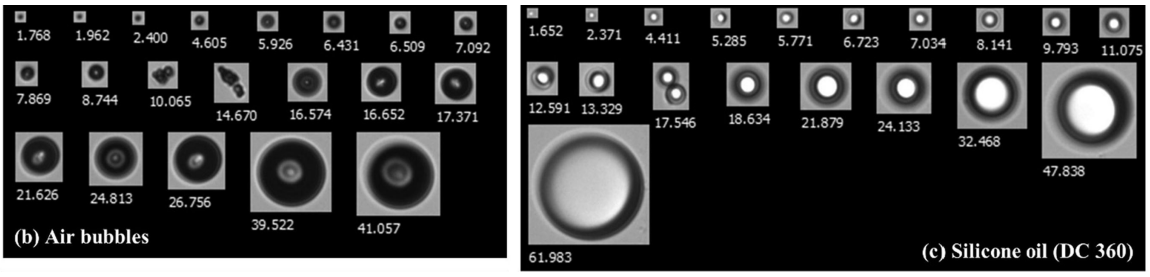

Figure 2.15: The morphology of artifically generated air bubbles (left) and silicone oil droplets (right) during FlowCAM. Both are spherical in nature. Note that the border of the air bubbles is thicker and that the silicone oil displays a central reflective spot (Kim et al., 2020)

.

FlowCAM identified the presence of subvisible particles in the protein solution, after having been subjected to mechanical stress and syringes without (Fig. 2.16) or with silicone lubrication (Fig. 2.17).

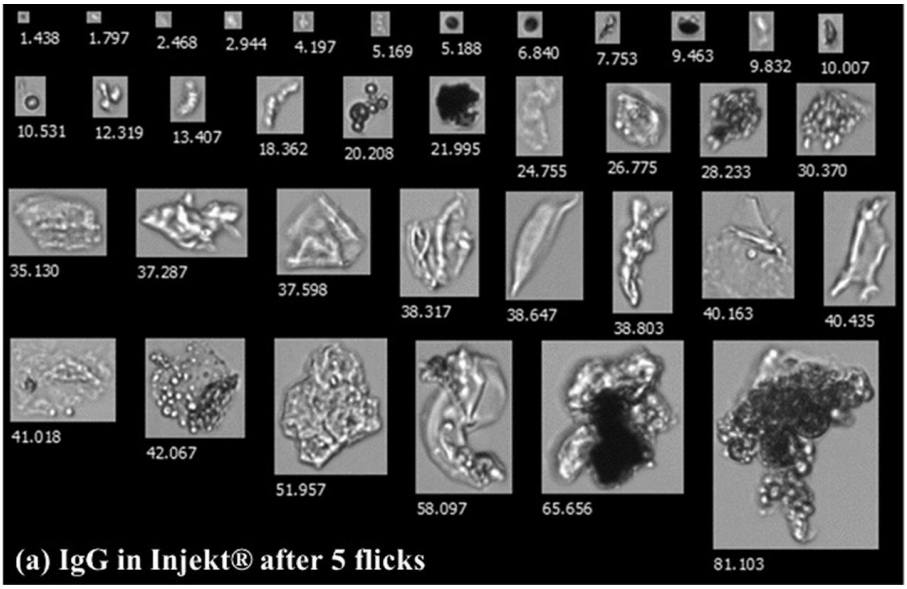

Figure 2.16: Characterization of a protein solution by FlowCAM. The solution had been subjected to mechanical stress (flicking 5 times) and a syringe without silicone lubrication. The sample contained amorphous stress-induced protein aggregates, which seemed larger and denser (appeared darker) than the particles which were found in the sample from the siliconized counterpart in Figure 2.17 below (Kim et al., 2020)

.

The proteinaceous particles in the solution from the silicone free syringe appeared denser. The authors suggested that this was because the protein aggregates self-associated in the absence of silicone (Kim et al., 2020).

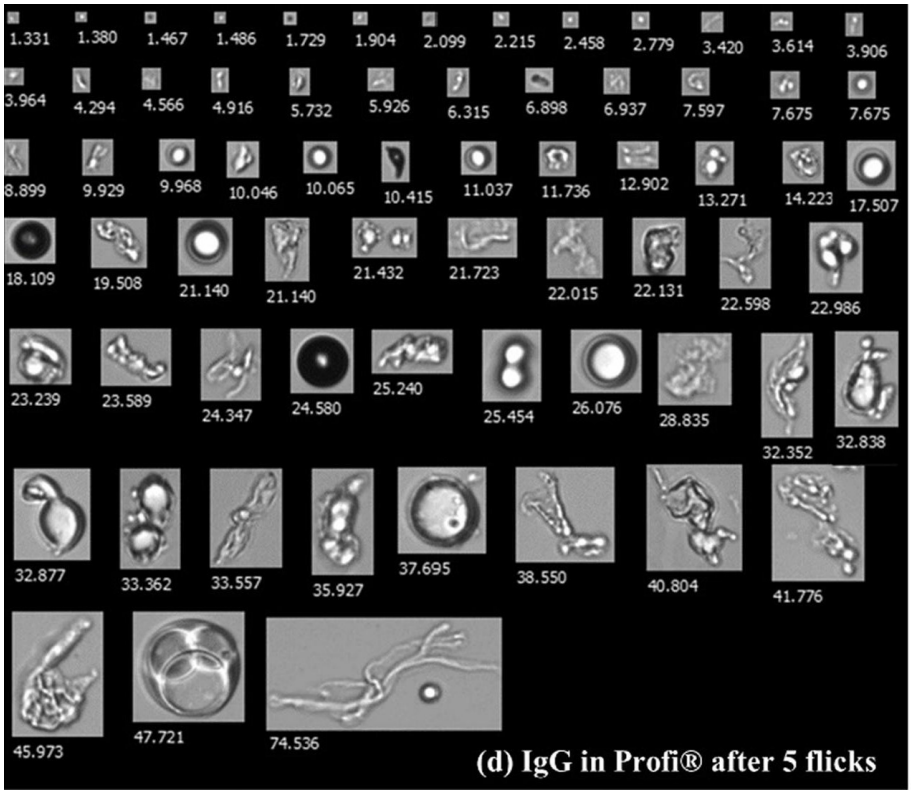

Figure 2.17: Characterization of a protein solution by FlowCAM. The solution had been subjected to mechanical stress (flicking 5 times) and a syringe with silicone lubrication. The sample contained particles such as air bubbles (spherical with thick border), silicone oil droplets (spherical with light lumen and thinner border) and fibril-like protein-adsorbed silicone oil particles of varying shapes and sizes (Kim et al., 2020)

.

It seems that it will be possible to distinguish the silicone oil droplets from other particles by their sphericity. Thus, filtering by this particle property could be used to sort them from other particles such as protein aggregates or chafed material from the device. A study by Jiao et al. (2020) found that AR ratio was effective, for the distinguishing of silicone oil from other particles in a protein solution without surfactant, when cutoff was set to 0.85. Some of the oil particles were found to be wrongly classified because they consisted of fused droplets, which had an more oblong shape. Studies which used multiparameter flow imaging models in order to more accurately identify the silicone particles have been performed. But the gained precision from using complex models have yet not proven to be beneficial (Jiao et al., 2020).

Kim et al. (2020) also examined the effect of dropping the filled syringes (Fig. 2.18). It

was concluded that the drop gave rise to aggregate formation, which might be due to the creation of short lived cavitation bubbles during the drop. The captured images from the syringes with silicone showed that the formed protein aggregates now seemed to be more like clumps, instead of the fibrillous structures seen above in Figure 2.17 (Kim et al., 2020).

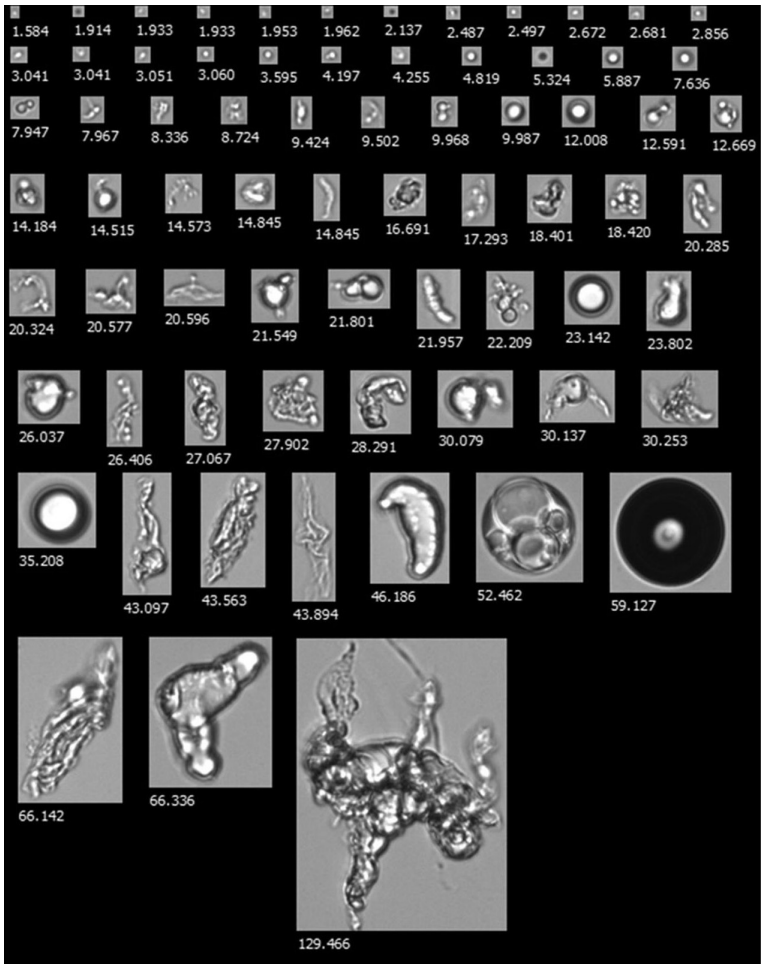

Figure 2.18: Characterization of a protein solution by FlowCAM. The solution had been subjected to mechanical stress (50 cm drop) and a syringe with silicone lubrication (IgG in Profi). The sample contained particles such as air bubbles (spherical with thick border), silicone oil droplets (spherical with light lumen and thinner border) and protein-adsorbed silicone oil particles (Kim et al., 2020)

.

Suggesting that there might be a link between the type of mechanical stress and the aggregate morphology (Kim et al., 2020).

2.3.4 SEC

Size exclusion chromatography build upon the principle that smaller particles will spend more time in the stationary phase than larger particles. Thus, the larger the particle (in relation to its hydrodynamic radius), the shorter will the retention time be. This is because the stationary phase has pores which the smaller particles will enter, while the larger particles will pass by the pores and follow the mobile phase out of the column. Size exclusion chromatography commonly used by the pharmaceutical industry for the investigation of aggregation in protein solutions. The method is regarded as mild and have a low chance of evoking conformational changes(Harris and Lucy, 2020; Fekete et al., 2014).

If an additional peak emerges for samples after mechanical stress, which elutes faster than the peak seen in the native solution. Then these peaks are expected to be associated with formed aggregates (Fig. 2.19)Zhou et al. (2016).

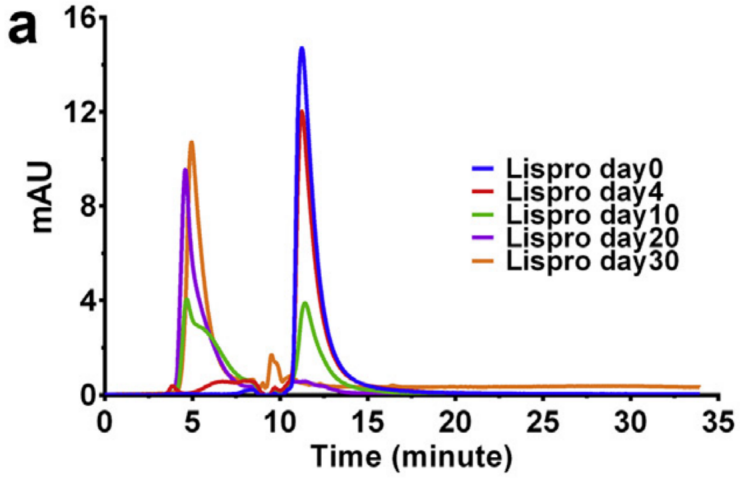

Figure 2.19: Evaluation of a protein solution with the insulin analog Lispro. The solution was incubated at 37°C for 30 days and analyzed by size size exclusion at different days. The retention time is presented on the x-axis and absorbance on y-axis. The incubation lead to a gradual aggregate formation, as peaks which eluated faster than the native peak emerged and grew larger as time passed. This was accompanied by a decrease of the native peak area, which might be due to consumption of the native protein to form aggregate Zhou et al. (2016)

.

Peak area can also be used, a decrease in native form peak area is a sign that this form has been lost, for example to create aggregates or by association to interfaces such as silicone oil droplets (Harris and Lucy, 2020; Fekete et al., 2014).

The study by Zhou et al. (2016) will be used as inspiration for the settings and material used when performing SEC analysis. The degree of aggregation will be evaluated by compar-

ing the peak areas of the mechanically stressed samples against the peak area of the native solution.

Chapter 3

Methodology

3.1 Material

3.1.1 Chemicals

Following chemicals were used during experimentation (Table 3.1).

Table 3.1: Utilized chemicals.

Product	Supplier	CAS nr.
Insulin analog	Sanofi	207748-29-6
Liquinox®	Alconox Inc.	25155- 30-0
Trizma® base	Sigma-Aldrich	77-86-1
Hydrochloric acid	VWR	7647-01-0
Sodium dihydrogen Phosphate dihydrate	Merck	13472-35-0
di-Sodium dihydrogen Phosphate dihydrate	Merck	10028-24-7
Sodium chloride	VWR	7647-14-5
Sodium azide	VWR	26628-22-8

3.1.2 Medical devices

Following syringes were used during experimentation (Table 3.2).

Table 3.2: Utilized syringes.

Product name	Supplier	Size	Silicone	Experiment
HENKE-JECT®	HSW	5 mL	Yes	Syringe setup optimization
HENKE-JECT®	HSW	3 mL	Yes	Syringe setup optimization
Terumo®	Terumo	1 mL	Yes	Syringe setup optimization
Inject® Solo	B. Braun	5 mL	No	Final output
Omnifix®	B. Braun	5 mL	Yes	Final output

Following needles were used during experimentation (Table 3.3).

Table 3.3: Utilized needles.

Product name	Supplier	Gauge	Size (mm)	Experiment
Hypodermic needle HENKE-JECT®	HSW	30G	0.3x12	Syringe setup optimization and final output
Neolus®	Terumo	27G	0.4x20	Syringe setup optimization
Microlance® 2	BD	25G	0.5x16	Syringe setup optimization

The 5 mL syringes in the final investigation, originated from the same manufacturer. They had identical internal geometry and both had a barrel made from polypropylene. The material of the plunger differed. The silicone free syringe had a plunger of polypropylene and the siliconized syringe had a plunger of polyethylene (vwr, n.d.*b*,n).

3.1.3 Preparation of stock solutions

Preparation of 0.01 M HCl solution, 50 mM TRIS buffer (pH 8.0) and 3.5 mg/mL insulin solution (pH 7.4), was done according to SOP (App. A and B). The insulin solution was formulated without excipients, but had the same concentration and pH as the product on market.

3.2 Analytical method

3.2.1 NanoDrop

Instrument

Thermo Fisher Scientific NanoDrop ND-1000 Spectrophotometer, USA.

Method

The machine was reset with Milli-Q water, followed by blanking with a buffer containing 50 mM TRIS buffer and 0.01 M HCl solution in a 5:4 ratio. The absorbance was measured at 280 nm and concentration was determined by Beers Law. The extinction coefficient (0.9521 $cm^{-1}/mL/mg^{-1}$) was assumed to be the same for the oligomeric and monomeric state of the native protein. Five absorbance measurements were performed and the average concentration was calculated. The insulin solution was diluted with buffer until concentration reached approximately 3.5 mg/mL. The risk of residual protein deposit on the lens of the NanoDrop was checked for by measuring buffer at the end of measurements.

3.2.2 Texture analyser

Instrument

Stable Micro Systems TA-XT2i Texture analyser with 5 kg loading cell, Great Britain.

Method

The force (N) was recorded by attaching a setup which fixated the device in a texture analyser and allowed the arm of the analyser to operate the plunger. The total extrusion force (F_{total}) was characterized in this Master thesis as the average total gliding force during expulsion of fluid (Fig. 2.4) and the friction force of the system was defined by the average gliding force. The friction force was measured on wetted syringes without needle. The degree of mechanical stress on the fluid was evaluated according the amount of shear stress to which it had theoretically been subjected to. As the protein concentration was low (3.5 mg/mL), the viscosity of the insulin solution was assumed equal to water and to behave as a Newtonian fluid.

All samples were recorded at room temperature (20 °C). The table of the texture analyser gradually became warmer during operation and styrofoam was placed between sample and

table to prevent heat transfer. Also, the time the sample spent on the table was minimized as much as possible. The texture analyser had a max movement speed limit of 40 mm/s.

A crude setup involving tape was used for investigation of the syringe setup optimization, where the solution consisted of water. Total force during expulsion was measured on manually prefilled syringes. Total force during aspiration (filling of the syringe) was measured by letting the arm of the texture analyser operate a syringe with the needle immersed in a beaker with water.

The total extrusion force was examined for three sizes of siliconized syringes (1, 3 and 5 mL) and three needle gauges (25G, 27G and 30G) at different plunger speeds. Friction force during expulsion was measured in the range of 0.5 - 12 mm/s and total extrusion force in the range of 0.5 - 40 mm/s.

The average total gliding force during aspiration was investigated for the 5 mL syringe with the three above mentioned needle gauges. During filling, friction force was measured at plunger speeds between 0.5 - 10 mm/s and total force at 0.5 - 8 mm/s. The data from this preliminary investigation was then evaluated against theoretically calculated hydrodynamic force (Eq. 2.4 and shear stress (Eq. 2.2)

The second design, with wood and welded part (Fig. 4.3a), was used for the gathering of output from buffer with and without silicone.

Final output was gathered with the 3D printed syringe setup (Fig. 4.3b).

The hydrodynamic force and the shear stress was then estimated according to Equation 2.3 respectively 2.2.

3.2.3 DLS

Instrument

Malvern panalytical Zetasizer Nano ZS, Great Britain.

Method

No filtration was performed prior to DLS. Dilution series with untreated insulin solution, encompassing 0.25 - 3.5 mg/mL, was created to find suitable concentration for DLS. Samples were diluted with a buffer containing 50 mM TRIS buffer and 0.01 M HCl solution in a 5:4 ratio. Suitable concentration was found to be to 3.5 mg/mL (view result, Table 4.1). The final investigation was performed as duplicates, with three measurement runs per each. Samples were kept cooled in refrigerator and analyzed within 24 hours after treatment in syringe setup. To ensure samples were representative, the test tube was turned upside down five times before taking out samples. They were then compared to untreated native insulin solution.

The duplicates consisting of 1 mL sample each, were put into polystyrene semi micro cuvettes and analyzed by backscatter (173°) at 25°C. Viscosity of solution was assumed same as 25°C water.

3.2.4 SEC

Instrument

Thermo Fisher Scientific UltiMate 3000 HPLC, USA. Equipped with Tosoh Bioscience G300SWX and TSK gel SWXL guard column, Japan,

Method

The test tube was tilted upside down five times before sample was taken out. The sample was diluted to 1 mg/mL in a 1.5 mL microcentrifuge tube and frozen. Sample was diluted with a buffer containing 50 mM TRIS buffer and 0.01 M HCl solution in a 5:4 ratio. It was then thawed and centrifuged for 10 min at 13400 rpm and visually checked for presence of pellet in bottom. Thereafter, 200 μL supernatant was transferred to a glass vial, crimped closed, installed in sample tray and kept at 6°C. The mobile phase consisted of 100 mM Sodium Phosphate buffer at pH 7 with 100 mM sodium chloride and 0,02 % Sodium azide. The flow rate was set to 1 mL/min, sample time 17 min and injection volume was 10 μL. Three replicates were investigated for each sample. During quantification, the total peak area of the native samples were considered as 100 % and the peak area of the other samples were evaluated in regards to them.

3.2.5 FlowCAM

Instrument

YOKOGAWA FlowCAM VS-IV-C B3, Japan.

Method

Measurements were performed with a 10x objective and a 100 µm by 2 mm Flow Cell. Autofocus was set with 15 µm beads, followed by manual focus fine tuning. Distance to nearest neighbor was set to 0 µm, minimum diameter 2 µm (ESD) and flow rate was 0.150 mL/min. No filtration was performed prior to FlowCAM. To ensure the sample was representative and uniform, the test tube was turned upside down five times before loading the sample into

funnel. Capturing of buffer which had undergone same treatment combination (the combination of three different speeds and two types of syringes) as the insulin solution would later be exposed to, was performed to help identify which parameters that were helpful when characterizing silicone oil particles. The buffer consisted of 50 mM TRIS buffer and 0.01 M HCl solution in a 5:4 ratio. Final investigation captured undiluted triplicates consisting of 0.5 mL for each sample of insulin solution. Between each sample, the system was flushed with 10 mL buffer, corresponding to ten times the system volume. When finished, Flow Cell was cleaned with 2 % Liquinox at 5 mL/min, followed by flushing with Milli-Q water. This ensured removal of silicone oil and protein particle residues.

Chapter 4

Method development

4.1 DLS optimization

A dilution series was created and analyzed in order to explore suitable concentrations for future investigations 4.1.

Table 4.1: DLS result from insulin dilution series of native insulin (3.5 mg/mL). The following parameters are listed; concentration (Conc.), size (Z-average), count rate, y-intercept of the correlogram (y-intercept), the time it took to perform one measurement (time) and quality report from software (Quality). The - denotes missing data.

Conc. (mg/mL)	Z-average (nm)	Count rate (kcps)	y-intercept	time (s)	Quality
0.25	4.354-13.33	39.2	0.433-0.460	360	All error
0.5	4.521-4.625	61.3	0.635-0.638	267	All error
1.0	4.490-5.102	92.5	0.737-0.753	206	2/3 met
1.5	-	142	-	180	All met
2.0	4.993-5.144	221	0.842-0.846	145	All met
2.5	-	215	-	-	All met
3.0	-	377,2	0.871	-	2/3 met
3.5	5.077-5.135	434.4	0.869-0.870	124	All met

The data in table 4.1 supports that 3.5 mg/mL was the most suitable concentration to investigate by DLS. Concentrations of 0.25 - 1.0 mg/mL were unsuitable as they prompted criteria complaints from the software, stating that data quality was too poor for distributive and cumulative fitting. Quality criteria were met for all 1.5 mg/mL measurements, but was less suitable than the higher concentrations as it was associated with low count rates. The apparent size (Z-average) overlapped for 2 and 3.5 mg/mL, suggesting that concentrations within this range are part of the DLS region. Their y-intercepts were almost similar, above 0.8, which indicated very good signal-to-noise ratio. The decrease in count rate between the two roughly corresponded to the dilution factor, hence no further dilution of native sample (3.5 mg/mL) was needed. This choice also offered the advantage of keeping the analysing time as short as possible. The native insulin solution was found to be moderately polydisperse with PDI between 0.17 - 0.20.

4.2 Syringe setup optimization

Needle gauges were evaluated on the basis of theoretical calculations of the shear stress (τ_w).The theoretical shear stress was plotted as a function of needle gauge (Fig. 4.1).

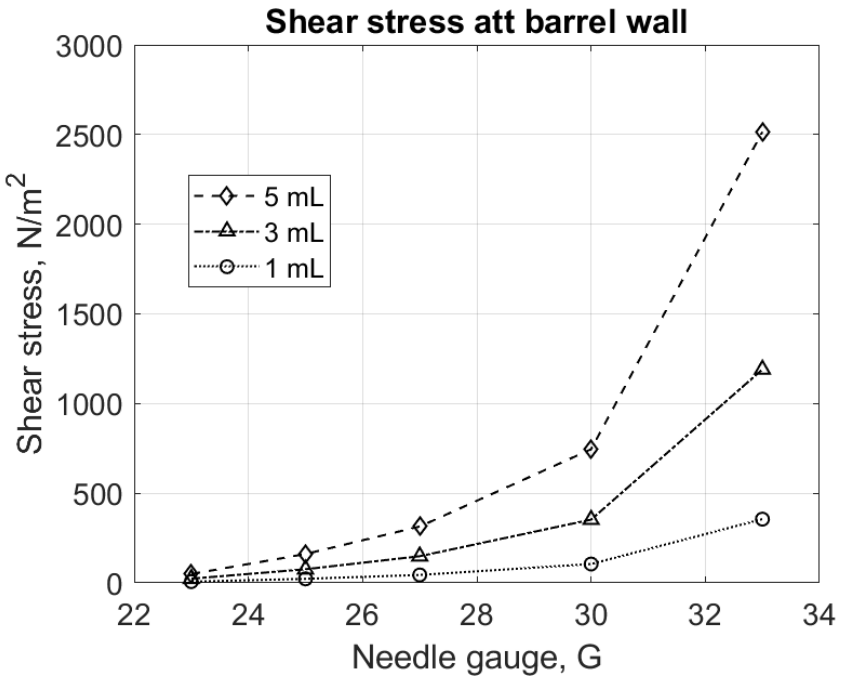

Figure 4.1: The dependency between syringe size, needle gauge and the theoretical shear stress. The plunger velocity was set as 2 mm/s. The inner diameter for each gauge corresponded to conventional sizes used in the industry.

This data was part of the decision-making process regarding which three needle sizes and syringes to investigate. The stress was calculated by combining Equation 2.2 with Equation 2.4. As expected, the highest mechanical stress was achieved when the largest syringe was combined with the thinnest needle gauge (Fig. 4.1). At the same time, thinner needle and larger syringe will lead to higher expulsion force. Thus, the question remained whether how thin the needle could be, before the force became so high that the texture analyser suffered from overload. To test this, a 5 mL syringe with 30G was filled with water and mounted in the crude setup. It showed that the texture analyser was overloaded at forces around around 70N and that the force was roughly 55 N at an expulsion speed of 2 mm/s. Thinner needles were thus deemed not of interest, and it was decided to investigate 30G, 27G and 25G. The texture analyser was used for preliminary investigation of 30G, 27G and 25G needles with 5, 3 and 1 mL syringes during expulsion and aspiration of 20°C water. It should be noted that these syringes and needles were not of the same as the ones used in the final setup (view. Tables 3.2 and 3.3), with the exception of the 30G needle. The friction forces of the wetted syringes during ejection of air without needles, were relatively small and negligible in comparison to the hydrodynamic forces at greater expulsion velocities. The friction was roughly 1.15 N for the two larger syringes and 0.5 N for the 1 mL syringe.

Findings during expulsion were plotted against theoretical values, represented in Figure 4.2.

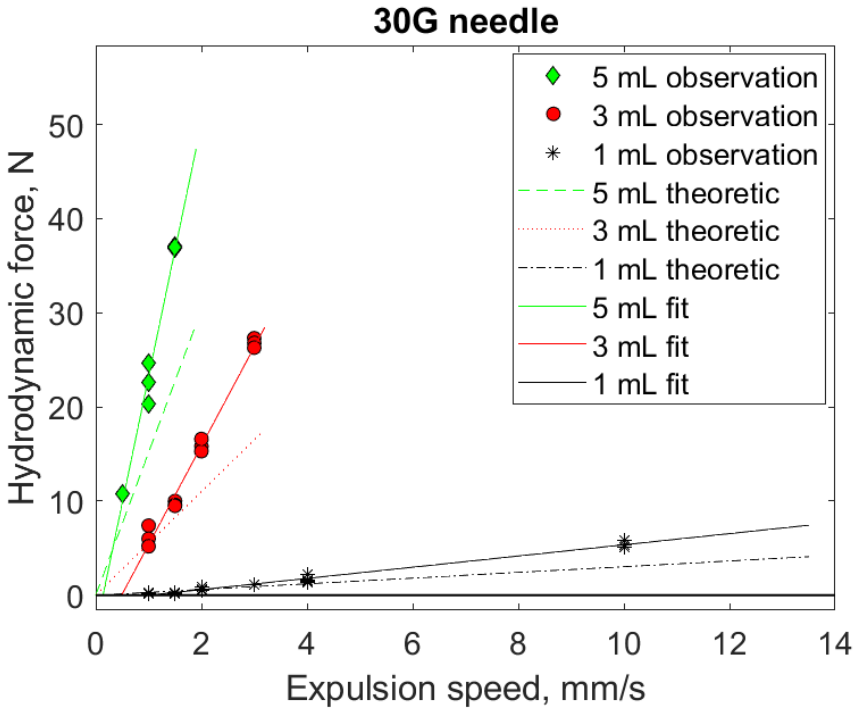

(a) 30G

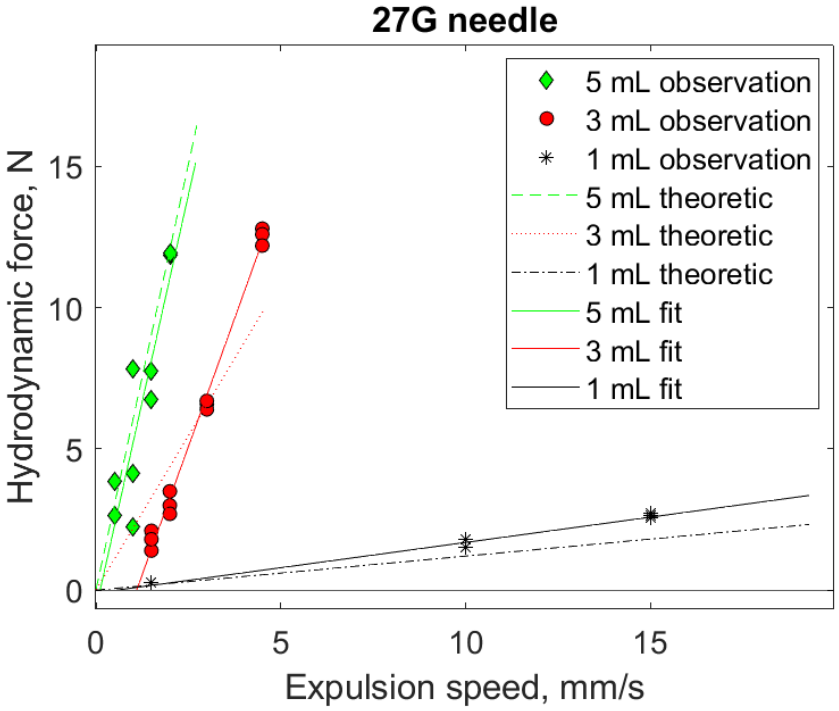

(b) 27G

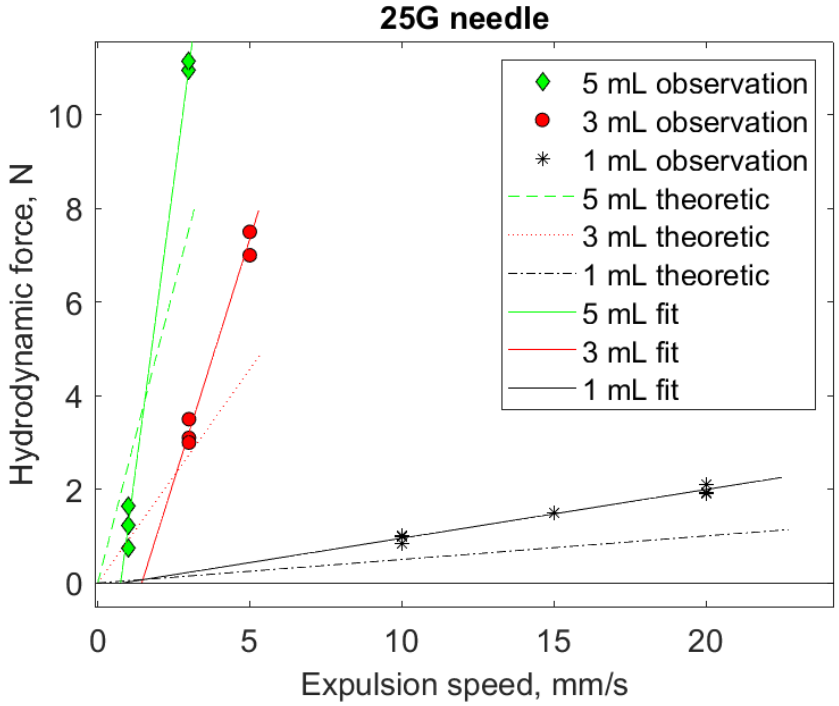

(c) 25G

Figure 4.2: Plunger velocity dependence of the hydrodynamic force during expulsion from three different needles (a, b and c) in combination with the three different syringe sizes. Only velocities associated with laminar flow (Re $\leq$ 2000) are presented in the graphs. Linear fitting of observed data is represented by solid lines. Dashed lines represent theoretic values originating from Equation 2.4.

The matlab code which were used to create the plots can be found in Appendix C.

According to theory (Eq. 2.2), a higher hydrodynamic force is associated with the exertion of higher mechanical stress (shear stress) on the expelled fluid. The goal of the final experimental setup was to be able to efficiently collect information from an as large as possible interval of shear stress during laminar flow, with the equipment at hand (texture analyser). While at the same time acquiring a large enough sample volume for further analysing by DLS, SEC and FlowCAM. This was best obtained by using the 5 mL syringe with 30G (Fig. 4.2a. The smaller syringes were determined unsuitable for the task as they required faster expulsion velocities and yielded lower sample volumes. The output from aspiration with 5 mL and the 30G syringe showed that an air pillar formed inside the syringe during the process even at the lowest investigated speed (0.5 mm/s). This along with the time limit for this project, led to the decision of running the aspiration at a constant speed of 0.1 mm/s during the final investigation.

The expulsion force of the 5 mL syringe with 30G will be greater than 40N and thus exceed the recommended force for manual injection. This was allowed to occur in the final setup, as it was desirable to be able to describe fluid which had suffered greater mechanical stress.

It was also of interest to investigate if the output supported that transition flow could be reached in a clinical setting. The lower limit for transitional flow was assumed as $Re \leq 2000$ for the needle. An rate of 0.3 mL/s during manual subcutaneous injection corresponds on average to a plunger speed of 2.4 mm/s for a 5 mL syringe, 4.1 mm/s for a 3 mL syringe and 17.3 mm/s for a 1 mL syringe. For intramuskular injections, the rate (0.1 mL/s) corresponded to a third of the plunger speeds given above for respective syringe size.

The output showed that there were combinations were transition flow could arise during the manual use of siliconized syringes. But only during the subcutaneous injections, when 40 N and 0.3 mL/s were set as clinically relevant limits for the maximal acceptable injection force and rate. Transitional flow could occur for the 3 and 1 mL syringe with 30G at injection forces of 30 - 40 N respectively 10 - 15 N. The other combinations were only clinically relevant at laminar flow.

Due to time restriction, paired with the gained knowledge from the preliminary study and risk of cell overload, it was decided to limit the investigation to:

- Explore one syringe size (5 mL) and two types of syringes (with or without silicone).
- One needle gauge (30G).
- A constant and low withdrawal speed of the plunger (0.1 mm/s) for all samples.
- Three different expulsion speeds within the laminar flow area (0.1, 0.9 and 1.7 mm/s).

- Three replicates for each combination of expulsion speed and syringe type.

Each run yielded 5 mL of sample, which was loaded into a plastic test tube. For comparison, the study included three replicates of insulin solution not subjected to mechanical treatment by syringe (native). The solution in test test tube was then subjected to investigation by DLS, SEC and FlowCAM. Due to error during investigation, one more replicate had to be manufactured of the 0.1 and the 0.9 mm/s with silicone. Thus, the presence of one more replicate for each of these combinations.

4.3 Design of syringe probe

A preliminary investigation of the analyser when operating 1, 3 and 5 mL syringes with 20°C water was done (Fig.4.2). During this trial, a crude setup which included electrical tape, sellotape and cable ties was used to operate the syringe. This was then further developed and resulted in the manufacture of a two part syringe holder (Fig. 4.3a).

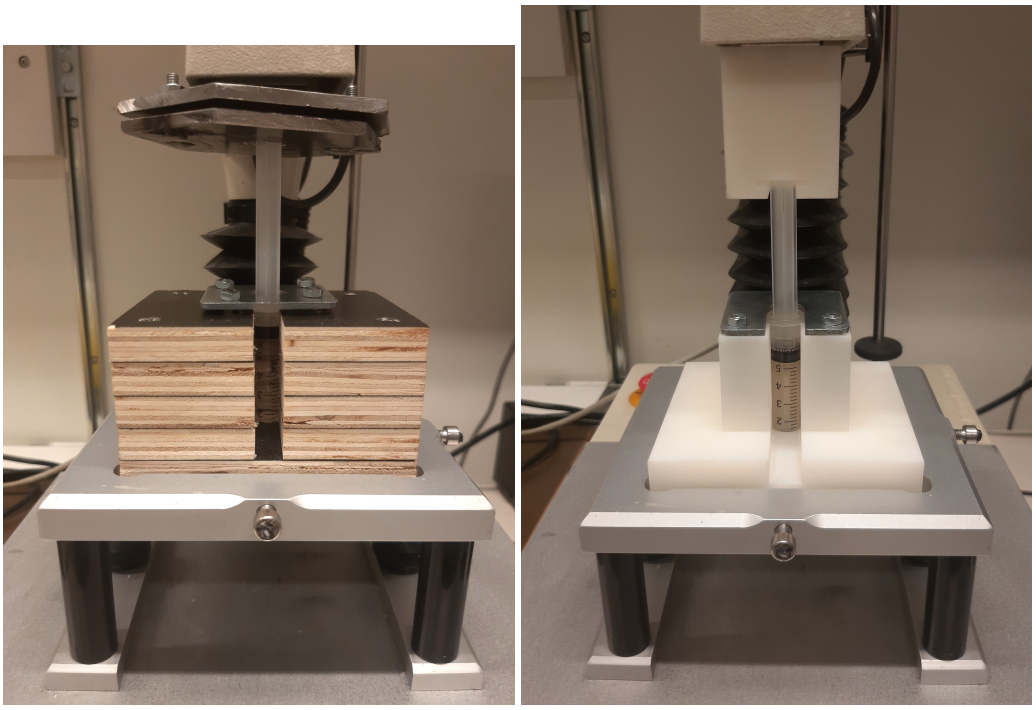

(a) **(b)**

Figure 4.3: Syringe setups for the filling and emptying of a 5 mL. The second design (a) consisted of an lower wooden part which held the barrel, locked into place by a square plate washer and an upper welded metal part which locked the plunger. Third and final 3D printed design (b).

This setup was unfortunately associated with askewness of the plunger during operation, resulting in abnormally high friction forces, which sometimes overloaded the loading cell. Subsequently, a third and final syringe holder which built upon the same principles as the former, was created by 3D printing (Fig. 4.3b). This design was responsible for the operation of the 5 mL syringes during gathering of the final output.

4.4 Selection of particle property

FlowCAM parameters for the categorizing of silicone oil from other aggregates, were investigated by comparing insulin solution in a non-siliconized to buffer in a siliconized syringe. Both had been exposed to an expulsion speed of 1.7 mm/s. Visual inspection of captured particles revealed that the buffer held mostly silicone oil particles, which could be identified by their smooth spherical appearance, with a dark border and they often contained a central reflective spot. The insulin solution on the other hand, primarily contained protein aggregates, which presented as translucent or dark opaque amorphous particles, often fibrous in nature with thinner and more irregular borders (Fig. 4.4).

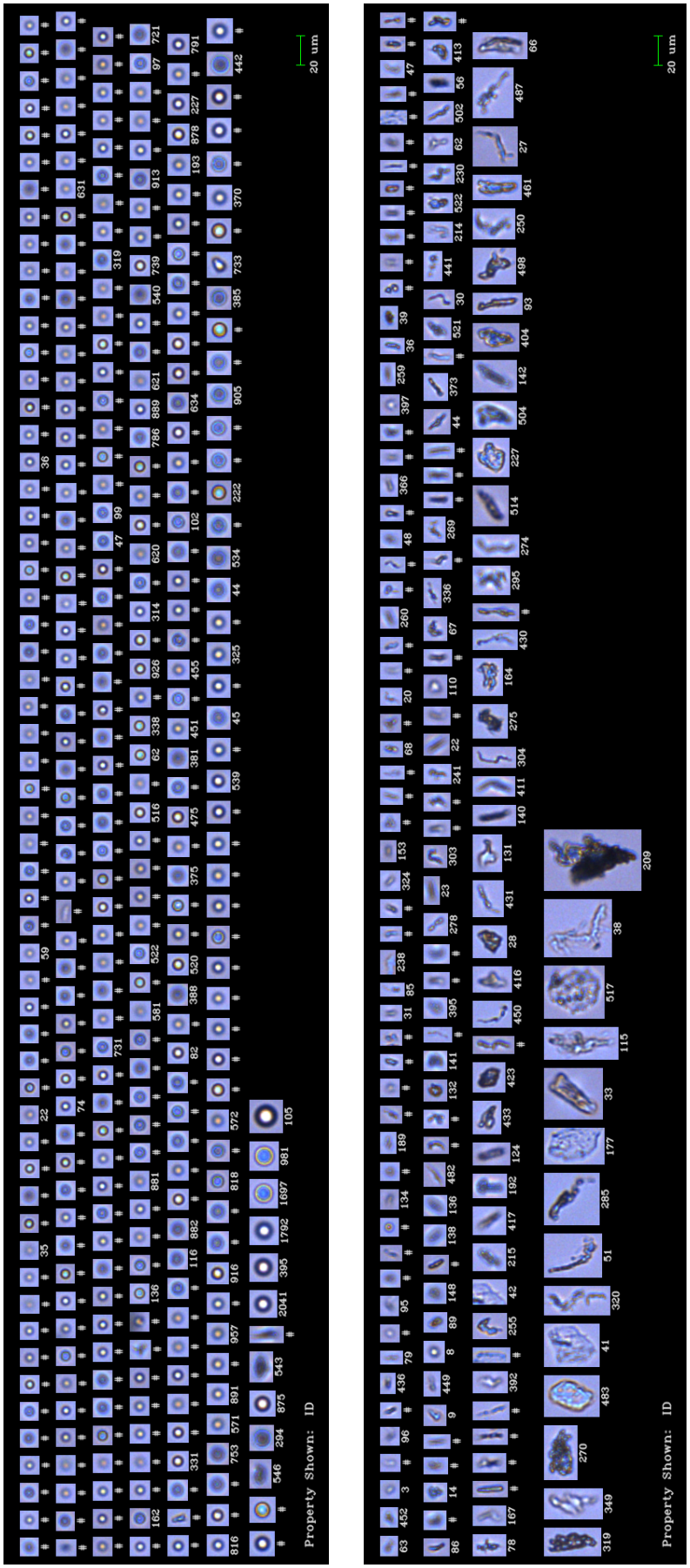

Figure 4.4: Captured particles (≥ 5 µm) from solution which had been exposed to expulsion speed of 1.7 mm/s. The buffer from siliconized syringe (top) chiefly contains spherical silicone oil particles while the insulin solution from syringe without silicone (bottom) mostly contains protein aggregates of fibrous or amorphous nature.

Two parameters for particles ≥ 5 µm were identified to be of interest for the identification of silicone oil particles. (Fig. 4.5).

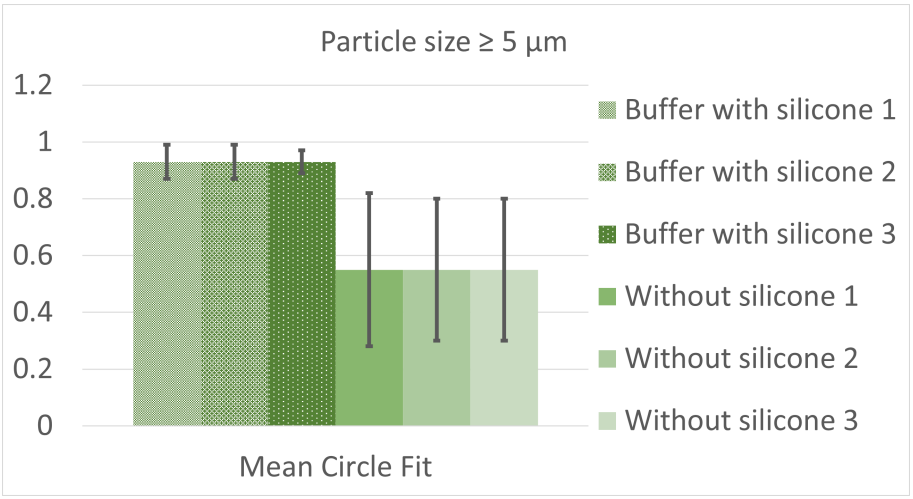

(a)

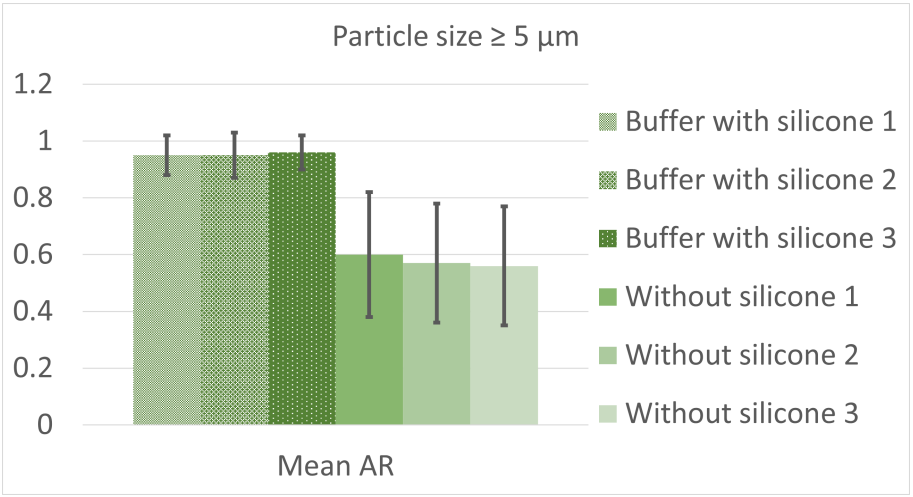

(b)

Figure 4.5: Mean circle fit (a) and mean aspect ratio (AR) (b) for particles ≥ 5 µm in buffer from siliconized syringe and insulin solution from silicon-free syringe. Three samples represent each (1, 2 and 3). Both of the solutions were exposed to expulsion speed 1.7 mm/s. Error bar denotes ± one standard deviation.

The two parameters were identified as the mean circle fit and the mean AR. The particles associated to the buffer with silicone were closer to 1 for both parameters, while the score was lower for the insulin solution without silicone (Fig. 4.5). This matched the the visual inspection of silicone oil particles as being more spherical in nature. The cutoff for silicone oil particle was determined to ≥ 0.85 for both parameters and particles in this range will be referred to as spherical. This was chosen on the basis of being in between ± one standard deviation for the buffer and protein solution. Visual inspection of the final output confirmed

that this setting primarily presented silicone oil particles, while particles below 0.85 mainly displayed captured protein aggregates. Thus, these setting were regarded as sufficient means to distinguish silicone oil particles from protein aggregates when particle size was ≥ 5 µm.

No parameter for the separation of silicone from protein aggregates could be found for particles ≤ 5 µm. Visual inspection of captured material also confirmed this. It revealed that particles of this size often appeared unfocused to a degree of where their origin could not be clearly determined.

Chapter 5

Results and discussion

Reader discretion is advised, this investigation was performed on insulin in buffer without the presence of stabilizing agents which are otherwise present. Thus, the result does not reflect the behavior of readily formulated insulin from the manufacturer and should not be used to promote such assumptions.

5.1 NanoDrop

Three batches of insulin solution were created and used for the investigation of the final result. The solutions were found to have the following concentrations (mg/mL) ; 3.46, 3.48 and 3.49.

5.2 Mechanical stress

The insulin solution was subjected to three different expulsion speeds and syringe with or without silicone. No clouding was observed afterwards in any of the treated samples during visual inspection. The average friction glide force of wet empty syringe (Fig. 5.1) and average total glide force with solution was recorded by the texture analyser.

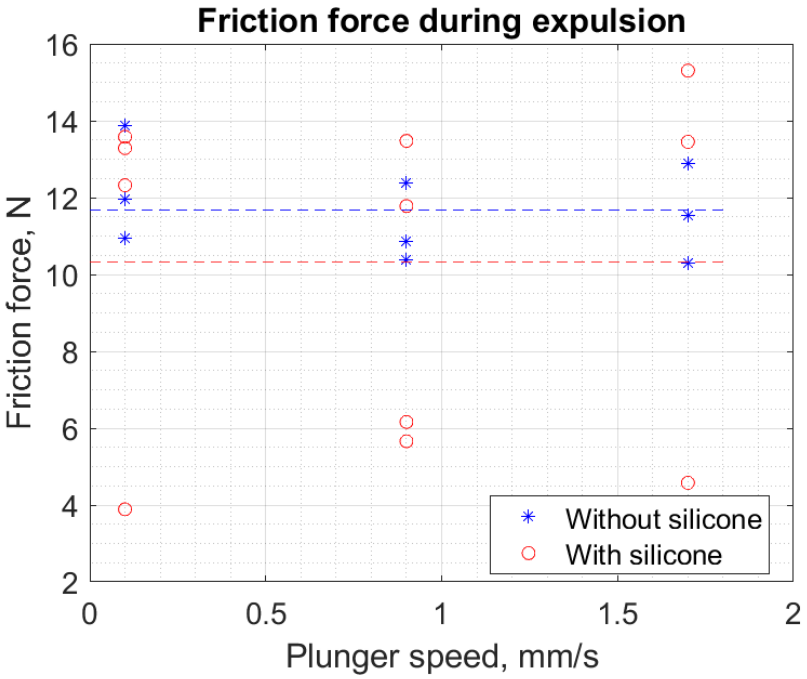

Figure 5.1: The average dynamic friction force at 0.1, 0.9 and 1.7 mm/s for the two types of syringes. The dashed lines in correspond to the average friction force for each syringe type across all three speeds.

Figure 5.1 shows that the frictional force was similar for the different combinations of syringe type and speeds. The output from the syringe without silicone seems to be more collected, indicating that the friction was more uniform for this syringe. Across expulsion speeds, the average frictional force was determined to 11±1 N and 10±4 N for the syringe without respectively with silicone.

The average hydrodynamic force was expressed as the difference between total glide force and friction glide force. Figure 5.2 shows that there was a positive correlation between hydrodynamic force and the expulsion speed, which is consistent with Equation 2.4. Linear fitting of data yielded $y = 26x - 6.0$ with a goodness of fit $R^2 = 0.98$ for the syringe without silicone. For the type with silicone, the trend line was $y = 24x + 1.6$ with $R^2 = 0.82$. Thus, the slope of the relationship was similar for both syringe types, but the output from the siliconized syringe look as though it might be slightly larger. The output from the non-siliconized syringe appears more tightly clustered and the lower goodness of fit for the siliconized syringe arises mainly due to the presence of an outlier (4 N at 0.9 mm/s). An explanation for this outlier could not be determined.

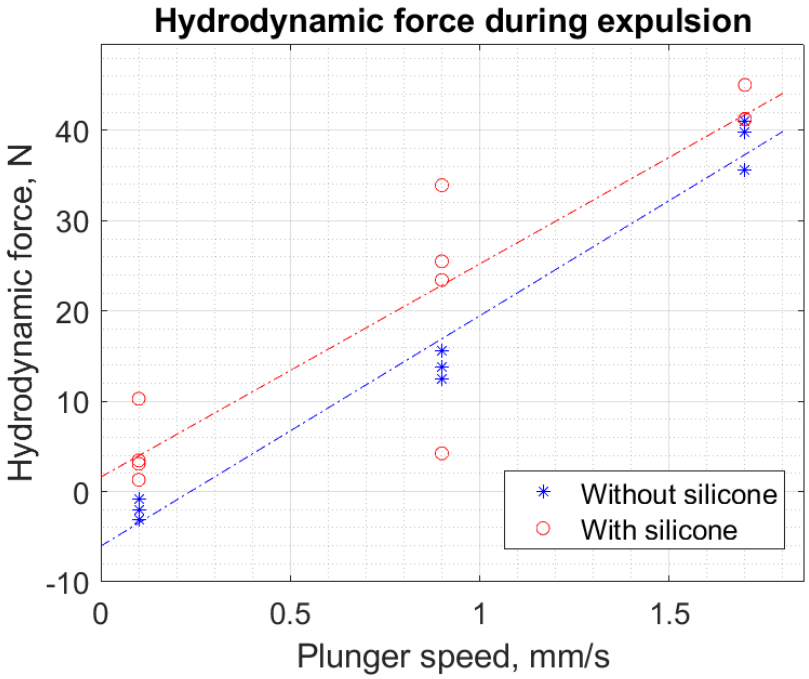

Figure 5.2: The average dynamic friction force at 0.1, 0.9 and 1.7 mm/s for the two types of syringes. The dashed lines in correspond to the average friction force for each syringe type across all three speeds.

.

For the silicone-free syringe at 0.1 mm/s, the friction force of the wet empty syringe was greater than the total force during expulsion of solution, resulting in negative hydrodynamic force in Figure 5.2. This might be explained by the texture analyser, which had a tendency to be inconsistent when measuring forces close to zero. It could also be explained by the gravitational pull of the fluid pillar inside the syringe. Where the gravitational force overshadows the smaller hydrodynamic force associated with emptying the syringe at the low speed of 0.1 mm/s.

The hydrodynamic force was used to theoretically calculate the shear stress on the solution at the barrel wall. The reasoning concerning the output from Figure 5.3 was consistent with the one made for Figure 5.2, The conversion from hydrodynamic force to shear stress at barrel wall essentially involves an multiplication of a constant (view Eq. 2.2). The linear relationship was $y = 643x - 152$ and $y = 596x + 40.7$ for the syringe with silicone respectively without silicone (Fig. 5.3).

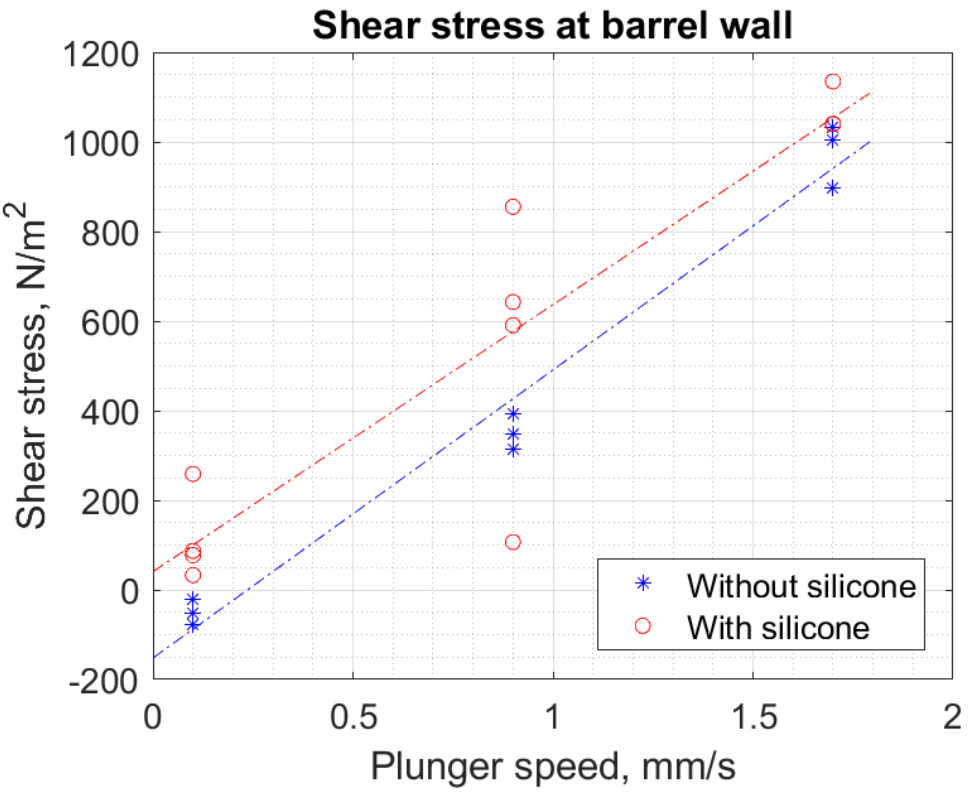

Figure 5.3: Theoretical shear stress at syringe barrel wall for the two types of syringes at three different expulsion speeds (0.1, 0.9 and 1.7 mm/s). The dashed lines represent the linear fittings to the output of each syringe type.

In total, the fluid had theoretically experienced a mechanical stress which ranged on average from 0 - 1000 N/m^2 in the laminar flow area. The theoretical average shear stress was -50.1, 351 and 978 N/m^2 for respective speed in the non-siliconized syringe and 114, 549 and 1072 N/m^2 for the siliconized.

All plotting in this section were made in Matlab, the code can be viewed in Appendix D.

5.3 DLS

Figure 5.4 displays the whole intensity size distribution obtained from the DLS of native solution and the different combinations of syringe type and expulsion speeds.

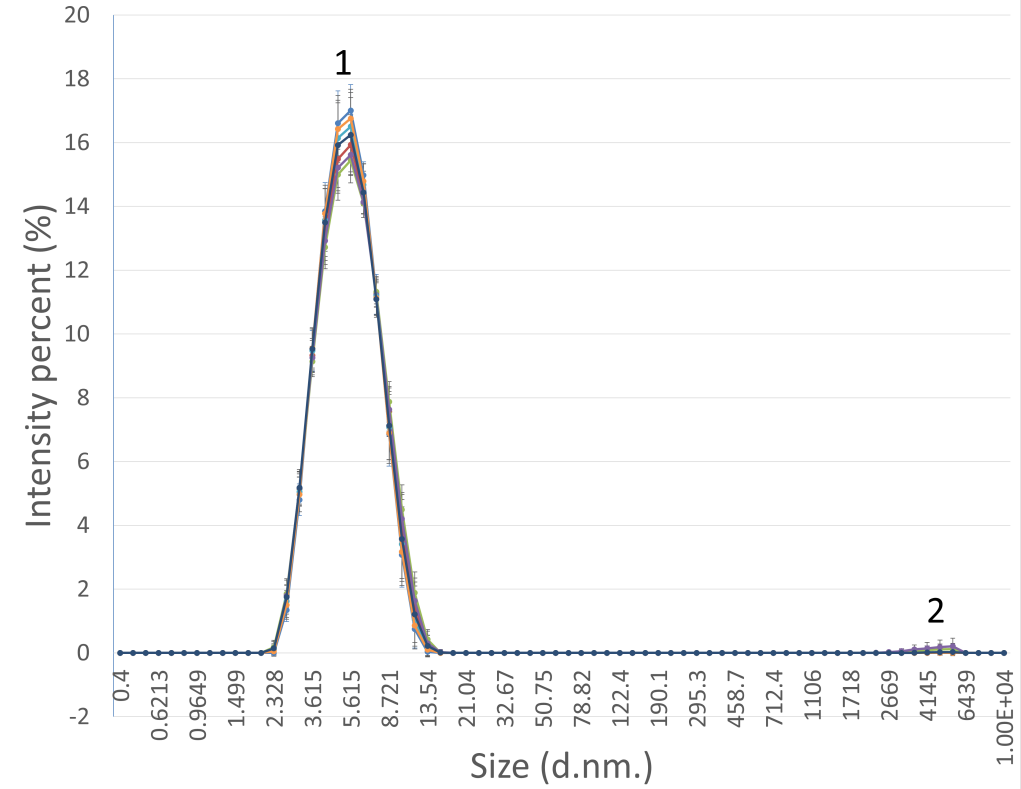

Figure 5.4: Complete intensity size distribution of native insulin and the three different expulsion speeds (0.1, 0.9 and 1.7 mm/s) with siliconized or non-siliconized syringe. Two peaks were identified, one large at 5.6 nm (1) and one small at approximately 5 µm. Error bar denotes ± one standard deviation.

Native - blue

With silicone 0.1 - red	Without silicone 0.1 - turquoise
With silicone 0.9 - green	Without silicone 0.9 - orange
With silicone 1.7 - purple	Without silicone 1.7 - dark blue

.

The intensity distribution(Fig. 5.4), contained a major peak at 5.6 nm (Fig. 5.5) for all combinations. This shows that the protein in the solution was mainly present in its hexamer form. No difference in the appearance of this peak could be detected between any of the combinations. There was no significant loss of peak height or shift of peak location. One standard deviation encompassed all. This points toward that there was no discernible reduction of hexamer in order to form larger aggregates.

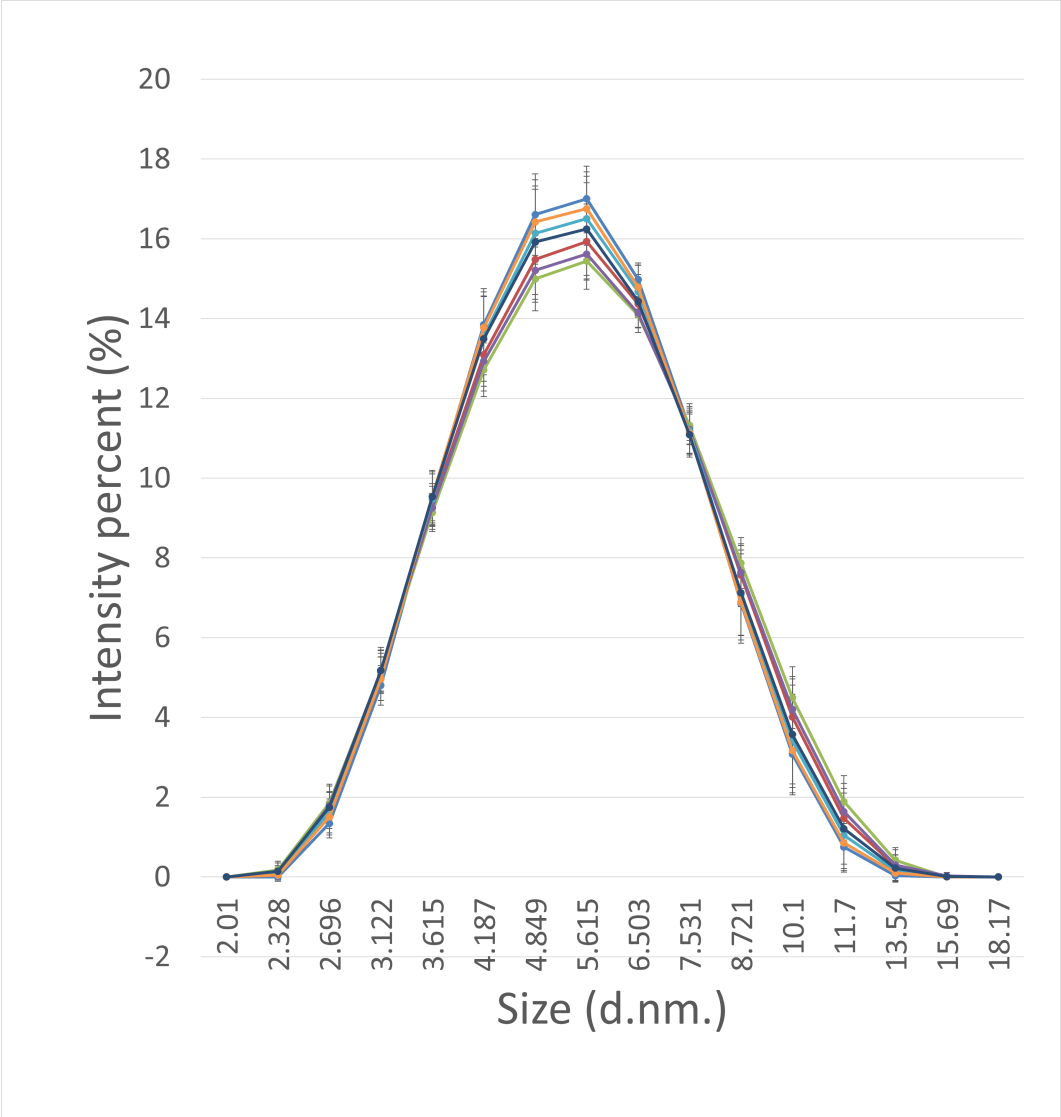

Figure 5.5: Close up of peak 1 in Figure 5.4. Intensity size distribution of native insulin and the three different expulsion speeds (0.1, 0.9 and 1.7 mm/s) with siliconized or non-siliconized syringe. Error bar denotes ± one standard deviation.

Native - blue

With silicone 0.1 - red	Without silicone 0.1 - turquoise
With silicone 0.9 - green	Without silicone 0.9 - orange
With silicone 1.7 - purple	Without silicone 1.7 - dark blue

.

A small peak (Fig. 5.6), emerged at approximately 5 µm during 1.7 mm/s for both syringe types and at 0.9 mm/s for siliconized syringes.

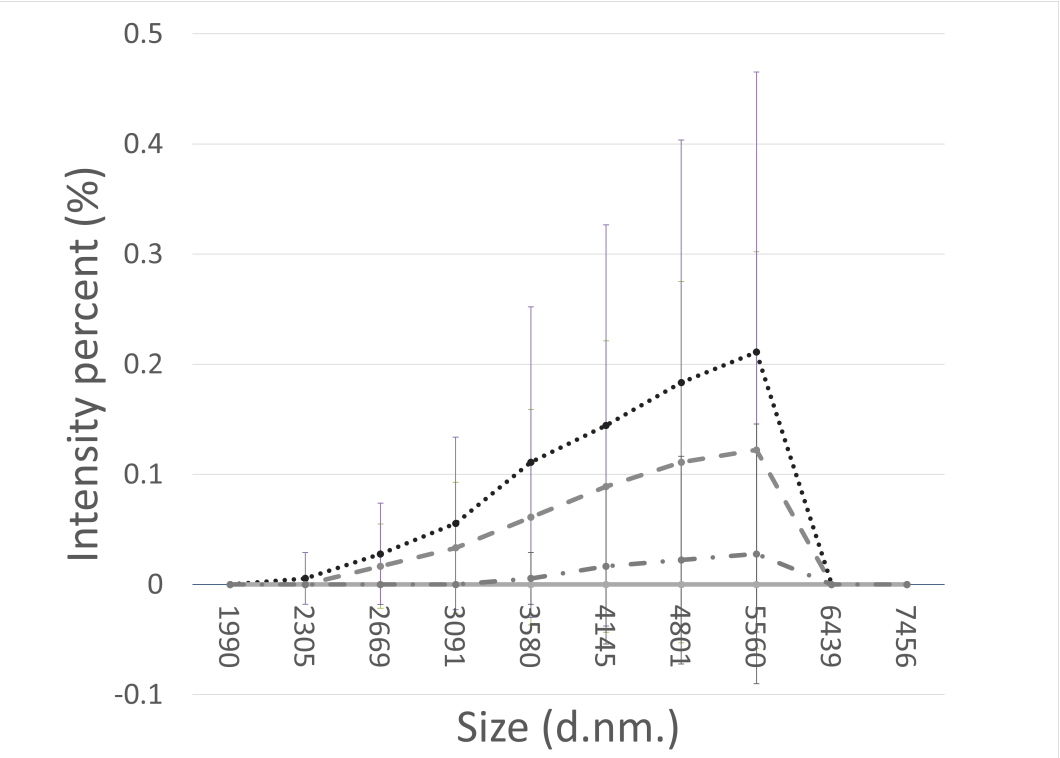

Figure 5.6: Close up of peak 2 in Figure 5.4. Intensity size distribution of native insulin and the three different expulsion speeds (0.1, 0.9 and 1.7 mm/s) with siliconized or non-siliconized syringe. Dotted line represents with silicone 1.7 mm/s, dashed line represents with silicone 0.9 mm/s and dash-dotted line represents without silicone 1.7 mm/s. The other combinations displayed no peak. Error bar denotes ± one standard deviation.

But, the emergence of the large aggregate could not be proven as its presence was inconsistent across outputs. This was reflected by the large standard deviation of peak nr. 2, which can be seen in Figure 5.6.

No notable difference was observed between the native solution and the other combinations regarding Z-average and PDI (Fig. 5.7).

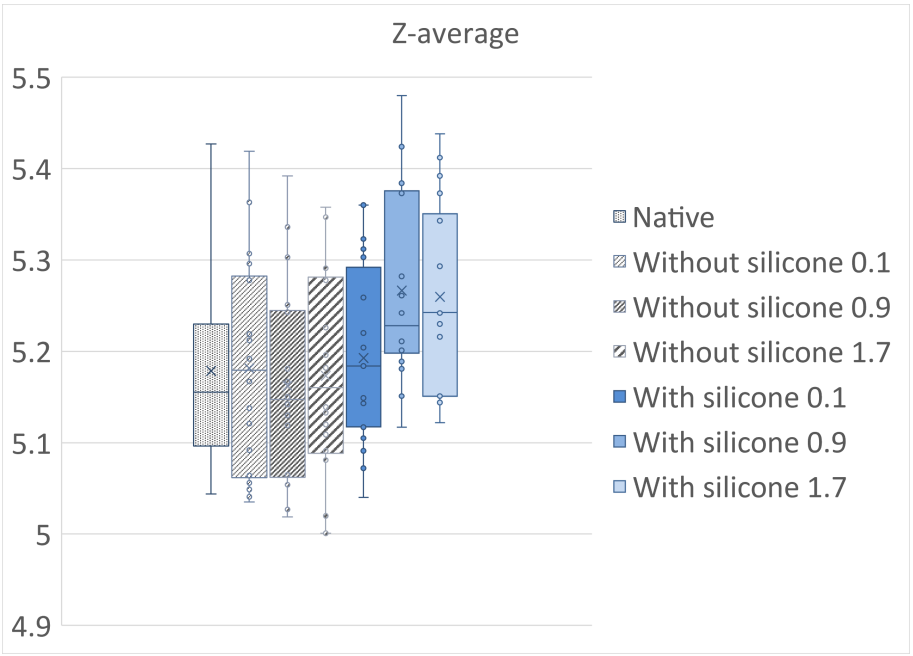

(a)

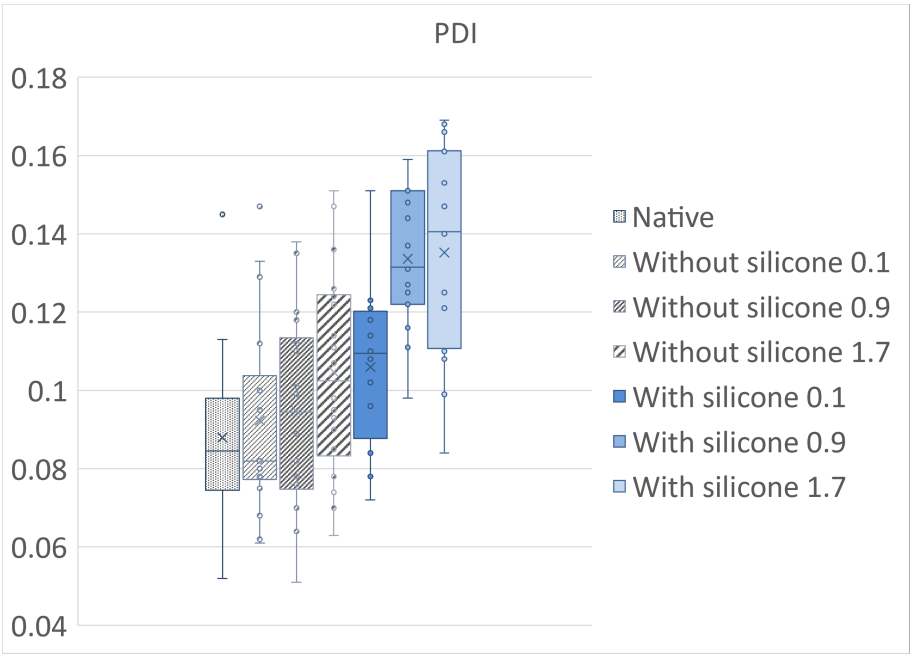

(b)

Figure 5.7: Box and whisker plot of the Z-average (a) and PDI (b) of native insulin and the three different expulsion speeds (0.1, 0.9 and 1.7 mm/s) with siliconized or non-siliconized syringe.

In general, Z-average was approximately 5.2 nm. The PDI ranged from 0.051-0.169, with an average across all samples of 0.108. The output values implied that the native solution was

monodisperse and remained relatively monodisperse after having been exposed to mechanical stress.

5.4 FlowCAM

Investigation by FlowCAM revealed the following particle size distributions (Fig. 5.8).

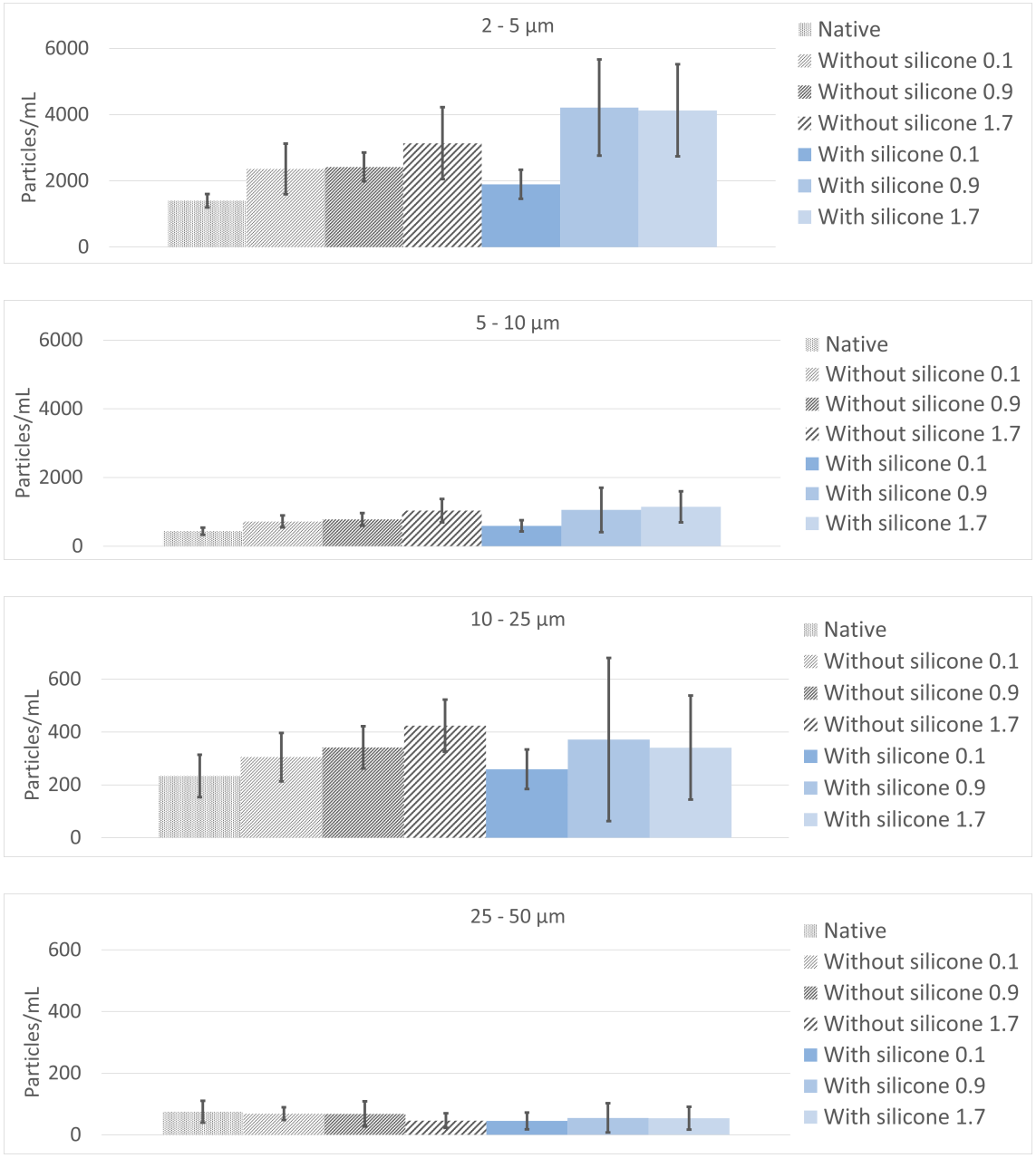

Figure 5.8: Particle size distribution in the native insulin and the three different expulsion speeds (0.1, 0.9 and 1.7 mm/s) with siliconized or non-siliconized syringe. Note that the y-axis for 10 - 25 µm and 25 - 50 µm are tenfold smaller than for the other two. Error bar denotes ± one standard deviation.

In general, FlowCAM reveals that the majority of the particles were small and belonging

to the 2-5 µm fraction (Fig. 5.8). Unfortunately, this also represented the fraction where the captured images often appeared unfocused and could not be categorized. The particle concentration gradually decreased when particle size increased, and the 25-50 µm particles represented the smallest fraction. For particles in the range of 2-10 µm, there might be a trend of increased particle count at the highest expulsion speed.

The proportion of particles (≥ 5 µm) with circle fit or AR 0.85 - 1 for the native sample and the different combinations are shown in Figure 5.9.

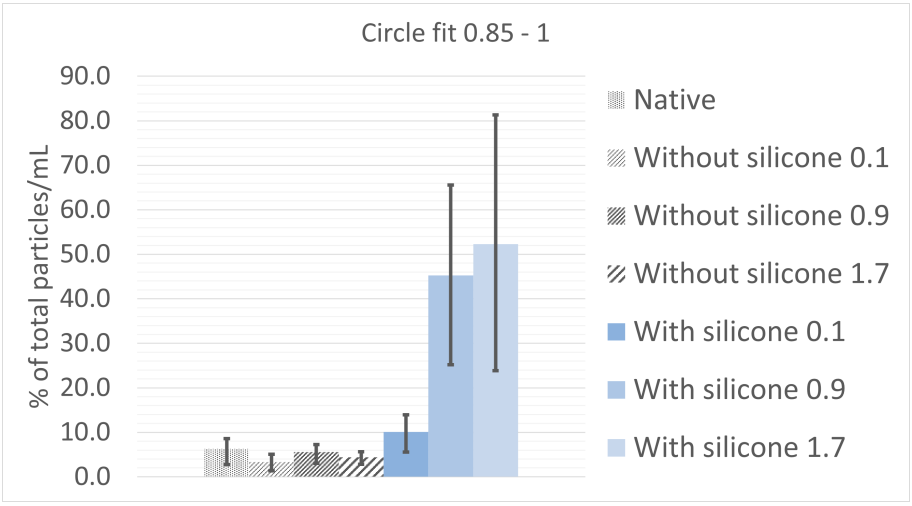

(a)

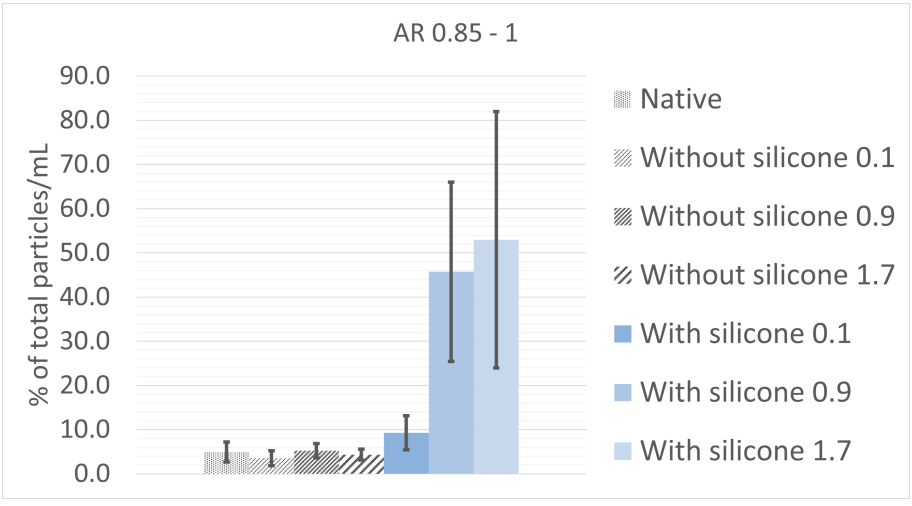

(b)

Figure 5.9: The proportion of particles of size ≥ 5 µm, with circle fit 0.85 - 1 (a) or aspect ratio (AR) 0.85 - 1 (b). Proportion output for native insulin and the three different expulsion speeds (0.1, 0.9 and 1.7 mm/s) with siliconized or non-siliconized syringe. Error bar denotes ± one standard deviation.

Circle fit and AR yielded similar proportions (Fig. 5.9). No difference in the proportions

of silicone oil particles could be determined between native solution and the silicon-free syringe. The same was true for the siliconized syringe at the lowest speed. Higher expulsion speeds in the siliconized syringe, led to a greater proportion of silicone particles and they made up roughly 50 % of the particles. This suggested that the increase in speed lead to more silicone being transferred from syringe to solution.

The particle morphology of the insulin solutions from siliconized and non-siliconized syringe at the highest expulsion speed (1.7 mm/s), can be viewed in Figure 5.10 on the next page. The siliconized syringe led to the introduction of silicone oil droplets. Note that occasional silicone oil droplets could be observed in the samples from the non-siliconized syringe. As mentioned before, the manufacturer commonly coats the needle silicone and this practice probably explains their presence. No clear difference in the protein aggregate morphology could be observed between the two different syringe types and there seemed to be a trend to form rod-shaped aggregates. This trend further suggests that it was appropriate to categorize by sphericity

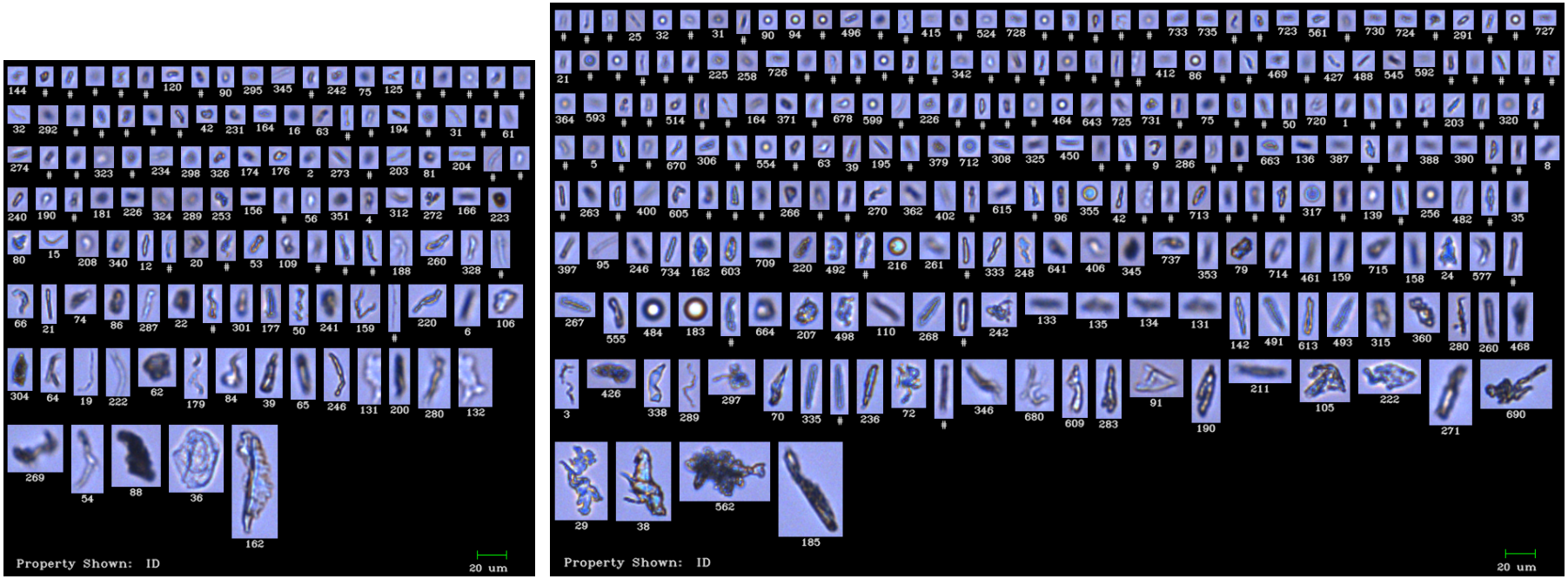

Figure 5.10: Captured particles from solution exposed to expulsion speed of 1.7 mm/s. The left image represents particles from non-siliconized syringe while particles from siliconized syringe are represented the image to the right. The non-siliconized syringe displays protein aggregates of varying shape along with occasional silicone oil droplet. The sample from from siliconized syringe displays spherical silicone oil droplets, protein aggregates and protein-adsorbed silicone oil particles.

The proportion of spherical (mainly silicone oil particles) and non-spherical particles (mainly protein aggregates) in native insulin and in the different combinations was compared. The circle fit and the AR yielded similar counts and seemed to preform equally well. Thus, only the output by circle fit will be presented (Fig. 5.11).

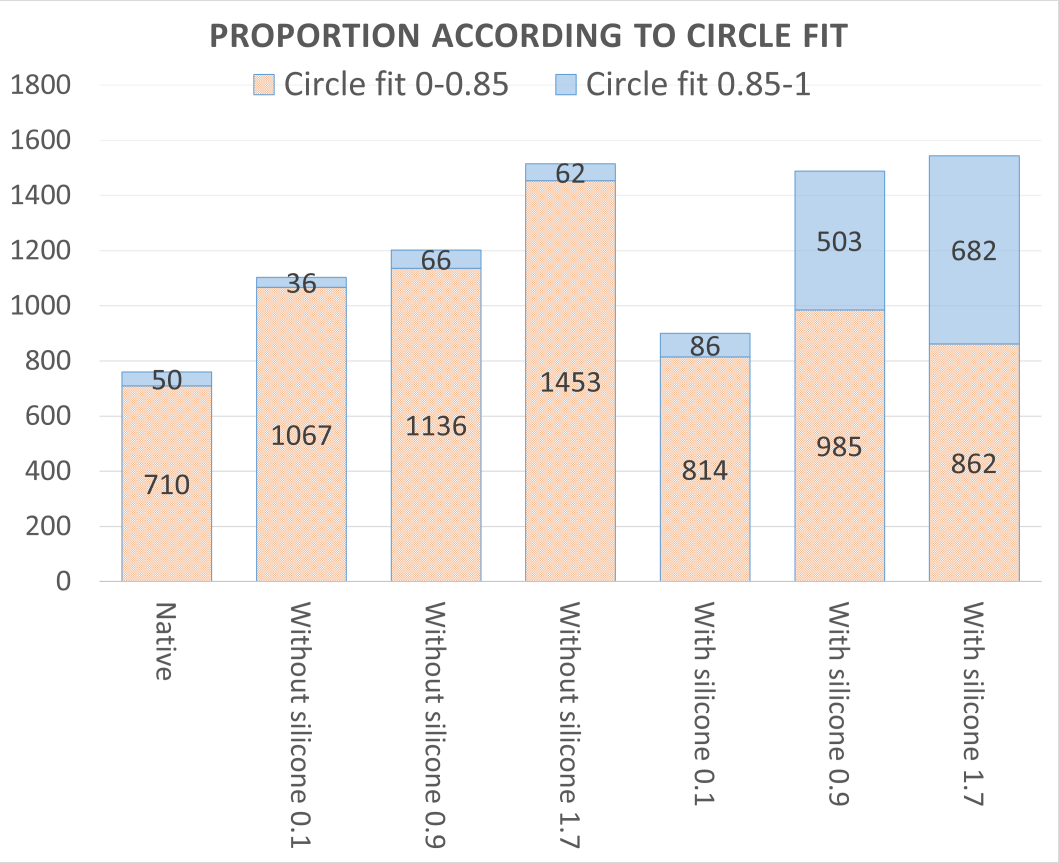

Figure 5.11: The particle count of spherical (blue) and non-spherical particles (patterned beige) (size ≥ 5 µm) according to mean circle Fit. Native insulin and the three different expulsion speeds (0.1, 0.9 and 1.7 mm/s) with siliconized and non-siliconized syringe. The output and y-axis represents particles/mL. Spherical was defined as having circle fit of 0.85-1.

Figure 5.11 shows that the protein aggregate concentration was lowest for the native solution which had never been subjected to any mechanical stress. The concentration of protein aggregates rose for the non-siliconized syringe as the speed increased. This confirmed what other studies had found, increase in mechanical stress leads to increased formation of protein aggregates. The same pattern was not observed in the siliconized syringe, where the concentration remained roughly the same across the different expulsion speeds and was only slightly higher than for the native solution. The observed lack of increase in protein aggregates for the siliconized syringes agree with the findings of other studies. The reason behind the lack

has been suggested to be because the protein will adsorb to the interface of the oil particles.

Figure 5.11 also shows that the concentration of silicone oil particles was roughly tenfold higher for the siliconized syringe at the two higher expulsion speeds (0.9 and 1.7 mm/s), and the count rose with increased speed. The total count of spherical particles was roughly the same across the five other combinations. It seems that the lowest expulsion speed exerted a shear stress which was not enough to increase the release of silicone. The observed rise in higher silicone oil particle count with increasing amount of mechanical stress, was consistent with other studies of siliconized syringes.

It should be noted that no regard to standard deviation was taken during the assumptions from Figure 5.11. Further investigation involving generation of more replicates and statistical testing would be recommended before assuming that there was a definite link between for example expulsion speed and degree of protein aggregation for the non-siliconized syringe.

5.5 SEC

The samples appeared clear after thawing and no pellet at bottom of the tube was observed in any of them after centrifugation. The chromatogram displayed one peak across all samples. When compared, the peaks from the mechanically stressed samples shared an almost identical retention time with the native samples (Fig. 5.12).

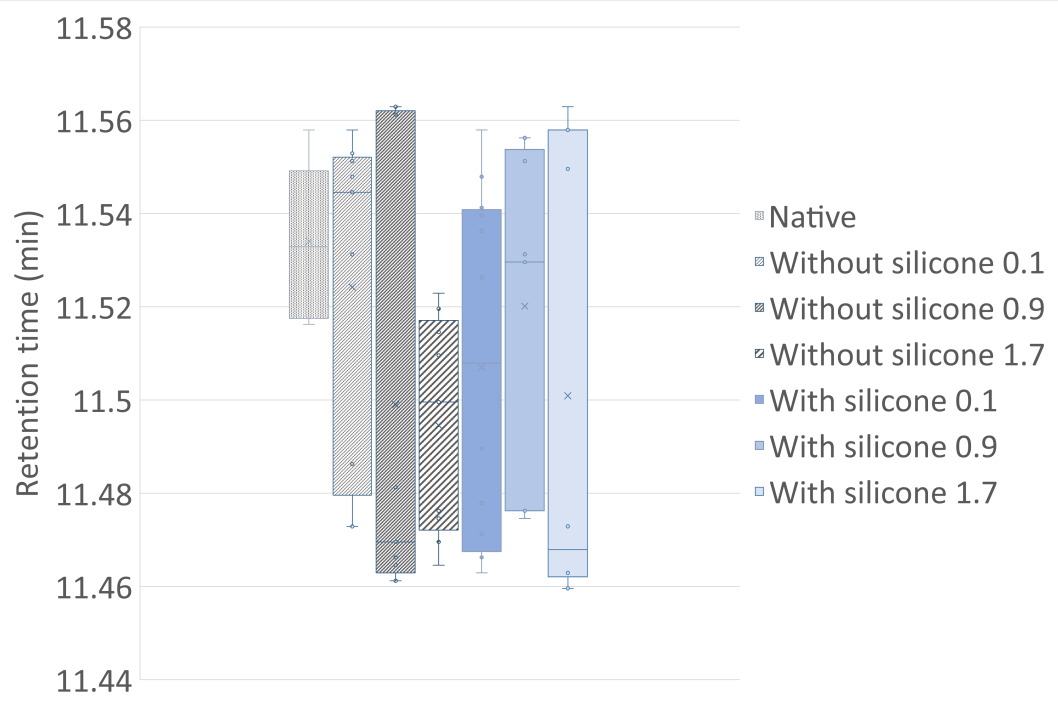

Figure 5.12: Box and whisker plot of retention time (min) for the native samples and each combination.

.

The mechanical stress and lubrication did not seem to have had an affect on the retention time (Fig. 5.12). The average retention time across all samples was 11.51 ± 0.04 min. Thus, the observed peak corresponded to the native forms of insulin. There seemed to be no indication of shift in the population of inhabited native forms and no emergence of potential aggregates could be observed in the chromatogram.

Figure 5.13, shows that the relative peak area was close to 100 % for all combinations and that the concentration of native form appeared lower for the samples from the siliconized syringes. The peak area was approximately 2.5 % lower than the untreated native sample, which represented a native protein loss of 87.5 µg/mL sample

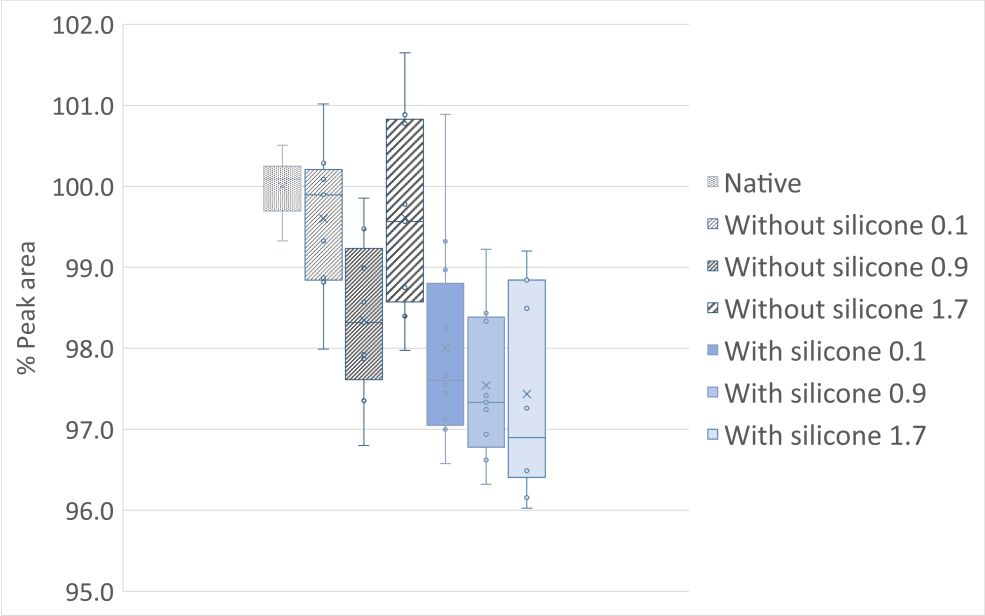

Figure 5.13: Box and whisker plot of % Peak area for the native samples and each combination. Peak area is given in relation to the average peak area of the native samples (which was set to 100 %).

.

The peak height was then evaluated (Fig. 5.14).

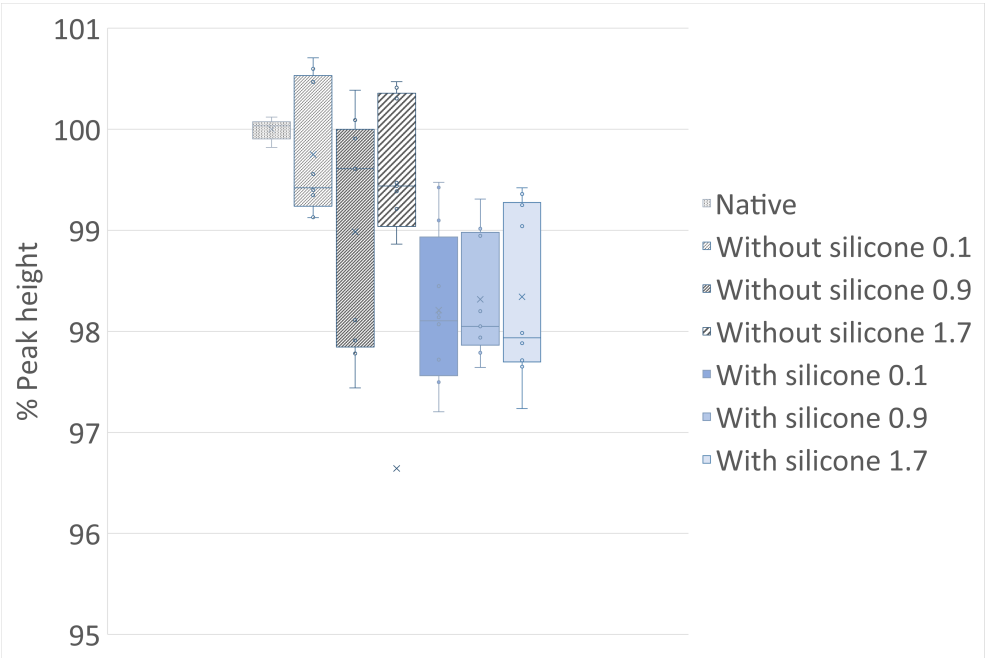

Figure 5.14: Box and whisker plot of % Peak height for the native samples and each combination. Peak height is given in relation to the average peak height of the native samples (which was set to 100 %).

.

This was performed to find out if the area loss was primarily associated to height, or if it was due to narrowing of the peak. Peak height for each combination, were given in relation to the average peak height of the native samples. The smaller area seems to be due to loss of peak height (Fig. 5.13), and the lower concentration in siliconized syringes was therefore regarded to mainly be due to loss of the most inhabited native protein forms.

A loss of 2.5 % might appear small at a first glance, but, when looking at the bigger picture it was actually quite large. The silicone interface area of the particles which were found during FlowCAM (Fig. 5.8), was estimated for the group which had been subjected to 1.7 mm/s and a siliconized syringe. The estimation was made under the assumption that silicone oil constituted roughly 50 % (Fig. 5.9) of the particles across sizes, and that the rest was protein aggregates. It was also assumed that the protein surface load was 1 mg/m^2. No considerations regarding packing or protein denaturation during adsorption were made. The silicone oil interface surface area was approximately 464*10^{-9} m^2/mL solution after the mechanical stress. This meant that the silicone oil particles could theoretically adsorb roughly 464*10^{-6} µg/mL, which only represented 5 ppm of the the protein loss found by SEC.

As some of the protein loss will also be in the form of aggregates, this loss was also estimated theoretically from the same FlowCAM output (Fig. 5.8). The protein aggregates were assumed as dense spheres with a density of 1.3 g/mL. The theoretical native protein loss due to aggregation was calculated to 1.82*10^{-}**12** µg/mL. Thus, the native protein loss due to pure protein aggregation was in theory significantly lower than the loss due to interface adsorption.

Thus, the formed silicone oil interface might contribute more to the loss than the formed aggregates, and only 5 ppm of the loss could be explained by the found particles in this investigation. It should be noted that FlowCAM only captured particles ≥ 2 µm, and the distribution pattern seems to display a trend were the particle count increases as the size decreases. The smaller particles might potentially present a large proportion of the particle area, how large is not known and their contribution to the loss could therefore not be included. Other sources of loss could for example be adsorption to interfaces of the device (syringe and needle) and other equipment which was used during the investigation. Further, some studies have found that FlowCAM was only able to capture a part of the particles in the investigated solution, not all. The real concentration is probably higher than the one obtained by FlowCAM and this should also be taken into consideration.

Chapter 6

Conclusion

This investigation managed to develop a method which could be used to describe the formation of subvisible particles in a syringe with needle during expulsion. The method involved development of a functioning probe, which made it possible for the texture analyser to exert and measure the expulsion force. The known force could then be translated to a theoretically estimated amount of shear stress, which represented how much mechanical stress the solution had been subjected to. Formation and size distribution of subvisible particles could be described by FlowCAM, while loss of native protein could be confirmed by SEC.

The following could be concluded:

- The in-house 3D printed probe, turned out to be an cost-effective alternative compared to other products on the market. It costed approximately one tenth of the commercially available probes and performed well.
- The investigation was possible to carry out within the set time frame. Theoretical calculations and experimental work was performed to support the choice of scope. FlowCAM investigation showed that two parameters regarding particle sphericity, circle fit and AR, were useful when separating silicone oil particles from protein aggregates. Cutoff at 0.85 was effective for characterization of particles ≥ 5 µm. This was confirmed by visual inspection. Particles ≤ 5 µm were captured out of focus and this fraction could not be properly characterized by FlowCAM. This was problematic as they accounted for the majority of the found particles. For example 70 % of the particles in the output from siliconized syringes at 1.7 mm/s were 2 - 5 µm.

- The insulin solution had experienced shear stress at laminar flow, which in theory roughly ranged from 0 - 1000 N/m^2 during expulsion. There was a positive correlation between plunger speed and the average hydrodynamic force, which was quite linear. The average dynamic friction force remained relatively constant across the different speeds and syringe types. The siliconized syringe was associated with a larger variation in force than the non-siliconized syringe.

- The DLS revealed that the insulin molecules were mainly present in their hexamer form at a concentration of 3.5 mg/mL and had a hydrodynamic diameter of 5.6 nm. Exposure to mechanical stress might promote the formation of 5 µm particles. But, the output was inconsistent and their presence could therefore not be reliably proven by DLS.

- According to FlowCam, shear stress led to increased concentrations of particles ≥ 2 µm. The increase was mainly due to protein aggregate formation in the non-siliconized syringe, while it was mainly due to silicone oil droplet formation in the siliconized syringe. Increased expulsion speed did not seem to give rise to increased concentration of protein aggregates for the siliconized syringe. Meanwhile, SEC showed that the siliconized syringe was associated with a substantial (2.5 %) loss of native protein. Other studies have suggested that his phenomenon can be due to adsorption of protein to the silicone oil interface or protein aggregation. The loss for the siliconized syringe at 1.7 mm/s was theoretically estimated from the particle distribution. The oil droplet interface seemed to represent a larger cause of loss than the protein aggregates. In total, the particles were found to only account for an extremely small part (5 ppm) of the loss found by SEC. Either were the assumptions during the theoretical calculations wrong, or other sources of loss were present. For example, in the form of smaller particles which belonged to the part of the size distribution which could not be described by FlowCAM, or FlowCAM underestimated the real particle count. The loss could also be due to the adsorption to other interfaces, such as the syringe, needle or equipment used for storage of sample.

- The 5 mL syringe with 30G and an expulsion speed of 0.9 mm/s, was within the limits of a manual subcutaneous injection, It was associated with a rise in the concentration of subvisible particles and loss of native protein. This scenario had the potential to arise in a clinical setting in real life.

Chapter 7

Future outlook

The next step would be to create more replicates for the syringe without silicone for investigation by FlowCAM, to statistically establish whether there is a significant relationship between plunger speed during expulsion and the protein aggregate concentration.

To facilitate the sorting of captured silicone particles from protein aggregates, it would be favourable to design an automatic categorisation for the capturing of future samples by the FlowCAM. The categorization filter could be based upon the two parameters, AR and circle Fit, which describe sphericity. Appropriate cutoff value could be 0.85 for both parameters. Where higher scores represented the circular silicone particles and lower than 0.85 represented the amorphous protein aggregates. To further improve the sorting, visual inspection could be combined with the automatic categorization. Occasional particles which had been placed in the wrong category, could hereby be visually identified and manually moved into the proper category.

The fraction of small particles (2-5 µm) constituted the largest proportion, but they could not be categorized due to problems with focus. The focus could possibly be improved by changing the objective and flow Cell to 20X/50 µm. Note should be taken that a change to thinner Flow Cell might be associated with clogging, which can be solved by dilution of the sample. Characterization by FlowCAM could possibly be further improved by utilizing the fluorescent mode or by finding some way to colour the silicone oil droplets without disturbing the protein. Further, a larger part of the particle size distribution could be described, if a FlowCAM Nano was paired with the currently used model.

This investigation only examined the effect of stress during expulsion at laminar flow.

The preliminary syringe setup optimization showed that it was possible to reach transitional flow during manual subcutaneous injection in a clinical setting. Further studies involving transitional flow and its effect on subvisible particles, could be performed by investigating for example 30G and a syringe size which lies between 1 and 3 mL.

The effect of dead space between the syringe nozzle and the needle hub could also be investigated. Dead space will lead to an unavoidable aspiration of air during the operation of the syringe, and air interfaces are known to potentially affect protein aggregation by adsorption to the interface.

Other studies could involve the effect of mechanical stress due to aspiration, as this was also not explored during this investigation. This type of study would require the use of a larger needle lumen or smaller syringe, as the 5 mL syringe with 30G displayed forces close to overload already at low aspiration speeds (0.1 mm/s).

To facilitate such studies, the homebuilt probe would need to be further improved, so that it would be able to operate other syringes than 5 mL. For example by 3D printing something that could be slipped around the smaller syringe, and allow it to fit snugly in the hole of the lower part of the probe. Another possibility would be to print a completely new version of the probe, which build upon the design, but allowed operation of different syringe sizes.

References

Adams, G. G., Meal, A., Morgan, P. S., Alzahrani, Q. E., Zobel, H. K., Lithgo, R., Kok, M. S., Besong, D. T. M., Jiwani, S. I., Ballance, S., Harding, S. E., Chayen, N. and Gillis, R. B. (2018), 'Characterisation of insulin analogues therapeutically available to patients', *PLOS ONE* **13**, 1–17.

Anselmo, A. C., Gokarn, Y. and Mitragotri, S. (2019), 'Non-invasive delivery strategies for biologics', *Nature Reviews Drug Discovery* **18**(1), 19–40.
URL: *https://www.nature.com/articles/nrd.2018.183*

Anton Paar (n.d.), 'Multiple detection angles in dynamic light scattering analysis'. accessed: 24.01.2023.
URL: *https://wiki.anton-paar.com/en/multiple-detection-angles-in-dynamic-light-scattering-analysis/*

Berteau, C., Filipe-Santos, O., Wang, T., Rojas, H. E., Granger, C. and Schwarzenbach, F. (2015), 'Evaluation of the impact of viscosity, injection volume, and injection flow rate on subcutaneous injection tolerance', *Medical Devices: Evidence and Research* **8**, 473–484.
URL: *https://www.tandfonline.com/doi/abs/10.2147/MDER.S91019*

Brookhaven Instruments (2019), 'Guide for dynamic light scattering (dls) sample preparation'. accessed: 24.01.2023.
URL: *https://www.brookhaveninstruments.com/guide-for-dls-sample-preparation/*

Burckbuchler, V., Mekhloufi, G., Giteau, A. P., Grossiord, J., Huille, S. and Agnely, F. (2010), 'Rheological and syringeability properties of highly concentrated human polyclonal immunoglobulin solutions', *European Journal of Pharmaceutics and Biopharmaceutics* **76**(3), 351–

356.
URL: *https://www.sciencedirect.com/science/article/pii/S0939641110002122*

Carpenter, J. F., Fradkin, A. H. and Vessely, C. (2015), 'Meeting biopharmaceutical analytical requirements for subvisible particle sizing and counting', *European Pharmaceutical Review* .
URL: *https://www.europeanpharmaceuticalreview.com/article/35952/meeting-biopharmaceutical-analytical-requirements-for-subvisible-particle-sizing-and-counting/*

Chisholm, C. F., Baker, A. E., Soucie, K. R., Torres, R. M., Carpenter, J. F. and Randolph, T. W. (2016), 'Silicone oil microdroplets can induce antibody responses against recombinant murine growth hormone in mice', *Journal of Pharmaceutical Sciences* **105**(5), 1623–1632.
URL: *https://www.sciencedirect.com/science/article/pii/S0022354916003828*

Chouchane, K., Frachon, T., Marichal, L., Nault, L., Vendrely, C., Maze, A., Bruckert, F. and Weidenhaupt, M. (2022), 'Insulin aggregation starts at dynamic triple interfaces, originating from solution agitation', *Colloids and Surfaces B: Biointerfaces* **214**, 112451.
URL: *https://www.sciencedirect.com/science/article/pii/S0927776522001345*

Connor, N. (2019), 'What is reynolds number for laminar flow – definition'. accessed: 28.03.2023.
URL: *https://www.thermal-engineering.org/what-is-reynolds-number-for-laminar-flow-definition/*

Correia, M., Neves-Petersen, M. T., Jeppesen, P. B., Gregersen, S. and Petersen, S. B. (2012), 'Uv-light exposure of insulin: pharmaceutical implications upon covalent insulin dityrosine dimerization and disulphide bond photolysis', *PloS one* **7**(12), e50733.
URL: *https://europepmc.org/articles/PMC3515625*

Dias Júnior, C. d. S., Cardoso, A. L., Figueiredo, A. G. d. A., Ota, S. and Melo, G. B. (2020), 'Agitation of the syringe and release of silicone oil', *Eye (London, England)* **34**(12), 2242—2248.
URL: *https://europepmc.org/articles/PMC7784962*

Dingman, R. and Balu-Iyer, S. V. (2019), 'Immunogenicity of protein pharmaceuticals', *Journal of Pharmaceutical Sciences* **108**(5), 1637–1654.
URL: *https://www.sciencedirect.com/science/article/pii/S002235491830813X*

Fekete, S., Beck, A., Veuthey, J.-L. and Guillarme, D. (2014), 'Theory and practice of size exclusion chromatography for the analysis of protein aggregates', *Journal of Pharmaceutical and Biomedical Analysis* **101**, 161–173. JPBA Reviews 2014.
URL: *https://www.sciencedirect.com/science/article/pii/S0731708514002027*

Fluid Imaging Technologies, Inc. (2017), 'Flowcam8000 series®dynamic imaging particle analyzer user guide'. accessed: 28.03.2023.
URL: *https://www.manualslib.com/manual/1494089/Fluid-Imaging-Technologies-Flowcam-8000-Series.html?page=9manual*

Galan, N. (2022), 'Choosing the right needle for your injections. what to know about syringe types and needle sizes'. accessed: 28.03.2023.
URL: *https://www.verywellhealth.com/how-to-select-the-correct-needle-size-for-an-injection-2616536*

Gecsey, J. (2015), 'Introduction to the new usp 787 -subvisible particulate matter in therapeutic protein injections'. accessed: 28.03.2023.
URL: *https://www.youtube.com/watch?v=Ot7jQar5gtY*

Harris, D. and Lucy, C. (2020), *Quantitative chemical analysis*, 10 edn, Macmillan International Higher Education. accessed: 06.04.2023.
URL: *https://search.ebscohost.com/login.aspxdirect=trueAuthType=ip,uiddb=cat07147aAN=lub.6516030site=eds-livescope=site*

Harrison, D. M. and Garratt, C. J. (1969), 'The accurate measurement of insulin molarity', *Biochemical Journal* **113**(4), 733–734.
URL: *https://doi.org/10.1042/bj1130733*

Hopkins, U. and Arias, C. Y. (2013), 'Large-volume im injections: A review of best practices', *Oncology Nurse Advisor* pp. 32–37.
URL: *https://www.oncologynurseadvisor.com/wp-content/uploads/sites/13/2019/01/onafeature0213injections10767.pdf*

Irvine, D. J., Su, X. and Kwong, B. (2013), *Routes of Delivery for Biological Drug Products*, John Wiley Sons, Ltd, chapter 22, pp. 1–48.
URL: *https://onlinelibrary.wiley.com/doi/abs/10.1002/9780470571224.pse521*

JAPAN BIO PRODUCTS (n.d.), 'Jbp nanoneedle'. accessed: 28.03.2023.
URL: *http://jbpglobal.placenta.co.jp/product/jbp-nanoneedle/*

Jiao, N., Barnett, G. V., Christian, T. R., Narhi, L. O., Joh, N. H., Joubert, M. K. and Cao, S. (2020), 'Characterization of subvisible particles in biotherapeutic prefilled syringes: The role of polysorbate and protein on the formation of silicone oil and protein subvisible particles after drop shock', *Journal of Pharmaceutical Sciences* **109**(1), 640–645.
URL: *https://www.sciencedirect.com/science/article/pii/S0022354919307385*

Kim, N. A., Kim, D. J. and Jeong, S. H. (2020), 'Do not flick or drop off-label use plastic syringes in handling therapeutic proteins before administration', *International Journal of Pharmaceutics* **587**, 119704.
URL: *https://www.sciencedirect.com/science/article/pii/S0378517320306888*

Li, J., Pinnamaneni, S., Quan, Y., Jaiswal, A., Andersson, F. I. and Zhang, X. (2012), 'Mechanistic understanding of protein-silicone oil interactions', *Pharmaceutical research* **29**(6), 1689—1697.
URL: *https://link.springer.com/article/10.1007/s11095-012-0696-6*

LS Instruments (n.d.), 'Experimental guidelines - dls sample preparation'. accessed: 24.01.2023.
URL: *https://lsinstruments.ch/en/theory/dynamic-light-scattering-dls/experimental-guidelines-dls-sample-preparation*

Ludwig, D., Carpenter, J. F., Hamel, J. and Randolph, T. W. (2010), 'Protein adsorption and excipient effects on kinetic stability of silicone oil emulsions', *Journal of Pharmaceutical Sciences* **99**(4), 1721–1733.
URL: *https://www.sciencedirect.com/science/article/pii/S0022354916305111*

Makurvet, F. D. (2021), 'Biologics vs. small molecules: Drug costs and patient access', *Medicine in Drug Discovery* **9**, 100075.
URL: *https://www.sciencedirect.com/science/article/pii/S2590098620300622*

Malvern Panalytical (2010), 'Dynamic light scattering: An introduction in 30 minutes'. accessed: 24.01.2023.
URL: *https://www.malvernpanalytical.com/en/learn/knowledge-center/technical-notes/TN101104DynamicLightScatteringIntroduction*

Malvern Panalytical (2017), 'Dynamic light scattering - common terms defined'. accessed: 25.01.2023.
URL: *https://www.malvernpanalytical.com/en/learn/knowledge-center/whitepapers/WP111214DLSTermsDefined*

Malvern Panalytical (n.d.), 'Zetasizer nano range. simple and versatile light scattering systems'. accessed: 27.01.2023.
URL: *https://www.malvernpanalytical.com/en/support/product-support/zetasizer-range/zetasizer-nano-range*

Melo, G. B., da Cruz, N. F. S., Emerson, G. G., Rezende, F. A., Meyer, C. H., Uchiyama, S., Carpenter, J., Shiroma, H. F., Farah, M. E., Maia, M. and Rodrigues, E. B. (2021), 'Critical

analysis of techniques and materials used in devices, syringes, and needles used for intravitreal injections', *Progress in Retinal and Eye Research* **80**, 100862.
URL: *https://www.sciencedirect.com/science/article/pii/S1350946220300343*

Nagel, N., Graewert, M. A., Gao, M., Heyse, W., Jeffries, C. M., Svergun, D. and Berchtold, H. (2019), 'The quaternary structure of insulin glargine and glulisine under formulation conditions', *Biophysical Chemistry* **253**, 106226.
URL: *https://www.sciencedirect.com/science/article/pii/S0301462219301383*

Narhi, L. O., Chou, D. K., Christian, T. R., Gibson, S., Jagannathan, B., Jiskoot, W., Jordan, S., Sreedhara, A., Waxman, L. and Das, T. K. (2022), 'Stress factors in primary packaging, transportation and handling of protein drug products and their impact on product quality', *Journal of Pharmaceutical Sciences* **111**(4), 887–902.
URL: *https://www.sciencedirect.com/science/article/pii/S0022354922000211*

Nobbmann, U. (2017), 'Polydispersity – what does it mean for dls and chromatography?'. accessed: 27.01.2023.
URL: *https://www.materials-talks.com/polydispersity-what-does-it-mean-for-dls-and-chromatography/*

Pandya, A. K. and Patravale, V. B. (2021), 'Computational avenues in oral protein and peptide therapeutics', *Drug Discovery Today* **26**(6), 1510–1520.
URL: *https://www.sciencedirect.com/science/article/pii/S1359644621001379*

Pharmacopea Europaea (2008), '2.9.19. particulate contamination: Sub-visible particles'. accessed: 28.03.2023.
URL: *http://uspbpep.com/ep60/2.9.19.%20particulate%20contamination-%20sub-visible%20particles%2020919e.pdf*

Polania Gutierrez, J. J. and Munakomi, S. (2022), *Intramuscular Injection*, StatPearls Publishing, Treasure Island (FL).
URL: *http://europepmc.org/books/NBK556121*

Poulsen, C., Langkjær, L. and Worsøe, C. (2007), 'Precipitation of insulin aspart and insulin glulisine products used for continuous subcutaneous insulin infusion', *Diabetes Technology and Therapeutics* **9**(1), 26–35.
URL: *https://doi.org/10.1089/dia.2006.0054*

PubChem (2023), 'Compound summary insulin analog'. accessed: 28.03.2023.
URL: *https://pubchem.ncbi.nlm.nih.gov/compound/Insulin-analog*

Rathore, N., Pranay, P., Bernacki, J., Eu, B., Ji, W. and Walls, E. (2012), 'Characterization of protein rheology and delivery forces for combination products', *Journal of Pharmaceutical Sciences* **101**(12), 4472–4480.
URL: *https://www.sciencedirect.com/science/article/pii/S0022354915313575*

RealHope (n.d.), 'Aiding in the development of more robust protein drugs and increasing safety for patients.'. accessed: 25.04.2023.
URL: *https://realhope.se/home/about-real-hope/*

Roy T Cherris (2018), 'United state pharmacopeia particle determination: Guidance for parenteral products'. accessed: 28.03.2023.
URL: *https://www.pharmout.net/wp-content/uploads/2018/02/NGVF-2016-D2.T2.2.2-Roy-Cherris-Particle-Determination-Guidance-for-Parenteral-Products.pdf*

Rudiuk, S., Cohen-Tannoudji, L., Huille, S. and Tribet, C. (2012), 'Importance of the dynamics of adsorption and of a transient interfacial stress on the formation of aggregates of igg antibodies', *Soft Matter* **8**, 2651–2661.
URL: *https://pubs.rsc.org/en/content/articlelanding/2012/sm/c2sm07017k*

Ruiz, M. E. and Scioli Montoto, S. (2018), *Routes of Drug Administration*, Springer International Publishing, Cham, pp. 97–133.
URL: *https://doi.org/10.1007/978-3-319-99593-9*$_6$

Schellekens, H. (2002), 'Immunogenicity of therapeutic proteins: Clinical implications and future prospects', *Clinical Therapeutics* **24**(11), 1720–1740.
URL: *https://www.sciencedirect.com/science/article/pii/S0149291802800753*

Smewing, J. (2014), 'Texture analysis in action: Universal syringe rig'. accessed: 28.03.2023.
URL: *https://textureanalysisprofessionals.blogspot.com/2014/12/texture-analysis-in-action-universal.html*

Spaulding, B. (2014), 'Flowcam manual version 3.4'.

Stable Micro Systems (n.d.a), 'Texture analysis – a beginner's guide'. accessed: 28.03.2023.
URL: *https://www.stablemicrosystems.com/BeginnersGuideToTextureAnalysis.html*

Stable Micro Systems (n.d.b), 'Ta.xtplusc texture analyser'. accessed: 28.03.2023.
URL: *https://www.stablemicrosystems.com/TAXTplus.html*

Svenska Institutet för Standarder (2016), 'Iso 7886-1:2016 sterile hypodermic syringes for single use — part 1: Syringes for manual use'. accessed: 28.03.2023.
URL: *https://www.sis.se/api/document/get/80003371*

SWEMED (n.d.), 'Bd insulinspruta med/utan stickskydd'. accessed: 28.03.2023.
URL: *https://res.onemed.com/SE/Produktblad/205051.pdf*

Thorlaksen, C., Stanciu, A.-M., Busch Neergaard, M., Jiskoot, W., Groenning, M. and Foderà, V. (2022), 'Subtle ph variation around ph 4.0 affects aggregation kinetics and aggregate characteristics of recombinant human insulin', *European Journal of Pharmaceutics and Biopharmaceutics* **179**, 166–172.
URL: *https://www.sciencedirect.com/science/article/pii/S0939641122001904*

Vargas, S. K., Eskafi, A., Carter, E. and Ciaccio, N. (2020), 'A comparison of background membrane imaging versus flow technologies for subvisible particle analysis of biologics', *International Journal of Pharmaceutics* **578**, 119072.
URL: *https://www.sciencedirect.com/science/article/pii/S0378517320300569*

vwr (n.d.*a*), 'Disposable syringes, omnifix®'. accessed: 10.04.2023.
URL: *https://se.vwr.com/store/product/573081/disposable-syringes-omnifix*

vwr (n.d.*b*), 'Single use syringes, 2-piece, injekt® solo'. accessed: 10.04.2023.
URL: *https://se.vwr.com/store/product/804884/single-use-syringes-2-piece-injekt-solo*

Watt, R. P., Khatri, H. and Dibble, A. R. (2019), 'Injectability as a function of viscosity and dosing materials for subcutaneous administration', *International Journal of Pharmaceutics* **554**, 376–386.
URL: *https://www.sciencedirect.com/science/article/pii/S0378517318308305*

Woods, R. J., Alarcón, J., McVey, E. and Pettis, R. J. (2012), 'Intrinsic fibrillation of fast-acting insulin analogs', *Journal of diabetes science and technology* **6**(2), 265—276.
URL: *https://europepmc.org/articles/PMC3380767*

Yokogawa Fluid Imaging Technologies, Inc (2023), 'How it works particle count, size, and morphology with flow imaging microscopy'. accessed: 28.03.2023.
URL: *https://www.fluidimaging.com/*

Yokogawa Fluid Imaging Technologies, Inc (n.d.), 'The ultimate guide to flow imaging microscopy'. accessed: 28.03.2023.
URL: *https://info.fluidimaging.com/hubfs/documents/white-papers-ebooks/ebook-the-ultimate-guide-to-flow-imaging-microscopy.pdf*

Zhou, C., Qi, W., Lewis, E. N. and Carpenter, J. F. (2016), 'Characterization of sizes of aggregates of insulin analogs and the conformations of the constituent protein molecules: A

concomitant dynamic light scattering and raman spectroscopy study', *Journal of Pharmaceutical Sciences* **105**(2), 551–558.
URL: *https://www.sciencedirect.com/science/article/pii/S0022354915000246*

Appendices

Appendix A

SOP insulin solution

SOP Insulin stock solution

This SOP describes the preparation of 20 mL 3.5 mg/mL insulin stock solution pH 7.4.

Abbreviations used:

Abbreviation	Description
mg/mL	milli gram/milli Litre
mL	milli Litre
mg	milli gram
TRIS	Tris(hydroxymethyl)aminomethane
HCl	Hydrochloric acid
µm	micrometre

Equipment and materials used:

Equipment	Number to be used/ additional details:
pH meter and calibration solutions	
Milli-Q water and drying paper for pH probe	
Analytical balance and weighing papers	
Microspatula	1 spatula
20 mL glass vials with rubber lids, sterilised	4 vials
Marker pen	1 pen
Insulin powder	Molar mass: 5822.64 g/mol
Filtered sterile 50 mM TRIS buffert pH 8.0	2 x 5 mL + 1.2 mL
Filtered sterile 0.01 M HCl	4 mL + 1 mL
Eppendorf pipettes and tips	500 - 5000 µL pipette and 3 tips 100 – 1000 µL Eppendorf pipette and 1 tip
Plastic test tube with lid, sterile	1 tube, hold 10 mL
Nanodrop	
Pipette and 10 µL tip without filter	Are next to Nanodrop
Deionised water and cleaning paper	Are next to Nanodrop
10 mL syringe	2 syringes
0.2 µm filter	2 filters
Vial for DLS sample	
DLS etc.	

Procedure:

All glassware to be used will be labelled with the analysts' initials, the date and contents.

Preparation of filtered 20 mL 3.5 mg/mL insulin stock solution pH 7.4

1. Calibrate pH meter. Retrieve Milli-Q water and paper for cleaning pH probe.
2. Using an analytical balance, weigh each of the 20 mL glass vials with lid. Label them and mark them "prov 1" and "prov 2".
3. Use a microspatula to weigh out 35 mg of insulin powder in each of the glass vials. Check and make sure all the powder is deposited in the bottom of the vials.
4. Add 5 mL of 50 mM TRIS buffert with the 500-5000 µL Eppendorf pipette to each of the vials. Weigh them.
5. Move the vials carefully with the bottom running along the table surface in figure of eights until the powder is dissolved.
6. Measure pH (should be around 7.8).
7. Add 4 mL of 0.01 M HCl with the 500-5000 µL Eppendorf pipette to each of the vials. Move vials carefully in figure of eights. Measure pH (should be around 7.4).
8. Weigh the vials.
9. Create a blank by measuring 5 mL 50 mM TRIS buffert and 4 mL 0.01 M HCl with the 500 – 5000 µL Eppendorf pipette and mix it in a plastic test tube with lid.
10. Check insulin concentration with Nanodrop. Use 10 µL pipette tips without filter.
    - OBS! Before use check two things: 1) Do not use the equipment if the grey machine (Rotorgene) next to it is running. 2) Check light on box (dosan), lamp no. 1 should be glowing green = the correct computer is in use.
    - Open NO 1000 icon.
    - Enter Protein A280.
    - Remove cotton from lens, moisten paper with deionised water and clean lens.
    - Deposit 1 µL of deionised water on the lens (no bubbles), close and press "Okay".
    - Open and wipe lens with dry paper.
    - Blank: deposit 1 µL of blank on the lens and close. Press "Okay".
    - Open, moisten paper with deionised water and clean lens, then wipe lens with dry paper.
    - Sample: sample type, choose other protein (E&MW). Enter e = 5.734 $cm^{-1}M^{-1}$ and M = 5822.64 g/mol.
    - Deposit 2 µL of sample on lens, close and measure concentration.
    - 3 replicates for each vial. Clean between each by: open, moisten paper with deionised water and clean lens, then wipe lens with dry paper, add new sample and close.
    - Concentration should be slightly higher than 3.5 mg/mL (roughly 3.89 mg/mL) as it was diluted to 9 mL.
11. If concentration higher than 3.5 mg/mL, dilute with blank. Check pH is still 7.4 and measure concentration with Nanodrop?
12. Allow to equilibrate 1 hour.
13. Filter the 2 solutions using 10 mL syringe with a 0.2 µm filter into 2 sterile and labelled glass vials with rubber lids, take out sample for DLS and put rest in fridge.

Appendix B

SOP TRIS buffer and 0.01 M HCl

SOP TRIS buffer, 0.01 M HCL and equipment

This SOP describes the preparation of sterile equipment and two solutions (TRIS buffer and 0.01 M HCl), which will later be used for the creation of insulin stock solution and blanks.

Abbreviations used:

Abbreviation	Description
mM	milli Molar
mL	milli Litre
TRIS	Tris(hydroxymethyl)aminomethane
HCl	Hydrochloric acid
µm	micrometre

Equipment and materials used:

Equipment	Number to be used/ additional details:
pH meter and calibration solutions	
Marker pen	1 pen
Spoon	1 spoon
Analytical balance and weighing papers	
400 mL glass beaker	1 beaker
TRIS base powder, 1:1 ratio	Molar mass: 121.14 g/mol
Milli-Q water	200 mL + 99 mL
Plastic transfer pipette	2 pipettes
Magnetic stirrer and magnetic flea	1 magnetic flea
Glass measuring cylinder	Able to measure 6 mL
1 M HCl	6.5 mL+ 1mL
50 mL syringe	1+1 syringe
0.2 µm filter	1+1 filter
150 mL Glass lab bottle with lid	2 bottles+1 bottle
Eppendorf pipettes and tips	1-5 mL pipette and tip
100 mL volumetric flask	1 flask
20 mL glass vials for insulin stock solution with rubber lid	Depends on how much insulin is to be prepared later and number of experiments
Autoclave	

Procedure:

All glassware to be used will be labelled with the analysts' initials, the date and contents.

Preparation of filtered 200 mL 50 mM TRIS buffer pH 8.0

1. Calibrate pH meter.
2. Using an analytical balance, weigh the cleaned and labelled 400 mL glass beaker.
3. Use a spoon to weigh out 1.2114 g of Tris base powder on a clean weighing paper.
4. Transfer the material from the weighing paper to the 400 mL glass beaker.
5. Weigh the now empty weighing paper, subtract weight of eventual powder residue on paper from 0.788 g to get total amount transferred to beaker.
6. Weigh the beaker while adding 190 g (=190 mL) of Milli-Q water to the beaker. Pour first, then top off last weight with a plastic transfer pipette.
7. Note weight of beaker with water and weigh the magnetic flea.
8. Add the magnetic flea and place beaker on a magnetic stirrer, start stirring. Allow adequate time for the solid Tris to dissolve completely.
9. Install pH probe in beaker, measure pH (should be around 10.52).
10. Add 6 mL of 1 M HCl with a glass measuring cylinder, stir, allow equilibrize and measure pH (should be around 8.12).
11. Carefully titrate 1 M HCl in a dropwise fashion with plastic transfer pipette, stir, allow equilibrize and measure pH until pH reaches 8.00. (Roughly 0.5 mL will be needed).
12. Weigh beaker, subtract from it the weight of magnetic flea and the weight of the beaker when containing the 190 mL of Milli-Q water. The difference in weight is equal to the amount of added 1 M HCl.
13. Further add an amount of Milli-Q water equal to 10 g minus the amount of added 1 M HCl with a plastic transfer pipette while weighing the beaker. The total added weight of Milli-Q water and 1 M HCl should be 200 g in finished solution. 190 g of Milli-Q water has already been added (step 6).
14. Filter the solution using a 50 mL syringe with a 0.2 µm filter and divide into two cleaned and labelled 150 mL flasks with lid.

Preparation of filtered 100 mL 0.01 M HCl

1. Transfer 1 mL 1 M HCl with an Eppendorf pipette into a 100 mL volumetric flask.
2. Add Milli-Q water until a volume of 100 mL is reached.
3. Filter the solution using a 50 mL syringe with a 0.2 µm filter into a cleaned and labelled 150 mL flask with lid.

Sterilisation of equipment

1. Gather the two flasks of TRIS buffer, one flask 0.01 M HCl and the 20 mL glass vials.
2. Check the water level of the autoclave and add water if water level is low.
3. Loosen the lids of the flasks and install all equipment in the autoclave. Put lid on autoclave.
4. Autoclave at 120°C, 20 min. Allow cooldown for at least 20 min before removal.
5. Tighten the lids of the flasks and put equipment in fridge.

Appendix C

Matlab script syringe setup optimization

```
% friction force 5,3 and 1 mL syringe

% examined speed (mm/s) respective syringe
v_fric_5mL = [0.5        1        1.25    2];
v_fric_3mL = [2 4        6        10];
v_fric_1mL = [1 8 12];

% friction force (N) syringe at examnied speeds

% 5 mL
F_fric_5mL = [0.97       1.45 1.22        0.9
   1.26];

% belonging speed vector
v_5mL = [0.5 1 1 1.25 2];

F_fric_5mL_average = [0.97 mean(F_fric_5mL(2:3)) 0.9
   1.26]; % averagefriction force at each speed
F_fric_5mL_total_average = repmat(mean(F_fric_5mL)
   ,1,100); % total averagefriction force, repeated
```

```
   in 1x100 vector

% 3 mL
F_fric_3mL = [1.5        0.8       1.2     1.7
              1.1        0.9       1                1.7
              1.20       0.7       1                1.6];
                 % friction force

% belonging friction force vector
F_fric_3mL_vector = [1.5 1.1 1.2 0.8 0.9 0.7 1.2 1 1
   1.7 1.7 1.6];
% speed vector
v_3mL = [2 2 2 4 4 4 6 6 6 10 10 10];

F_fric_3mL_average = [mean(F_fric_3mL(:,1)) mean(
   F_fric_3mL(:,2)) mean(F_fric_3mL(:,3)) mean(
   F_fric_3mL(:,4))]; % averagefriction force at each
    speed
F_fric_3mL_total_average = repmat(mean(
   F_fric_3mL_average),1,100); % total
   averagefriction force, repeated in 1x100 vector

% 1 mL
F_fric_1mL = [0.1 0.30 0.4 0.2 0.4 0.5 0.7];

 %  2, 3 and 4 at 8 mm/s
 %  5, 6 and 7 at 12 mm/s.
% belonging speed vector
v_1mL = [1 8 8 8 12 12 12];

F_fric_1mL_average = [0.1 mean(F_fric_1mL(2:4)) mean(
   F_fric_1mL(5:end))];  % averagefriction force at
   each speed
F_fric_1mL_total_average = repmat(mean(F_fric_1mL)
   ,1,100); % total averagefriction force, repeated
   in 1x100 vector
```

```
%%
% plot of friction force as funktion of speed for
   three different syringes

% 5 mL syringe
figure (1)
plot (v_5mL,F_fric_5mL,'gd','MarkerFaceColor','g');
hold on
plot (v_fric_5mL,F_fric_5mL_average,'g:'); % average
   for each speed
hold on
plot(linspace(0,v_fric_5mL(end)),
   F_fric_5mL_total_average,'g--'); % total average (
   average for all speeds)

xlabel('expulsion velocity, mm/s');
ylabel('Friction force, N');
title ('Friction force 5 mL syringe');
legend ('Observation','Mean each velocity','Total
   mean');
hold off

%%
% 3 mL syringe
figure (2)
plot (v_3mL,F_fric_3mL_vector,'bd','MarkerFaceColor',
   'b');
hold on
plot (v_fric_3mL,F_fric_3mL_average,'b:'); % average
   for each speed
hold on
plot(linspace(0,v_fric_3mL(end)),
   F_fric_5mL_total_average,'b--');

xlabel('expulsion velocity, mm/s');
ylabel('Friction force, N')
title ('Friction force 3 mL syringe')
```

```
legend ('Observation','Mean each velocity','Total
   mean');
hold off

%%
% 1 mL syringe
figure (3)
plot (v_1mL,F_fric_1mL,'rd','MarkerFaceColor','r');
hold on
plot (v_fric_1mL,F_fric_1mL_average,'r:'); % average
   for each speed
hold on
plot(linspace(0,v_fric_1mL(end)),
   F_fric_1mL_total_average,'r--');

xlabel('expulsion velocity, mm/s');
ylabel('Friction force, N')
title ('Friction force 1 mL syringe');
legend ('Observation','Mean each velocity','Total
   mean');
hold off

%%
% Expulsionsforce 5, 3, and 1 mL syringe with 30G, 27
   G and 25G needle, water

% Observations
% 5 mL syringe

% 30G diffferent speeds
v_30G_5mL = [0.5   1     1    1    1.5   1.5    1.5
      2    2   2]; % mm/s, speedvector
F_30G_5mL = [11.9 23.8 25.8 21.5    38   38.3   38.1
    55.8 54 57.8]; % expulsionsforcevector
F_30G_5mL_hydro = F_30G_5mL -
   F_fric_5mL_total_average(1); % vector without
   friction
```

```
% 27G diffferent speeds
v_27G_5mL = [0.5 0.5  1   1   1   1.5   1.5   1.5
         2    2     2     3     3    3     4    4
   4     4.5  4.5  4.5]; % mm/s, speedvector
F_27G_5mL = [3.8  5  5.3  9  3.4  7.9   8.9   7.9
   13  13.1  13.1  24.6  25.4  24.9  39 39.3 40.1
   48.8  48 55.7];% expulsionsforcevector
F_27G_5mL_hydro = F_27G_5mL -
   F_fric_5mL_total_average(1); % vector without
   friction

% 25G diffferent speeds
v_25G_5mL = [1     1    1    3     3     3     5
        5    5     6.5   6.5   6.5]; % mm/s,
   speedvector
F_25G_5mL = [2.8  1.9  2.4  12.1  12.1  12.3  31.5
   33.2  33.9   56    56    55.6]; %
   expulsionsforcevector
F_25G_5mL_hydro = F_25G_5mL -
   F_fric_5mL_total_average(1); % vector without
   friction

%%
% 3 mL syringe

% 30G diffferent speeds
v_30G_3mL = [1     1    1       1.5       1.5   1.5
     2    2     2       3    3    3     4    4]; % mm
   /s, speedvector
F_30G_3mL = [8.6  7.2  6.4  11.2  10.8  10.7  17
   16.5  17.8   28.5  28  27.5   44.8  45]; %
   expulsionsforcevector
F_30G_3mL_hydro = F_30G_3mL -
   F_fric_3mL_total_average(1); % vector without
   friction
```

```
% 27G diffferent speeds
v_27G_3mL = [1.5  1.5  1.5  2    2    2    3    3
   3    4.5   4.5    4.5   6    6    6    8       8
       8     9      9       9 ]; % mm/s, speedvector
F_27G_3mL = [3.3  2.6   3  4.7  4.2  3.9  7.8  7.6
   7.9   14   13.8   13.4  21   21  20.4  36.8   37.9
      37.7  46.4   46.9   48.1]; % expulsion force
   vector
F_27G_3mL_hydro = F_27G_3mL -
   F_fric_3mL_total_average(1); % vector without
   friction

% 25G diffferent speeds
v_25G_3mL = [3     3    3     5     5     5    6.5
   6.5   6.5    8          8     8      10    10
   10    12     12   12]; % mm/s, speedvector
F_25G_3mL = [4.7  4.3  4.2   8.7   8.2   8.7   12.8
   12.9  12.6  18.2   18.2  18.3   30.2  30.2  30.4
   42.8   42.9  43]; % expulsionsforcevector
F_25G_3mL_hydro = F_25G_3mL -
   F_fric_3mL_total_average(1); % vector without
   friction

%%
% 1 mL syringe

% tendency  friction increase  linear with speed
% linear fitting of friction gave:
% friction_1mL = 0.0411*v + 0.013; % N

% 30G diffferent speeds
v_30G_1mL = [ 1     1     1    1.5       1.5   1.5
      2     2    2   2    3         3    3     4
           4     4     4     10     10    10     20
       20    20]; % mm/s, speedvector
F_30G_1mL = [0.16  0.27  0.16  0.37  0.24  0.33  0.63
    0.58 0.97 0.7  1.19  1.22 1.23  2.3  1.48  1.68
```

```
   1.72   6.25  5.46   5.79  17.68  17.91  17.55]; %
   expulsions force vector
F_30G_1mL_hydro = F_30G_1mL - 0.0411.*v_30G_1mL +
   0.013; % vector without friction

% 27G diffferent speeds
v_27G_1mL = [1.5    10    10     10    15          15
      15    20         20     20    25    25     25
        30     30     30];% mm/s, speedvector
F_27G_1mL = [0.31  2.21  1.91   1.9   3.33   3.17
   3.24  4.27  4.49   4.56  4.16   4.3   4.54    4.54
     4.34   4.24]; % expulsionsforcevector
F_27G_1mL_hydro = F_27G_1mL - 0.0411.*v_27G_1mL +
   0.013; % vector without friction

% 25G diffferent speeds
v_25G_1mL = [10     10    10     15         20     20
       20    30          30   30    40     40     40];
    % mm/s, speedvector
F_25G_1mL = [1.23  1.39  1.42   2.1   2.74   2.73
   2.91  2.64   2.8   2.9  2.86   2.84   2.78]; %
   expulsionsforcevector
F_25G_1mL_hydro = F_25G_1mL - 0.0411.*v_25G_1mL +
   0.013; % hydrodynamic force vector, frictionen go
%%
% OBS!!! check for limit for laminary flow (for Re
   >2000 theoretical equations not valid)
% Reynolds tal?
%Re = speed vfluid*hydraulic diameter/kinematic
   viskosity water

% hydraulisc diameter = needle diameter

kin_viscosity_water = 1.004*10^-6; % m2/s, water 20
   grader

% fluid speed in needle?
```

```
%           v = F/A
%           A = cross section area  needle = pi*
   r_needle^2
%           F = flow in syringe = speed syringe*cross
    section area syringe
%           = v_syringe*pi*r_syringe^2
%           dvs v_needle = ( v_syringe*pi*r_syringe^2
    )/pi*r_needle^2 = v_syringe*r_syringe^2 /r_needle
   ^2

% Inner diameter syringe and needle...?
% length needle?
L_30G = 12*10^-3; % m,length 30G needle
L_27G = 20*10^-3; % m,length 27G needle
L_25G = 16*10^-3; % m,length 25G needle

% inner radie needle?
r_30G = confidential
r_27G = confidential
r_25G = confidential

% inner radie syringe?
r_5mL = confidential
r_3mL = confidential
r_1mL = confidential

% what speed does it take in respective needle for Re
   >2000?
v_Re2000_30G = 2000*kin_viscosity_water/(2*r_30G); %
   13.5219 m/s for 30G needle
v_Re2000_27G = 2000*kin_viscosity_water/(2*r_27G); %
    9.4494 m/s for 27G needle
v_Re2000_25G = 2000*kin_viscosity_water/(2*r_25G); %
    8.032 m/s for 25G needle

% at what expulsionsspeed  is limit for not purely
   laminar flow respective syringe and needle
```

```
   combination?
% 5 mL syringe
v_Re2000_30G_5mL = (v_Re2000_30G*r_30G^2)/(r_5mL^2);
   % m/s, limit  at 1.9 mm/s for 5mL with 30G
v_Re2000_27G_5mL = (v_Re2000_27G*r_27G^2)/(r_5mL^2);
   % m/s, limit  at 2.7 mm/s for 5mL with 27G
v_Re2000_25G_5mL = (v_Re2000_25G*r_25G^2)/(r_5mL^2);
   % m/s, limit  at 3.2 mm/s for 5mL with 25G

% 3 mL syringe
v_Re2000_30G_3mL = (v_Re2000_30G*r_30G^2)/(r_3mL^2);
   % m/s, limit  at 3.2 mm/s for 3mL with 30G
v_Re2000_27G_3mL = (v_Re2000_27G*r_27G^2)/(r_3mL^2);
   % m/s, limit  at 4.5 mm/s for 3mL with 27G
v_Re2000_25G_3mL = (v_Re2000_25G*r_25G^2)/(r_3mL^2);
   % m/s, limit  at 5.3 mm/s for 3mL with 25G

% 1 mL syringe
v_Re2000_30G_1mL = (v_Re2000_30G*r_30G^2)/(r_1mL^2);
   % m/s, limit  at 13.5 mm/s for 1mL with 30G
v_Re2000_27G_1mL = (v_Re2000_27G*r_27G^2)/(r_1mL^2);
   % m/s, limit  at 19.3 mm/s for 1mL with 27G
v_Re2000_25G_1mL = (v_Re2000_25G*r_25G^2)/(r_1mL^2);
   % m/s, limit  at 22.7 mm/s for 1mL with 25G

%%
% theoretical equation for calculation of
   hydrodynamic force
% Kan then be plotted and compaired to collected data

% based on Hagen-Poiseuille equation
% F_hydro = (8*pi**v_b*my*L_n*r_b^4/r_n^4)

my_water = 1.0016*10^-3; % Pa s, dynamic viscosity of
    water at 20 degree celcius

% theoretic hydrodynamic force
```

```
% 5 mL
v_hydro_30G_5mL = linspace (0,v_Re2000_30G_5mL*10^3);
    % mm/s, linear speed of stopper, vector
   containing the velocity below Re=2000
F_hydro_30G_5mL = ((8*pi*my_water*L_30G*(r_5mL^4))/(
   r_30G^4)).*(v_hydro_30G_5mL.*10^-3); % N,
   hydrodynamic force 5mL syringe with 30G

v_hydro_27G_5mL = linspace (0,v_Re2000_27G_5mL*10^3);
    % mm/s, linear speed of stopper, vector
   containing the velocity below Re=2000
F_hydro_27G_5mL = ((8*pi*my_water*L_27G*(r_5mL^4))/(
   r_27G^4)).*(v_hydro_27G_5mL.*10^-3); % N,
   hydrodynamic force 5mL syringe with 27G

v_hydro_25G_5mL = linspace (0,v_Re2000_25G_5mL*10^3);
    % mm/s, linear speed of stopper, vector
   containing the velocity below Re=2000
F_hydro_25G_5mL = ((8*pi*my_water*L_25G*(r_5mL^4))/(
   r_25G^4)).*(v_hydro_25G_5mL.*10^-3); % N,
   hydrodynamic force 5mL syringe with 25G

% 3 mL
v_hydro_30G_3mL = linspace (0,v_Re2000_30G_3mL*10^3);
    % mm/s, linear speed of stopper, vector
   containing the velocity below Re=2000
F_hydro_30G_3mL = ((8*pi*my_water*L_30G*(r_3mL^4))/(
   r_30G^4)).*(v_hydro_30G_3mL.*10^-3); % N,
   hydrodynamic force 3mL syringe with 30G

v_hydro_27G_3mL = linspace (0,v_Re2000_27G_3mL*10^3);
    % mm/s, linear speed of stopper, vector
   containing the velocity below Re=2000
F_hydro_27G_3mL = ((8*pi*my_water*L_27G*(r_3mL^4))/(
   r_27G^4)).*(v_hydro_27G_3mL.*10^-3); % N,
   hydrodynamic force 3mL syringe with 27G
```

```
v_hydro_25G_3mL = linspace (0,v_Re2000_25G_3mL*10^3);
    % mm/s, linear speed of stopper, vector
   containing the velocity below Re=2000
F_hydro_25G_3mL = ((8*pi*my_water*L_25G*(r_3mL^4))/(
   r_25G^4)).*(v_hydro_25G_3mL.*10^-3); % N,
   hydrodynamic force 3mL syringe with 25G

% 1 mL

v_hydro_30G_1mL = linspace (0,v_Re2000_30G_1mL*10^3);
    % mm/s, linear speed of stopper, vector
   containing the velocity below Re=2000
F_hydro_30G_1mL = ((8*pi*my_water*L_30G*(r_1mL^4))/(
   r_30G^4)).*(v_hydro_30G_1mL.*10^-3); % N,
   hydrodynamic force 1mL syringe with 30G

v_hydro_27G_1mL = linspace (0,v_Re2000_27G_1mL*10^3);
    % mm/s, linear speed of stopper, vector
   containing the velocity below Re=2000
F_hydro_27G_1mL = ((8*pi*my_water*L_27G*(r_1mL^4))/(
   r_27G^4)).*(v_hydro_27G_1mL.*10^-3); % N,
   hydrodynamic force 1mL syringe with 27G

v_hydro_25G_1mL = linspace (0,v_Re2000_25G_1mL*10^3);
    % mm/s, linear speed of stopper, vector
   containing the velocity below Re=2000
F_hydro_25G_1mL = ((8*pi*my_water*L_25G*(r_1mL^4))/(
   r_25G^4)).*(v_hydro_25G_1mL.*10^-3); % N,
   hydrodynamic force 1mL syringe with 25G

%%

% plot

% 5 mL syringe, diffferent needlegauge and speed,
   friction force gone
```

```
figure (4)
plot (v_30G_5mL,F_30G_5mL_hydro,'ko','MarkerFaceColor
   ','m');
hold on
plot (v_27G_5mL,F_27G_5mL_hydro,'ko');
hold on
plot (v_25G_5mL,F_25G_5mL_hydro,'ko','MarkerFaceColor
   ','c');

% plot in limit for Re>2000 for respective
   needlegauge
y_5mL = linspace(0,60); % vector for y varden,100 st
   varden 0-60
x_Re2000_30G_5mL = repmat(v_Re2000_30G_5mL
   *10^3,1,100); % row matrix with 1x100 radvector
   only consist of limit for Re>2000
x_Re2000_27G_5mL = repmat(v_Re2000_27G_5mL
   *10^3,1,100); % row matrix with 1x100 radvector
   only consist of limit for Re>2000
x_Re2000_25G_5mL = repmat(v_Re2000_25G_5mL
   *10^3,1,100); % row matrix with 1x100 radvector
   only consist of limit for Re>2000

hold on
plot (x_Re2000_30G_5mL,y_5mL,'m--');
hold on
plot (x_Re2000_27G_5mL,y_5mL,'k--');
hold on
plot (x_Re2000_25G_5mL,y_5mL,'c--');

%hold on
%plot (v_hydro_30G_5mL,F_hydro_30G_5mL,'m:'); % plot
   in theoretical hydrodynamic force 5mL 30G
%hold on
%plot (v_hydro_27G_5mL,F_hydro_27G_5mL,'k:'); % plot
   in theoretical hydrodynamic force 5mL 27G
```

```
%hold on
%plot (v_hydro_25G_5mL,F_hydro_25G_5mL,'c:'); % plot
   in theoretical hydrodynamic force 5mL 25G

xlabel('expulsion velocity, mm/s');
ylabel('Hydrodynamic force, N');
title ('Hydrodynamic force 5 mL syringe at different
   needle gauges');
legend ('30G','27G','25G','Limit 30G','Limit 27G','
   Limit 25G');
hold off

%%

% 3 mL syringe, diffferent needlegauge and speed,
   remove friction force

figure (5)
plot (v_30G_3mL,F_30G_3mL_hydro,'ko','MarkerFaceColor
   ','m');
hold on
plot (v_27G_3mL,F_27G_3mL_hydro,'ko');
hold on
plot (v_25G_3mL,F_25G_3mL_hydro,'ko','MarkerFaceColor
   ','c');

% plot in limit for Re>2000 for respective
   needlegauge
y_3mL = linspace(0,60); % vector for y values,100
   values 0-60
x_Re2000_30G_3mL = repmat(v_Re2000_30G_3mL
   *10^3,1,100); % row matrix with 1x100 radvector
   only consist of limit for Re>2000
x_Re2000_27G_3mL = repmat(v_Re2000_27G_3mL
   *10^3,1,100); % row matrix with 1x100 radvector
   only consist of limit for Re>2000
x_Re2000_25G_3mL = repmat(v_Re2000_25G_3mL
```

```
    *10^3,1,100); % row matrix with 1x100 radvector
    only consist oflimit for Re>2000

%hold on
%plot (v_hydro_30G_3mL,F_hydro_30G_3mL,'m:'); % plot
    in theoretical hydrodynamic force 3mL 30G
%hold on
%plot (v_hydro_27G_3mL,F_hydro_27G_3mL,'k:'); % plot
    in theoretical hydrodynamic force 3mL 27G
%hold on
%plot (v_hydro_25G_3mL,F_hydro_25G_3mL,'c:'); % plot
    in theoretical hydrodynamic force 3mL 25G

hold on
plot (x_Re2000_30G_3mL,y_3mL,'m--');
hold on
plot (x_Re2000_27G_3mL,y_3mL,'k--');
hold on
plot (x_Re2000_25G_3mL,y_3mL,'c--');

xlabel('expulsion velocity, mm/s');
ylabel('Hydrodynamic force, N');
title ('Hydrodynamic force 3 mL syringe at different
    needle gauges');
legend ('30G','27G','25G','Laminar limit 30G','
    Laminar limit 27G','Laminar limit 25G');
hold off

%%

% 1 mL syringe, diffferent needlegauge and speed

figure (6)
plot (v_30G_1mL,F_30G_1mL,'mo','MarkerFaceColor','m')
    ;
hold on
plot (v_27G_1mL,F_27G_1mL,'ko');
```

```
hold on
plot (v_25G_1mL,F_25G_1mL,'co','MarkerFaceColor','c')
   ;

% plot in limit for Re>2000 for respective
   needlegauge
y_1mL = linspace(0,30); % vector for y varden,100 st
   varden 0-60
x_Re2000_30G_1mL = repmat(v_Re2000_30G_1mL
   *10^3,1,100); % row matrix with 1x100 radvector
   only consist of limit for Re>2000
x_Re2000_27G_1mL = repmat(v_Re2000_27G_1mL
   *10^3,1,100); % row matrix with 1x100 radvector
   only consist of limit for Re>2000
x_Re2000_25G_1mL = repmat(v_Re2000_25G_1mL
   *10^3,1,100); % row matrix with 1x100 radvector
   only consist of limit for Re>2000

hold on
plot (x_Re2000_30G_1mL,y_1mL,'m--');
hold on
plot (x_Re2000_27G_1mL,y_1mL,'k--');
hold on
plot (x_Re2000_25G_1mL,y_1mL,'c--');

%hold on
%plot (v_hydro_30G_1mL,F_hydro_30G_1mL,'m:'); % plot
   in theoretical hydrodynamic force 1mL 30G
%hold on
%plot (v_hydro_27G_1mL,F_hydro_27G_1mL,'k:'); % plot
   in theoretical hydrodynamic force 1mL 27G
%hold on
%plot (v_hydro_25G_1mL,F_hydro_25G_1mL,'c:'); % plot
   in theoretical hydrodynamic force 1mL 25G

xlabel('expulsion velocity, mm/s');
ylabel('expulsion force, N');
```

```
title ('Expulsion force 1 mL syringe at different
   needle gauges');
legend ('30G','27G','25G','Limit 30G','Limit 27G','
   Limit 25G');
hold off

%%
% compare diffrent size syringes with same needle
   size at diffferent speeds
%OBS! frictionforce removed for 5 and 3 mL syringe (=
    hydrodyn force) but not for 1 mL(= expulsionforce
   )!

% 30G needle with 5, 3 and 1 mL syringe diffferent
   speeds
figure (7)
plot (v_30G_5mL,F_30G_5mL_hydro,'go');
hold on
plot (v_30G_3mL,F_30G_3mL_hydro,'bo');
hold on
plot (v_30G_1mL,F_30G_1mL,'ro');

xlabel('expulsion velocity, mm/s');
ylabel('Force, N');
title ('30G needle at different syringe sizes');
legend ('5 mL','3 mL','1 mL');
hold off

%%
% 27G needle with 5, 3 and 1 mL syringe diffferent
   speeds

figure (8)

plot (v_27G_5mL,F_27G_5mL_hydro,'go');
hold on
plot (v_27G_3mL,F_27G_3mL_hydro,'bo');
```

```
hold on
plot (v_27G_1mL,F_27G_1mL,'ro');

xlabel('expulsion velocity, mm/s');
ylabel('Force, N');
title ('27G needle at different syringe sizes');
legend ('5 mL','3 mL','1 mL');
hold off

%%
% 25G needle with 5, 3 and 1 mL syringe diffferent
   speeds
figure (9)
plot (v_25G_5mL,F_25G_5mL_hydro,'go');
hold on
plot (v_25G_3mL,F_25G_3mL_hydro,'bo');
hold on
plot (v_25G_1mL,F_25G_1mL,'ro');

xlabel('expulsion velocity, mm/s');
ylabel('Force, N');
title ('25G needle at different syringe sizes');
legend ('5 mL','3 mL','1 mL');
hold off

%%

% comparison between collected data and theoretic
   equation for laminar flow

% 30 G needle different syringes, plotted only data
   which fulfill speed in needle  Re>2000
figure (10)

% collected data for 30G
%       limit for laminar flow is:
%                                 v_Re2000_30G_5mL: % m
```

```
    /s, 1.9 mm/s for 5 mL 30 G
%                                   v_Re2000_30G_3mL: % m
    /s, limit  at 3.2 mm/s for 3mL with 30G
%
    v_Re2000_30G_1mL_hydro: % m/s, OBS! now friction
    removed

plot (v_30G_5mL(1,1:7),F_30G_5mL_hydro(1,1:7),'kd','
    MarkerFaceColor','g');
hold on
plot (v_30G_3mL(1,1:12),F_30G_3mL_hydro(1,1:12),'ko',
    'MarkerFaceColor','r');
hold on
plot (v_30G_1mL(1,1:20),F_30G_1mL_hydro(1,1:20),'k*',
    'MarkerFaceColor','k'); % OBS!! friction force
    removed
hold on

% equations linear fitting to data:
v_linear_fit_30G_5mL = linspace (0.1372,1.9); % mm/s,
     genererar speedvector
Linear_fit_30G_5mL = 26.9.*v_linear_fit_30G_5mL -
    3.69; % N, linear fitting to collected data, OBS!
    only in lamninar area
% R^2 for fit = 0.981, norm of residuals = 3.45

v_linear_fit_30G_3mL = linspace (0.4886,3.2); % mm/s,
     generate speedvector
Linear_fit_30G_3mL = 10.5.*v_linear_fit_30G_3mL -
    5.13; % N, linear fitting to collected data, OBS!
    only in lamninar area
% R^2 for fit = 0.988, norm of residuals = 3

v_linear_fit_30G_1mL = linspace (0.9966,13.5); % mm/s
    , generate speedvector
Linear_fit_30G_1mL = 0.595.*v_linear_fit_30G_1mL -
    0.593; % N, linear fitting to collected data, OBS!
```

```
    only in lamninar area
% R^2 for fit = 0.983, norm of residuals = 1.01

% theoretical values for 30G
hold on
plot (v_hydro_30G_5mL,F_hydro_30G_5mL,'g--'); % plot
   in theoretical hydrodynamic force 5mL 30G
hold on
plot (v_hydro_30G_3mL,F_hydro_30G_3mL,'r:'); % plot
   in theoretical hydrodynamic force 3mL 30G
hold on
plot (v_hydro_30G_1mL,F_hydro_30G_1mL,'k-.'); % plot
   in theoretical hydrodynamic force 1mL 30G

% Plot of fit on collected data
hold on
plot (v_linear_fit_30G_5mL,Linear_fit_30G_5mL,'g');
hold on
plot (v_linear_fit_30G_3mL,Linear_fit_30G_3mL,'r');
hold on
plot (v_linear_fit_30G_1mL,Linear_fit_30G_1mL,'k');

hold on
plot (linspace(0,14),linspace(0,0),'k','LineWidth',1)
   ;

xlabel('Expulsion speed, mm/s');
ylabel('Hydrodynamic force, N');
title ('30G needle');
%legend('Location','eastoutside')
legend ('5 mL observation','3 mL observation','1 mL
   observation','5 mL theoretic','3 mL theoretic','1
   mL theoretic','5 mL fit','3 mL fit','1 mL fit');

hold off
%%
```

```
% 27G needle diffferent sprutor, plotted only data
   which fulfills speed in needle which dont give Re
   >2000

figure (11)

% collected data for 27G
%       limit for laminar flow is:
%                                   v_Re2000_27G_5mL: % m
   /s, limit  at 2.7 mm/s for 5mL with 27G
%
%                                   v_Re2000_27G_3mL: % m
   /s, limit  at 4.5 mm/s for 3mL with 27G
%
%                                   v_Re2000_27G_1mL: % m
   /s, limit  at 19.3 mm/s for 1mL with 27G
%

plot (v_27G_5mL(1,1:11),F_27G_5mL_hydro(1,1:11),'kd',
   'MarkerFaceColor','g');
hold on
plot (v_27G_3mL(1,1:12),F_27G_3mL_hydro(1,1:12),'ko',
   'MarkerFaceColor','r');
hold on
plot (v_27G_1mL(1,1:7),F_27G_1mL_hydro(1,1:7),'k*','
   MarkerFaceColor','k'); % % OBS!! friction force
   removed, extrapolated

% equations linear fitting to data:

v_linear_fit_27G_5mL = linspace (0.1142,2.7); % mm/s,
     speedvector
Linear_fit_27G_5mL = 5.86.*v_linear_fit_27G_5mL -
   0.669; % N, linear fitting to collected data, OBS!
    only in lamninar area
% R^2 for fit = 0.808, norm of residuals = 5.06
```

```
v_linear_fit_27G_3mL = linspace (1.1019,4.5); % mm/s,
    genererar speedvector
Linear_fit_27G_3mL = 3.63.*v_linear_fit_27G_3mL - 4;
   % N, linear fitting to collected data, OBS! only
   in lamninar area
% R^2 for fit = 0.992, norm of residuals = 1.29

v_linear_fit_27G_1mL = linspace (0.5642,19.3); % mm/s
   , genererar speedvector
Linear_fit_27G_1mL = 0.179.*v_linear_fit_27G_1mL -
   0.101; % N, linear fitting to collected data, OBS!
    only in lamninar area
% R^2 for fit = 0.976, norm of residuals = 0.337

% theoretical values for 27G

hold on
plot (v_hydro_27G_5mL,F_hydro_27G_5mL,'g--'); % plot
   in theoretical hydrodynamic force 5mL 27G
hold on
plot (v_hydro_27G_3mL,F_hydro_27G_3mL,'r:'); % plot
   in theoretical hydrodynamic force 3mL 27G
hold on
plot (v_hydro_27G_1mL,F_hydro_27G_1mL,'k-.'); % plot
   in theoretical hydrodynamic force 1mL 27G


% Plot of fit collected data
hold on
plot (v_linear_fit_27G_5mL,Linear_fit_27G_5mL,'g');
hold on
plot (v_linear_fit_27G_3mL,Linear_fit_27G_3mL,'r');
hold on
plot (v_linear_fit_27G_1mL,Linear_fit_27G_1mL,'k');

hold on
plot (linspace(0,20),linspace(0,0),'k');
```

```
xlabel('Expulsion speed, mm/s');
ylabel('Hydrodynamic force, N');
title ('27G needle');
legend ('5 mL observation','3 mL observation','1 mL
   observation','5 mL theoretic','3 mL theoretic','1
   mL theoretic','5 mL fit','3 mL fit','1 mL fit');

hold off
%%

% 25G needle diffferent sprutor,  plotted only data
   which fulfills speed in needle which dont give Re
   >2000


figure (12)

% collected data for 25G
%       limit for laminar flow:
%                                   v_Re2000_25G_5mL: % m
   /s, limit  at 3.2 mm/s for 5mL with 25G
%                                   v_Re2000_25G_3mL: % m
   /s, limit  at 5.3 mm/s for 3mL with 25G
%                                   v_Re2000_25G_1mL: % m
   /s, limit  at 31.4 mm/s for 1mL with 25G

plot (v_25G_5mL(1,1:6),F_25G_5mL_hydro(1,1:6),'kd','
   MarkerFaceColor','g');
hold on
plot (v_25G_3mL(1,1:6),F_25G_3mL_hydro(1,1:6),'ko','
   MarkerFaceColor','r');
hold on
plot (v_25G_1mL(1,1:7),F_25G_1mL_hydro(1,1:7),'k*','
   MarkerFaceColor','k');

% equations linear fitting to data:
```

```
% equation under behover goras om, bara 2 diffferent
   speeds
v_linear_fit_25G_5mL = linspace (0.7531,3.2); % mm/s,
    genererar speedvector
Linear_fit_25G_5mL = 4.9.*v_linear_fit_25G_5mL -
   3.69; % N, linear fitting to collected data, OBS!
   only in lamninar area
% R^2 for fit = 0.997, norm of residuals = 0.658

% equation under behover goras om, bara 2 diffferent
   speeds
v_linear_fit_25G_3mL = linspace (1.45,5.3); % mm/s,
   generates speedvector
Linear_fit_25G_3mL = 2.07.*v_linear_fit_25G_3mL - 3;
   % N, linear fitting to collected data, OBS! only
   in lamninar area
% R^2 for fit = 0.988, norm of residuals = 0.554

v_linear_fit_25G_1mL = linspace (0.8,22.5); % mm/s,
   genererate speedvector
Linear_fit_25G_1mL = 0.104.*v_linear_fit_25G_1mL -
   0.0827; % N, linear fitting to collected data, OBS
   ! only in lamninar area
% R^2 for fit = 0.974, norm of residuals = 0.205

% theoretical values for 25G
hold on
plot (v_hydro_25G_5mL,F_hydro_25G_5mL,'g--'); % plot
   theoretical hydrodynamic force 5mL 25G
hold on
plot (v_hydro_25G_3mL,F_hydro_25G_3mL,'r:'); % plot
   theoretical hydrodynamic force 3mL 25G
hold on
plot (v_hydro_25G_1mL,F_hydro_25G_1mL,'k-.'); % plot
   theoretical hydrodynamic force 1mL 25G
```

```
% Plot of fit on collected data
hold on
plot (v_linear_fit_25G_5mL,Linear_fit_25G_5mL,'g');
hold on
plot (v_linear_fit_25G_3mL,Linear_fit_25G_3mL,'r');
hold on
plot (v_linear_fit_25G_1mL,Linear_fit_25G_1mL,'k');

hold on
plot (linspace(0,25),linspace(0,0),'k');

xlabel('Expulsion speed, mm/s');
ylabel('Hydrodynamic force, N');
title ('25G needle');
legend ('5 mL observation','3 mL observation','1 mL
   observation','5 mL theoretic','3 mL theoretic','1
   mL theoretic','5 mL fit','3 mL fit','1 mL fit');

hold off

%%
% OBS!!! chech for laminar flow, otherwise equations
   not valid

% Reynolds number?
%Re = speed fluid*hydraulic diameter/kinematic
   viskosity water

% hydraulic diameter = needlee diameter

% kin_viscosity_water = 1.004*10^-6; % m2/s, water 20
    degrees


% fluid speed in needle?
%           v = F/A
%           A = cross section area needle = pi*
```

```
   r_needle^2
%           F = flowt i syringe = speed syringe*cross
    section area syringe
%           = v_syringe*pi*r_syringe^2
%           dvs v_needle = ( v_syringe*pi*r_syringe^2
    )/pi*r_needle^2 = v_syringe*r_syringe^2 /r_needle
   ^2

% take the highest speed for each combination
% calculate speed on fluid in needle
% 5 mL syringe
v_needle_30G_5mL = (2*10^-3*(r_5mL^2))/(r_30G^2); % m
   /s, 2 mm/s in syringe,  14.1709 m/s
v_needle_27G_5mL = (4.5*10^-3*(r_5mL^2))/(r_27G^2);
   % m/s, 4.5 mm/s in syringe, 15.5709 m/s
v_needle_25G_5mL = (6.5*10^-3*(r_5mL^2))/(r_25G^2);
   % m/s, 6.5 mm/s in syringe,  16.25 m/s

% 3 mL syringe
v_needle_30G_3mL = (4*10^-3*(r_3mL^2))/(r_30G^2); % m
   /s, 4 mm/s in syringe,  17.0667 m/s
v_needle_27G_3mL = (9*10^-3*(r_3mL^2))/(r_27G^2); % m
   /s, 9 mm/s in syringe, 18.7529 m/s
v_needle_25G_3mL = (12*10^-3*(r_3mL^2))/(r_25G^2); %
   m/s, 12 mm/s in syringe, 18.0653 m/s

% 1 mL syringe
v_needle_30G_1mL = (20*10^-3*(r_1mL^2))/(r_30G^2); %
   m/s, 20 mm/s in syringe,  20.0342 m/s

v_needle_27G_1mL = (20*10^-3*(r_1mL^2))/(r_27G^2); %
   m/s, 20 mm/s in syringe,  9.7838 m/s
v_needle_27G_1mL_30 = (30*10^-3*(r_1mL^2))/(r_27G^2);
    % m/s, 30 mm/s in syringe,  14.6757 m/s

v_needle_25G_1mL = (20*10^-3*(r_1mL^2))/(r_25G^2); %
   m/s, 20 mm/s in syringe,  7.0688 m/s
```

```
v_needle_25G_1mL_40 = (40*10^-3*(r_1mL^2))/(r_25G^2);
    % m/s, 40 mm/s in syringe,  14.1376 m/s

%%
% Reynolds number?

% 5 mL syringe
Re_30G_5mL = v_needle_30G_5mL*2*r_30G/
   kin_viscosity_water; % gives 2096.0
Re_27G_5mL = v_needle_27G_5mL*2*r_27G/
   kin_viscosity_water; % gives 3295.6
Re_25G_5mL = v_needle_25G_5mL*2*r_25G/
   kin_viscosity_water; % gives 4046.3

% 3 mL syringe
Re_30G_3mL = v_needle_30G_3mL*2*r_30G/
   kin_viscosity_water; % gives 2524.3
Re_27G_3mL = v_needle_27G_3mL*2*r_27G/
   kin_viscosity_water; % gives 3969.1
Re_25G_3mL = v_needle_25G_3mL*2*r_25G/
   kin_viscosity_water; % gives 4498.3

% 1 mL syringe
Re_30G_1mL = v_needle_30G_1mL*2*r_30G/
   kin_viscosity_water; % gives 2963.2
Re_27G_1mL = v_needle_27G_1mL_30*2*r_27G/
   kin_viscosity_water; % gives 3106.2
Re_25G_1mL = v_needle_25G_1mL_40*2*r_25G/
   kin_viscosity_water; % gives 3520.3

% what speed does it take in each needle for Re>4000?
v_Re4000_30G = 4000*kin_viscosity_water/(2*r_30G); %
   gives  27.0438 m/s for 30G needle
v_Re4000_27G = 4000*kin_viscosity_water/(2*r_27G); %
   gives 18.8988 m/s for 27G needle
v_Re4000_25G = 4000*kin_viscosity_water/(2*r_25G); %
   gives 16.0640 m/s for 25G needle
```

Appendix D

Matlab script mechanical stress

```
% Estimation of shear stress and shear rate at barrel
    wall

r_barrel = confidential
r_needle = confidential
L_needle = 12*10^-3; % length needle, m

v_plunger = [0.1 0.1 0.1 0.9 0.9 0.9 1.7 1.7 1.7]; %
   linear speed of plunger, mm/s

% without silicone
F_hydro = [-0.881        -3.065   -2.021 12.426
   15.539   13.773 40.98     39.782   35.609]; %
   hydrodynamic force (N) at 0.1, 0.9 and 1.7 mm/s

v_plunger_sili = [0.1 0.1 0.1 0.1 0.9 0.9 0.9 0.9 1.7
    1.7 1.7]; % linear speed of plunger, mm/s

% with silicone
F_hydro_sili = [1.307    3.457    10.27    3.075 33.925
```

```
        4.232   23.433  25.494 41.233   41.271
    45.027]; % hydrodynamic force (N) at 0.1, 0.9 and
    1.7 mm/s

%%

% vectors for plot of linear fit to data in figure
v_linefit = linspace (0,1.8); % generate vector with
    100 values of plunger speed 0-1.8 mm/s
F_hydro_linefit = 25.5.*v_linefit - 6.03; % generate
    vector corresponding to linear fit of data without
     silicone at speed 0-1.8 mm/s
F_hydro_linefit_sili = 23.6.*v_linefit + 1.61; %
    generate vector corresponding to linear fit of
    data with silicone at speed 0-1.8 mm/s

%plot
figure (1)
plot (v_plunger,F_hydro,'b*') % plot of data without
    silicone, R2 = 0.975, y = 25.5x - 6.03, norm of
    residuals = 7.97
grid on
grid minor
hold on
plot (v_plunger_sili,F_hydro_sili,'ro') % plot of
    data with silicone, R2 = 0.822, y = 23.6x + 1.61,
    norm of residuals = 23.1
hold on
plot (v_linefit,F_hydro_linefit,'b-.') % linear fit
    to data without silicone
hold on
plot (v_linefit,F_hydro_linefit_sili,'r-.') % linear
    fit to data with silicone
ylabel ('Hydrodynamic force, N');
xlabel ('Plunger speed, mm/s');
legend ('Without silicone','With silicone')
title('Hydrodynamic force during expulsion')
```

```
hold off




%%
% Plot of shear stress

% Shear stress
% without silicone
tau_w = (F_hydro./(pi*((r_barrel)^2)))*((r_needle)
   /(2*L_needle)); % Shear stress, N/m^2


% with silicone
tau_w_sili = (F_hydro_sili./(pi*((r_barrel)^2)))*((
   r_needle)/(2*L_needle)); % Shear stress, N/m^2

% vectors for plot of linear fit to data in figure
tau_w_linefit = 643.*v_linefit - 152; % generate
   vector corresponding to linear fit of data without
    silicone at speed 0-1.8 mm/s
tau_w_linefit_sili = 596.*v_linefit + 40.7; %
   generate vector corresponding to linear fit of
   data with silicone at speed 0-1.8 mm/s

%plot
figure (2)
plot (v_plunger,tau_w,'b*') % plot of data without
   silicone, R2 = 0.975, y = 643x - 152, norm of
   residuals = 201
grid on
grid minor
hold on
plot (v_plunger_sili,tau_w_sili,'ro') % plot of data
   with silicone, R2 = 0.822, y = 596x + 40.7, norm
```

```
   of residuals = 584
hold on
plot (v_linefit,tau_w_linefit,'b-.') % linear fit to
   data without silicone
hold on
plot (v_linefit,tau_w_linefit_sili,'r-.') % linear
   fit to data with silicone
ylabel ('Shear stress, N/m^2');
xlabel ('Plunger speed, mm/s');
legend ('Without silicone','With silicone')
title('Shear stress at barrel wall')
hold off

% average shear stress?
% without silicone
average_tau = [mean(tau_w(1:3)) mean(tau_w(4:6)) mean
   (tau_w(7:9))]; % at 0.1 mm/s (-50.1 N/m^2), at 0.9
    mm/s (351 N/m^2) and at 1.7 mm/s (978 N/m^2)
average_tau_sili = [mean(tau_w_sili(1:4)) mean(
   tau_w_sili(5:8)) mean(tau_w_sili(9:11))]; % at 0.1
    mm/s (114 N/m^2), at 0.9 mm/s (549 N/m^2) and at
   1.7 mm/s (1072 N/m^2)

%%

% frictional force

% without silicone
F_fric = [13.872        10.953   11.958 12.376    10.39
      10.863 12.883    11.537   10.286]; % friction
   force (N) at 0.1, 0.9 and 1.7 mm/s
F_fric_vector = repmat (mean (F_fric),1,100); % row
   vector repeating the average fricton force (N)
   across speed 100 times

% with silicone
F_fric_sili = [13.287    12.322   3.889    13.581 11.78
```

```
        13.476   6.161    5.66 13.451      15.305
    4.578];  % friction force (N) at 0.1, 0.9 and 1.7
    mm/s
F_fric_vector_sili =  repmat (mean (F_fric_sili)
    ,1,100);  % row vector repeating the average
    fricton force (N) across speed 100 times


figure (3)
plot (v_plunger,F_fric,'b*') % plot of data without
    silicone
grid on
grid minor
hold on
plot (v_plunger_sili,F_fric_sili,'ro') % plot of data
     with silicone
hold on
plot (v_linefit,F_fric_vector,'b--') % linear fit to
    data without silicone
hold on
plot (v_linefit,F_fric_vector_sili,'r--') % linear
    fit to data with silicone
ylabel ('Friction force, N');
xlabel ('Plunger speed, mm/s');
legend ('Without silicone','With silicone')
title('Friction force during expulsion')
hold off



%%
```

EXAMENSARBETE Methods to study device induced aggregation of proteins
STUDENT Therese von Wowern
HANDLEDARE Marie Wahlgren (LTH), Anna Kjellström (LTH)
EXAMINATOR Lars Nilsson (LTH)

En metod för att undersöka om sprutor orsakar partiklar i proteinläkemedel

POPULÄRVETENSKAPLIG SAMMANFATTNING **Therese von Wowern**

Främjar användandet av sprutor med nål bildandet av potentiellt skadliga partiklar i proteinläkemedel?

Läkemedel som består av skräddarsydda proteiner används idag för att behandla bland annat diabetes. De ges traditionellt som injektioner och detta misstänks vara kopplat till skapandet av skadliga partiklar. Sprutan och nålen är ofta silikoniserade för att underlätta hantering och deras användning utsätter det känsliga proteinet för mekaniska krafter. Detta tros leda till bildandet av partiklar i form av silikon droppar och protein klumpar (aggregat). Detta arbete utvecklade därför en metod för att undersöka effekten av sprutor med nål på ostabiliserat insulin. En 3D printad spruthållare till en maskin som kan trycka och dra samtidigt som den mäter kraften (texturometer) designades för att kunna manövrera sprutan (se bild nedan).

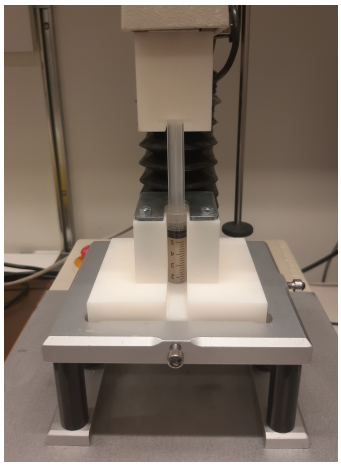

Effekten av mekanisk påverkan undersöktes genom att variera tömningshastighastighen av sprutan. Endast hastigheter som var associerade med laminärt flöde underöktes. Osilikoniserade sprutor jämfördes mot silikoniserade. Tre vanligt förekommande analysmetoder (dynamisk ljusspridning, storlekskromatografi (SEC) och FlowCam) användes för att mäta partikelkoncentration och storlek. Spruthållaren i vit nylonplast presterade bra, tog tre dagar att skapa och kostade en tiondel av färdiga alternativ på marknaden. FlowCam mätningarna visade att partikelkoncentrationerna höll sig under tillåtna nivåer och steg med ökad tömningshastighet. FlowCam tog bilder av de individuella partiklarna i proven. Dessa kunde sedan användas för att se vilka slags partiklar proven innehöll. Silikondroppparna var helt sfäriska med slät kant och hade ibland en reflektiv mitt. Det visade sig att koncentrationsökningen i den silikoniserade sprutan berodde på ökat antal silikonoljedroppar. I den osilikoniserade sprutan berodde ökningen istället på ett ökat antal partiklar som var ojämna, mörkare och med skrovlig kant. Dessa antogs vara proteinaggregat.

Metoden som utvecklades kan i framtiden användas för att undersöka andra proteiner eller effekten av andra faktorer såsom övergångsflöde, uppdragshastighet eller luftintroduktion.